STRUCTURAL AND FUNCTIONAL STUDIES OF

ELECTRON TRANSFER COMPLEXES

By

XING GONG

Bachelor of Science
Lanzhou University
Gansu, P. R. China
1996

Master of Science
Lanzhou University
Gansu, P. R. China
1999

Submitted to the Faculty of the
Graduate College of the
Oklahoma State University
in partial fulfillment of
the requirements for
the Degree of
DOCTOR OF PHILOSOPHY
December, 2005

STRUCTURAL AND FUNCTIONAL STUDIES OF

ELECTRON TRANSFER COMPLEXES

Thesis Approved:

Chang-An Yu
Thesis Adviser

Linda Yu

Robert L. Matts

Richard C. Essenberg

Robert L. Burnaps

A. Gordon Emslie
Dean of the Graduate College

ACKNOWLEDGEMENTS

I wish especially to express my sincere appreciation to my adviser, Dr. Chang-An Yu, for his intelligent supervision, constructive guidance, and inspiration through my graduate program. I am also equally grateful to Dr. Linda Yu for her supervision, guidance and encouragement during my study. Many particular thanks I owe to them for their constant concern and direction in my research work and my future career.

My deep gratitude extends to my committee members: Dr. Richard Essenberg, Dr. Robert Matts, and Dr. Robert Burnap, whose guidance, assistance, and encouragement are also invaluable for my study and future life.

I am also very thankful for the cooperation from Dr. Di Xia from NIH and Drs. Hesterberg Micaela and Dierk Scheide in Dr. Thorsten Friedrich's group from Germany. My sincere gratitude also goes to all of members in Dr. Yu's lab for their marvelous hospitality and stimulating conversations about the research and life during my graduate study.

Surely, I must acknowledge with deep appreciation to my wife, Xiaoying Liu, and to my parents, Heping Liu and Haiwen Gong, as well as to my parents-in-law, Professors Li Yang and Zhongli Liu, and to other relatives in China and the US. Their understanding, support, love, encouragement, inspiration, and patience throughout these years, especially at the times of difficulty, are the driving-force of my study and life.

TABLE OF CONTENTS

LIST OF TABLES

LIST OF FIGURES

NOMENCLATURE

ADP	Adenosine diphosphate
ATP	Adenosine triphosphate
$[^3H]$Azido-Q	3-Azido-2-methyl-5-methoxy$[^3H]$-6-decyl-1,4-benzoquinone
b_H or b_{562}	High potential cytochrome *b*
b_L or b_{566}	Low potential cytochrome *b*
Complex I	NADH:ubiquinone oxidoreductase
Complex II	Succinate:ubiquinone oxidoreductase
Complex III	Ubiquinol:cytochrome *c* oxidoreductase or cytochrome bc_1
Complex IV	Cytochrome *c* oxidase
Complex V	ATP-synthase
DATA	N,N’-diallyltartardiamide
DM	Dodecylmaltoside
DMSO	Dimethylsulfoxide
DSC	Differential scanning calorimetry
E. coli	*Escherichi coli*
EPR	Electron paramagnetic resonance
ET	Electron transfer
FAD	Flavin adenine dinucleotide, oxidized form
$FADH_2$	Flavin adenine dinucleotide, reduced form

FMN	Flavin mononucleotide
HPLC	High performance liquid chromatography
HQNO	Heptylhydroxyquinoline-N-oxide
ICM	Intra-cytoplasmic membrane
IMS	Intermembrane space
ISP	Rieske iron-sulfur protein
MCLA	2-Methyl-6-(-*p*-methoxyphenyl)-3,7-dihydroimidazo[1,2-α]pyrazin-3-one hydrochloride; or methyl *Cypridina* luciferin analog
β-ME	β-Mercaptoethanol
MIM	Mitochondrial inner membrane
MOAS	Methoxyacrylate stilbene
NAD	Nicotinamide adenine dinucleotide, oxidized form
NADH	Nicotinamide adenine dinucleotide, reduced form
NADP	Nicotinamide adenine dinucleotide phosphate, oxidized form
NADPH	Nicotinamide adenine dinucleotide phosphate, reduced form
N. crassa	*Neurospora crassa*
Ni-NTA	Nickel-nitrilotriacetic acid
OG	Octylglucoside
$O_2^{\cdot -}$	Superoxide anion
Pi	Inorganic phosphate
PMSF	Phenylmethylsulfonyl fluoride
Q_1	2,3-Dimethoxy-5-methyl-6-isoprenoyl-1,4-benzoquinone

$Q_0C_{10}Br$	2,3-Dimethoxy-5-methyl-6-(10-bromodecyl)-1,4-benzoquinone
$Q_0C_{10}BrH_2$	2,3-Dimethoxy-5-methyl-6-(10-bromodecyl)-1,4-benzoquinol
Q	Ubiquinone
QH_2	Ubiquinol
Qi site	Ubiquinone reduction site
Qo site	Ubiquinol oxidation site
R. sphaeroides	*Rhodobacter sphaeroides*
SD	Standard deviation
ST-EPR	Saturation transfer electron paramagnetic resonance
TM	Transmembrane
[2Fe-2S]	Iron-sulfur cluster of Rieske iron-sulfur protein
UHDBT	5-Undecyl-6-hydroxy-4,7-dioxobenzothiazole
XO	Xanthine oxidase

CHAPTER I

INTRODUCTION

Bioenergetics and Electron Transfer Chain

Living cells require a continual input of energy to maintain the living state. More than 90% of the energy needed for aerobic cells is provided through a process known as oxidative phosphorylation. This process is carried out in the inner mitochondrial membrane by the electron transfer chain and adenosine triphosphate (ATP) synthase (1,2) (see Figure 1).

The electron transfer chain is composed of four enzyme complexes: NADH:ubiquinone oxidoreductase (complex I), succinate:ubiquinone oxidoreductase (complex II), cytochrome bc_1 complex (ubiquinol:cytochrome *c* oxidoreductase or Complex III), and cytochrome *c* oxidase (complex IV). Electrons are passed through these complexes from lower to higher standard reduction potentials. Complex I catalyzes the transfer of electrons from reduced nicotinamide adenine dinucleotide (NADH) to coenzyme Q (CoQ). Complex II catalyzes the oxidation of flavin adenine dinucleotide ($FADH_2$) by CoQ. Since this redox reaction does not release sufficient free energy to synthesize ATP, complex II functions only to extract the electrons from $FADH_2$ and transfer them into the electron transfer chain. CoQ then carries electrons to complex III,

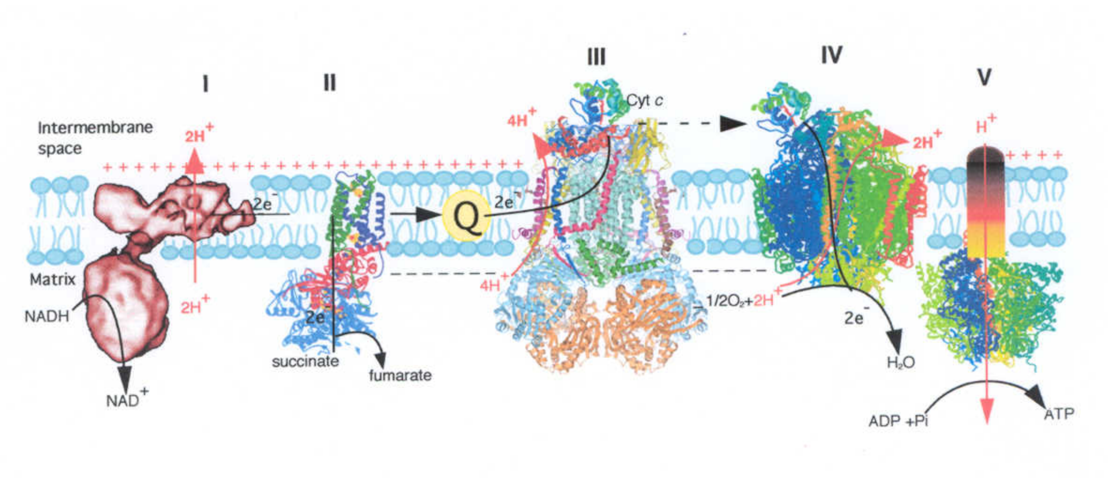

Figure 1. The enzymes of the mitochondrial inner membrane involved in oxidative phosphorylation. The oxidation of NADH and $FADH_2$ is catalyzed by the respiratory or electron transport chain, a series of four enzyme complexes: NADH:ubiquinone oxidoreductase (complex I), succinate:ubiquinone oxidoreductase (complex II), cytochrome *bc*$_1$ complex (ubiquinol:cytochrome *c* oxidoreductase or complex III) and cytochrome *c* oxidase (complex IV). The other complex is the ATP synthase (complex V), which catalyzes the synthesis of ATP from ADP and inorganic phosphate (P_i).

which catalyzes the oxidation of reduced CoQ by cytochrome *c*. Reduced cytochrome *c* is finally oxidized by donating the electrons to molecular oxygen by complex IV producing water. Electrons transferred through complexes I, III and IV are accompanied with translocation of protons across the mitochondrial inner membrane to generate a proton gradient and a membrane potential used by ATP synthase (complex V) that synthesize ATP from ADP and inorganic phosphate (Pi). The chemiosmotic theory (3) proposed by the Nobel Prize laureate Peter Mitchell is the general mechanistic principle of oxidative and phosphorylation. It explains the coupling between respiration and ATP synthesis and has become a paradigm in the intellectual framework of bioenergetics since the mid-1970's. To this date, the electron transfer and proton translocation in the electron transfer chain are the main points of bioenergetics.

NADH:Ubiquinone Oxidoreductase

<u>The Function and Subunit Composition of NADH:Ubiquinone Oxidoreductase</u>--NADH:ubiquinone oxidoreductase (commonly known as complex I) is the first segment of the energy-conserving electron transfer chains of mitochondria and many respiratory and some bacteria (4) (see Figure1). This complex catalyzes electron transfer from NADH to ubiquinone (Q) and concomitantly translocates protons across the membrane to generate a membrane potential and proton gradient for ATP synthesis (5,6). Forty-six different subunits have been identified in complex I from bovine heart mitochondria with a molecular mass of almost 1000 kDa (7). Seven subunits (ND1 to ND6 plus ND4L) are products of the mitochondrial genome (8,9). The rest are nuclear gene products that are imported into the mitochondria from the cytoplasm (10). The bacterial complex I has a

mass close to 550 kDa and contains only 13 or 14 subunits (designated NuoA-N for *Escherichi* (*E.*) *coli* and Nqo1-14 for *Paracoccus denitrificans* and *Thermus thermophilus*) (6,11). All of the subunits of bacterial complex I have analogues in the mitochondrial enzyme (4) (see Table 1). Because the subunit composition of complex I from bacteria is relatively simple compared to that of its mitochondrial counterpart, the bacterial enzyme is a useful model system for studying the structure and function of complex I (12).

The Structures of Complex I--Unlike other electron-transport chain complexes, the X-ray crystal structure of complex I is not available at this moment because of its complexity. However, electron microscopy (EM) analysis of two dimensional crystals has shown that both the mitochondrial and the bacterial enzyme have two arms arranged perpendicular to each other forming a characteristic L-shaped structure (11). A model for the architecture of this enzyme is illustrated in Fig. 2A. One arm is embedded in the mitochondrial inner membrane, the other, so called the peripheral arm, protrudes into the mitochondrial matrix or bacterial cytoplasm. This was demonstrated at about 20 to 30 Å resolution for the enzyme from fungus *Neurospora crassa* (13,14), yeast *Yarrowia lipolytica* (15), beef heart mitochondria (16), *E. coli* (11,17), and the thermophile *Aquifex aeolicus* (18). Recently, however, Dr. Friedrich's group reported that *E. coli* complex I has an additional stable conformation, with the two arms arranged side by side, resulting in a horseshoe-shaped quaternary structure (see Fig. 2B). The global L-shaped conformation existed under high ionic strength conditions and the "horseshoe"-like conformation at low ionic strength. The transition between these two comformations was reversible. This "horseshoe"-like conformation is native, based on the fact that the complex exhibited

Table 1: Subunits and cofactors of complex I

Bovine complex I	*E. coli* and *Rhodobacter* complex I	*Paracoccus* and *Thermus* complex I	Cofactors	Fe-S center	*Em* (mV)
51 K	NuoF	Nqo1	FMN[b]		-340
			[4Fe-4S]	N3	-250
24 K	NuoE	Nqo2	[2Fe-2S]	N1a	-370
75 K	NuoG	Nqo3	[2Fe-2S]	N1b	-250
			[4Fe-4S]	N4	-250
			[4Fe-4S]	N5	-250
			[4Fe-4S]	N1c[c]	N/A
49 K	NuoD[a]	Nqo4			N/A
30 K	NuoC[a]	Nqo5			N/A
PSST	NuoB	Nqo6	[4Fe-4S]	N2	-50 to -150
TYKY	NuoI	Nqo9	2[4Fe-4S]	N6	N/A
ND1	NuoH	Nqo8			N/A
ND2	NuoN	Nqo14			N/A
ND3	NuoA	Nqo7			N/A
ND4	NuoM	Nqo13			N/A
ND4L	NuoK	Nqo11			N/A
ND5	NuoL	Nqo12			N/A
ND6	NuoJ	Nqo10			N/A
> 32 other subunits	none	none	Phospho-pantetheine, NADPH		N/A

[a] In some species of bacteria, for example *E. coli*, NuoC and NuoD are fused. [b] FMN is flavin mononucleotide. [c]This [4Fe-4S] cluster is only present in some species of bacteria (e.g., *E. coli, T. thermophilus*).

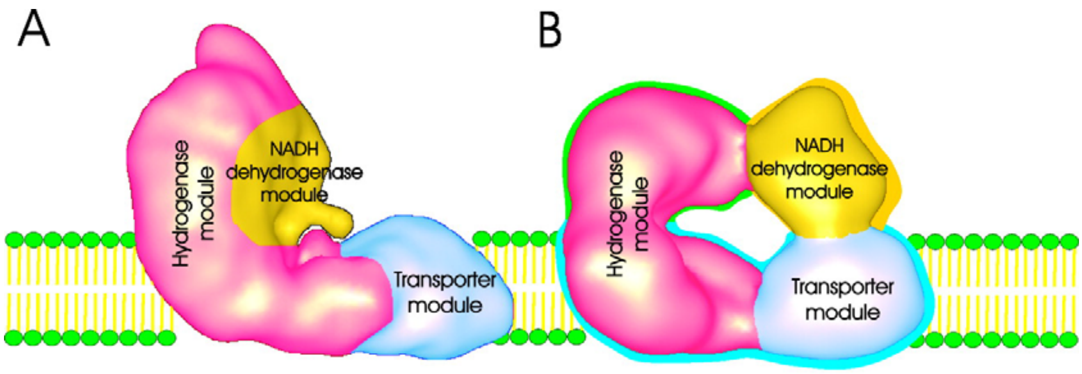

Figure 2. Speculative conformational models of complex I from *E. coli* in a buffer of high (*A*) and low (*B*) ionic strength (19). The soluble NADH dehydrogenase module comprising subunits NuoE, -F, and -G is drawn in *yellow*. All subunits of the connecting fragment (NuoB, -CD, and –I) together with the hydrophobic subunits NuoH and -L of the membrane fragment constitute the so-called hydrogenase module shown in *red*. The remaining subunits of the membrane fragment, namely NuoA, -J, -K, -M, and -N, build the so-called transporter module indicated in *blue frame* in *B*.

NADH:ubiquinone oxidoreductase activity solely in this conformation (19).

Subfraction of complex I with chaotropes and detergents indicates that all the redox centers of the enzyme (flavin mononucleotide (FMN) and up to 8-9 iron-sulfur [Fe-S] clusters) are located in the peripheral arm (10,11,20,21) (Table 1). The peripheral arm of bovine enzyme has been resolved into two fractions, a flavoprotein fraction and an iron-sulfur protein fraction. The main components of the flavoprotein fraction are the 51-kDa (NuoF in *E. coli*) and 24-kDa (NuoE) subunits, whereas the iron-sulfur protein fraction comprises mainly the 75- (NuoG), 49-, and 30-kDa (NuoCD, fused in *E. coli*) and PSST (NuoB) subunits (22). With the *E. coli* enzyme, the peripheral arm is resolved into a NADH dehydrogenase fragment and a connecting fragment (23). The soluble NADH dehydrogenase fragment is the electron input part of the complex, which comprises the subunits NuoE, NuoF and NuoG as well as harbors the FMN, and the electron paramagnetic resonance (EPR)-detectable FeS clusters of N1a, N1b, N1c, N3, and N4 (21). The NuoF subunit contains the NADH-binding site as it has been shown for complex I from beef heart (24) by photoaffinity labeling using arylazido-beta-[3-^{3}H]-alanyl NAD^{+}.

The connecting fragment consists of NuoB, NuoCD and NuoI (bovine TYKY) subunits and contains the EPR-detectable FeS cluster N2 and the UV-visible-detectable clusters N6a and N6b (25).

The membrane arm of the enzyme, which seemingly lacks known cofactors, such as flavin or iron-sulfur clusters, has been studied far less than the peripheral arm. However, the membrane arm of bovine complex I was resolved into two subcomplexes, designated Iβ and Iγ (20,26). The Iβ fragment contains subunits ND4 (NuoM in *E. coli*) and ND5 (NuoL) along with 11 accessory subunits, which do not directly participate in the electron and proton transport function. The Iγ fragment is composed of ND1 (NuoH), ND2 (NuoN), ND3 (NuoA), and ND4L (NuoK) along with 1 accessory subunit. Recently, the membrane arm of complex I from *E. coli* has been disrupted into fragments containing NuoL/M/N, NuoA/K/N, and NuoH/J subunits, respectively (27). Sequence comparisons have suggested that subunits ND2 (NuoN), ND4 (NuoM) and ND5 (NuoL) evolved from a common ancestor related to K^+ or Na^+/H^+ antiporters and thus are likely to be involved in the proton translocation (28).

<u>The Interaction between Q and Complex I</u>--The mechanisms of electron transfer and proton translocation in complex I is poorly understood. The interaction between complex I and Q is the central part of the enzymatic mechanism of this complex since Q is the final electron acceptor in this enzyme complex and may take part in electron recycling and/or proton transport processes. At the present time, the number or location of the Q-binding sites in this complex is still under debate (29,30); up to three sites have been proposed (31). The Q-binding site has long been thought to be located at the membrane arm due to its lipophilic nature. ND1 (NuoH in *E. coli*) was identified as a Q- and rotenone-binding protein by photoaffinity labeling using two rotenone analogs (32,33). The result of rotenone binding was used to indicate that Q binds to the same site. Pyridaben is another potent inhibitor of complex I. Using a pyridaben photoaffinity ligand the hydrophilic subunit PSST (NuoB in *E. coli*) was specifically labeled (34). The PSST subunit was proposed to house iron-sulfur cluster N2, which has the highest redox potential (see Table 1) and is therefore considered to be the site of electron transfer to the Q molecules (35). Fenpyroximate has been established to be a potent inhibitor of complex I (36,37). ND5 (NuoL) subunit was indicated as one of the possible candidates

representing a Q-binding site since it was specifically labeled by [^{3}H](trifluoromethyl)phenyldiazirinylfenpyroximate (38).

Another approach to locate the Q-binding site involved the use of bioinformatics (39). On the basis of the known 3D structures of enzyme complexes bearing Q, the following sequence motifs of Q-binding sites were deduced: L-$(X)_3$-H-$(X)_{2\text{-}3}$-T/S or A/L-$(X)_3$-H-$(X)_2$-L. A search of the SWISSPROT database identified that the sequence L-$(X)_3$-H-$(X)_3$-S was located in a well-conserved region of a diverse range of ND4 (NuoM in *E. coli*) sequences. The histidine residue was fully conserved and the triad itself was conserved in 96% of the 71 full-length sequences in the database. Alignment of representative ND4 (NuoM) and ND5 (NuoL) sequences indicates that a histidine residue (His328 in the bovine sequence) is also fully conserved in the equivalent position in the 91 full-length ND5 sequences. The triad sequence around the histidine residue in ND5 is most commonly (59%) the L-$(X)_3$-H-$(X)_2$-T. Taking these bioinformatics together, ND4 (NuoM)/ND5 (NuoL) are considered to be candidates for the locations of Q-binding sites in complex I. The ND4 (NuoM)/ND5 (NuoL) pair might harbor two separate Q sites or a single site could be formed from elements of both subunits.

Mutational analysis is the third powerful method to obtain the information about the Q-binding site(s). Several subunits were identified as the Q-binding site(s) in complex I based on the mutational studies. Human mutation on ND1 (NuoH) was reported to have a marginal effect on the NADH-dependent respiration and this effect was taken as genetic indication for the involvement of ND1 in the binding of Q (40-42). ND4 (NuoM) and the ND5 (NuoL) subunits were suggested as the Q-binding sites based on the fact that null mutants lacking the ND4 (NuoM) and the ND5 (NuoL) subunits had NADH-$K_3Fe(CN)_6$

reductase activity but lack NADH-ubiquinone reductase activity (43,44). Additionally, 49-kDa subunit (NuoD) was proposed to be involved in Q binding due to the inhibitor resistance conferred by a point mutation in this subunit (45).

Thus, the Q-binding site is most likely involved in NuoB (PSST), NuoD (49-kDa), NuoH (ND1), NuoM (ND4) and NuoL (ND5) in complex I. To unambiguously identify the Q-binding site(s) in this complex, we used a labeled azido-Q derivative, 3-azido-2-methyl-5-methoxy[^{3}H]-6-decyl-1,4-benzoquinone ([^{3}H]azido-Q), to study the interaction between Q and complex I from *E. coli* through photoaffinity labeling (46). Contrary to the experiments carried out previously, NuoM subunit was identified as the Q-binding site. Because the binding of [^{3}H]azido-Q was not affected by addition of inhibitors, the inhibitor binding site(s) might not be identical to the Q binding site(s) although these binding site(s) for inhibitors were partially overlapped. The detailed conditions for photoaffinity labeling of this enzyme with [^{3}H]azido-Q and the isolation procedure for the Q-binding peptide will be presented in Chapter II of this thesis.

<u>Supernumerary Subunits in Complex I</u>--As described above, mitochondrial complex I has at least 32 more subunits than its bacterial counterpart. These “extra” subunits are called “accessory” or “supernumerary”. Although the function of supernumerary subunits is not fully understood, it has been speculated that these subunits form a scaffold around the 14 minimal subunits preventing the high energy electrons from escaping the complex to react with oxygen to generate reactive oxygen species (11).

Using the technique of gene manipulation, Videira *et al*. (47,48) constructed null mutants of several *Neurospora* (*N.*) *crassa* supernumerary subunits and their effects on complex I were investigated (see Table 2). In some cases, like mutants *nuo21.3b*, *nuo20.9*, *nuo20.8*, *nuo19.3* and *nuo12.3*, the membrane arm was disrupted although the peripheral arm of complex I could still be formed. In the other case, like mutant *nuo29.9*, the peripheral arm seems to be totally disrupted without interference with the formation of the membrane arm of the enzyme. In the case of the ACP mutant, the peripheral arm seems to be totally disrupted and the membrane arm of complex I cannot assemble properly. All of these data indicate that subunits 29.9/B13, 21.3b/B14.7, 20.9, 20.8/PGIV, 19.3/PEST, 12.3/PDSW, and ACP/SDAP have a role in the assembly and/or stability of complex I.

A possible role for the 39K supernumerary subunit in bovine complex I (40K in *N. crassa*) was also investigated. Complex I isolated from *N. crassa* contains tightly bound NADPH and further experiments with null mutants suggest that this tightly bound NADPH of complex I is present in the *N. crassa* 40K subunit (49). Furthermore, the finding of 39K subunit of bovine complex I (40K in *N. crassa*) can be labeled by [^{32}P]NADPH (50) supports that this subunit has NADPH-binding activity which may be involved in intramitochondrial fatty acid synthesis (4). These observations point to the presence of NADH/NADPH-binding sites other than the substrate NADH-binding site.

The MWFE subunit, a short protein composed of 70 amino acid residues, was imported into mitochondria and assembled into complex I without requiring proteolytic processing. Two of the mutations of this subunit in Chinese hamster cell, a conservative substitution (R50K) and a short C-terminal deletion, make complex I completely inactive (51). In fact, in the absence of MWFE, complex I was not even detectable by blue native gel electrophoresis. On the basis of these data it can be concluded that the MWFE subunit is essential for functional activity in mammalian complex I.

Table 2: Properties of supernumerary subunits as determined by null mutants of *N. crassa* complex I

N. crassa subunit	Bovine homologue	Subunit Location	Effect on complex I assembly
40	39K	peripheral	no
29.9	B13	peripheral	yes
21.3a		peripheral	no
21.3b	B14.7	membrane	yes
21	AQDQ	peripheral	no
20.9		membrane	yes
20.8	PGIV	membrane	yes
19.3	PEST	peripheral	Yes
12.3	PDSW	membrane	Yes
ACP	SDAP	peripheral	Yes
9.8	MWFE	membrane	Unknown

Cytochrome *bc*$_1$ Complex

The Function and Subunits of the Cytochrome *bc*$_1$ Complex--The cytochrome *bc*$_1$ complex is an essential segment of the electron transfer chains of mitochondria (see Figure 1) and many respiratory and photosynthetic bacteria. This complex catalyzes electron transfer (ET) from ubiquinol to cytochrome *c* with concomitant translocation of protons across the inner mitochondrial or bacterial plasma membrane to generate a proton gradient and membrane potential for ATP synthesis (52,53).

All the cytochrome *bc*$_1$ complexes share three core subunits carrying prosthetic groups. These are *b*-type cytochrome with one low potential heme (b_L or b_{566}) and one high potential heme (b_H or b_{562}), one *c*-type cytochrome with a covalently attached heme c_1, and the Rieske iron sulfur protein (ISP) containing a high potential Rieske [2Fe-2S] cluster (54-56). These three subunits form a monomer that dimerizes to yield an active cytochrome *bc*$_1$ with two active sites per monomer, referred to as Qo (QH_2 oxidation) and Qi (Q reduction) sites. The Qo site, where QH_2 is oxidized to Q, is near the positive side of the membrane (P-site, mitochondrial inter-membrane space side or periplasmic side in prokaryotes). The Qi site, where Q is reduced to QH_2, is close to the negative side of the membrane (N-site, mitochondrial matrix side or cytoplasmic side in prokaryotes). In addition to these three core subunits, the cytochrome *bc*$_1$ complex also contains varying number (one to eight) of non-redox containing subunits, known as supernumerary subunits (56). Although the function of these supernumerary subunits is not very clear, Chen *et al.* (57) reported that the complexes containing none or less supernumerary subunits were less stable and had lower activity than those with more supernumerary subunits. Therefore, it is possible that the increased enzymatic activity and stability for the mitochondrial complexes result from the interactions between core subunits and their neighboring supernumerary subunits. In addition, subunit I and II of yeast bc_1 complex have been reported to be essential for maintaining the proper conformation of cytochrome *b* to aid in the addition of heme (58,59); subunit VI is involved in manipulating dimer/monomer transition (60,61); subunits VII and VIII are essential for assembly of the complex (62); subunit IX interacts with the iron-sulfur protein, cytochrome *b* and cytochrome c_1 (63). Recently, subunit I and II of plant or bovine bc_1 complex have been found to possess the mitochondrial processing peptidase activity (64,65).

The Catalytic Mechanism of the Cytochrome bc_1 Complex: Protonmotive Q-cycle--The most favorable mechanism for electron transfer and proton translocation in the cytochrome bc_1 complex is the "protonmotive Q-cycle", first proposed by Peter Mitchell and later modified by several groups (53,66-69) (see Figure 3). According to the Q-cycle mechanism, the Qo site of the cytochrome bc_1 oxidizes one QH_2 from the membrane Q_{pool}, releases two protons, and transfers the two electrons into two different electron acceptor chains either in a concerted mechanism (53,70-72) or in a sequential mechanism (73-77). In the concerted mechanism, two electrons from QH_2 are transferred simultaneously in a bifurcated pathway: an electron is transferred to heme b_L as soon as the other electron is transferred to ISP. Therefore, no ubisemiquinone at the Qo site is generated (see Fig. 3A). In the sequential mechanism, the heme b_L is reduced by an intermediate ubisemiquinone generated at the Qo site after the first electron is transferred to ISP (see Fig. 3B).

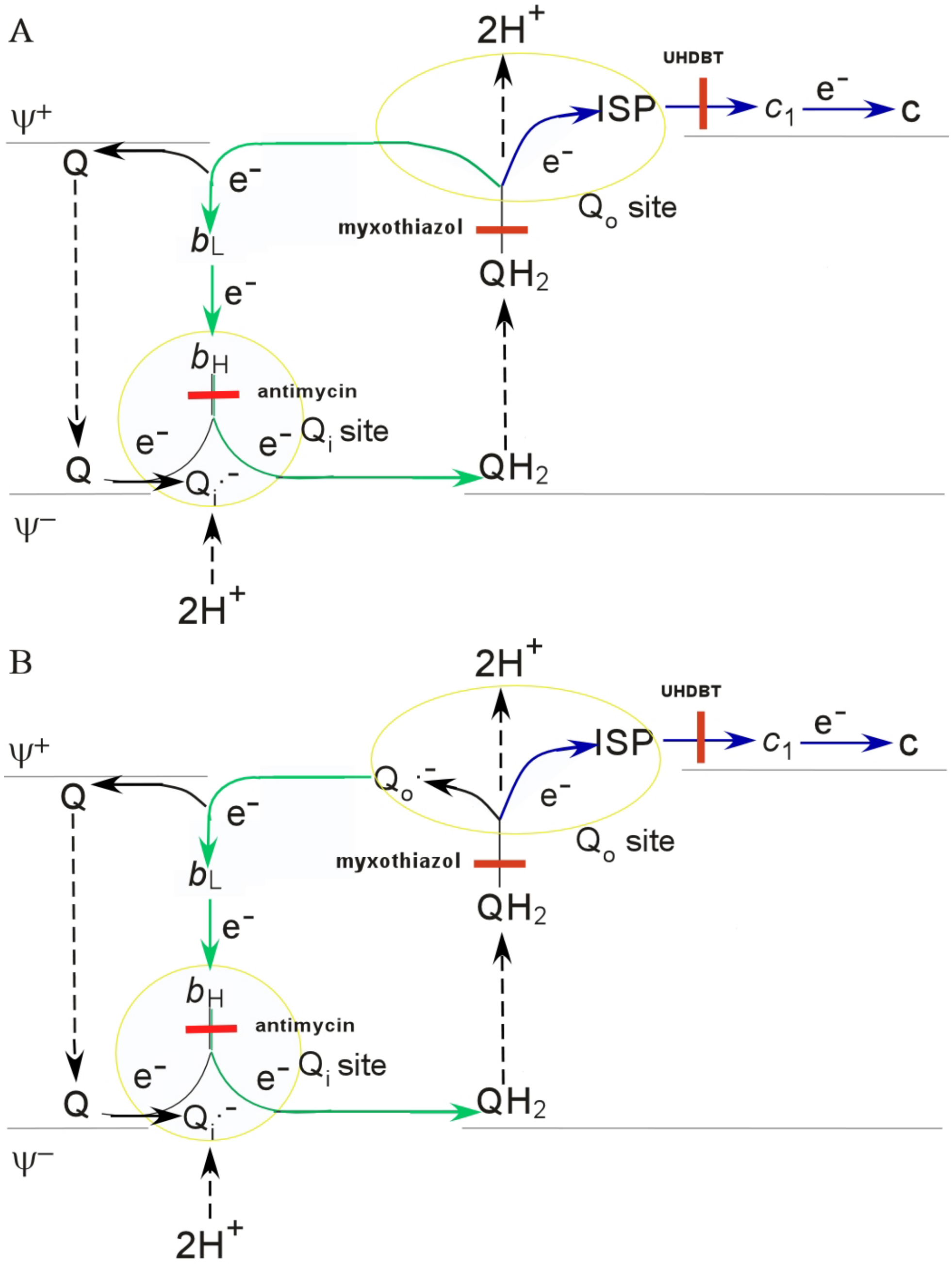

Figure 3. The protonmotive Q-cycle mechanism with (A) concerted and (B) sequential bifurcated reaction at Qo site in the dimeric cytochrome *bc*$_1$ complex. UHDBT, 5-undecyl-6-hydroxy-4,7-dioxobenzothiazole; ISP, Reske iron-sulfur protein; QH_2, ubiquinol; $Q^{\cdot-}$, ubisemiquinone; Q, ubiquinone. Blue and green lines indicate the electron transfer between redox centers. The red bars show the sites, at which inhibitors block electron transfer within the complex.

In both mechanisms, the electron, which has been transferred to ISP, is then transferred to cytochrome c_1 and then to cytochrome *c* (c_2 in bacteria). Ultimately, this electron reaches a terminal acceptor such as cytochrome *c* oxidase in mitochondria, or the oxidized photochemical reaction center in photosynthetic systems. The other electron from QH_2 is transferred via the heme b_L and heme b_H of the cytochrome *b* to the Qi site, where it reduces a Q to a detectable ubisemiquinone (SQ). At this point, the reaction is only half complete, with only one of the two electrons from QH_2 being transferred to cytochrome *c*. In the second half of the Q-cycle, all steps are repeated: one QH_2 is oxidized, one cytochrome *c* is reduced, two protons are deposited into the positive side of the membrane, and the heme b_H is reduced via the heme b_L. At the Qi site, the SQ, which is generated in the first half of the Q-cycle, accepts another electron from the heme b_H and uptakes two protons from the negative side of the membrane to form QH_2 to complete one Q-cycle. Overall, one complete Q-cycle generates one molecule of oxidized ubiquinone, two molecules of reduced cytochrome *c*, uptakes two protons from the negative side of the membrane, and deposits four protons to the positive side of the membrane, as summarized in Equation 1.

$$QH_2 + 2\text{ cytochrome } c^{3+} + 2H^+_N \Leftrightarrow Q + 2\text{ cytochrome } c^{2+} + 4H^+_P \qquad (1)$$

The discovery of two sets of inhibitors that bind specifically to Qo and Qi sites (78) is crucial for this Q-cycle mechanism. One set of inhibitors, so called class I inhibitors, blocks the oxidation of QH_2 and bind at or near the Qo site. Class I inhibitors are further divided into three sub-classes (Ia, Ib, and Ic) based on chemical characteristics of the inhibitors, and on spectroscopic and biophysical effects of the b_L heme and the iron-sulfur cluster of ISP upon binding of inhibitors. Class Ia inhibitors typically contain a βmethoxyacrylate (MOA) group and are referred to as the MOA inhibitors; they presumably block the electron transfer from quinol to ISP, accompanied by a red shift in the α and β-bands of the reduced heme b_L spectrum. Examples of the class Ia inhibitors are myxothiazol, azoxystrobin, famoxadone and methoxyacrylate stilbene (MOAS). Class Ib inhibitors possess a chromone ring and are believed to inhibit electron transfer from ISP to cyt c_1; they generate a pronounced increase in redox potential of ISP and, like class Ia inhibitors, also cause a red shift of the reduced heme b_L spectrum. Stigmatellin is a representative of class Ib inhibitors. Class Ic inhibitors are 2-hydroxy quinone analogues such as 5-undecyl-6-hydroxy-4,7-dioxobenzothiazole (UHDBT); they block the electron transfer in a similar way as the chromone inhibitors, but cause a smaller positive redox potential shift of ISP and have no effect on the spectrum of b_L heme. The other set of inhibitors, namely class II inhibitors, bind to the Qi site of the enzyme complex blocking the ubiquinone reduction. Antimycin and heptyldroxyquinoline-N-oxide (HQNO) belong to class II inhibitors (79,80). The chemical structures of these inhibitors are summarized in Figure 4.

Although Q-cycle hypothesis can explain many experimental observations very well, the question concerning why the branched electron transfer at the Qo site is under kinetic control instead of thermodynamic control is still waiting for an answer. There is no QH_2 found at the Qo site in the available structures and no ubisemiquinone detected at Qo site during the catalysis so far. Thus, the exact nature of QH_2 binding at the Qo site is unknown and becomes a central issue in understanding the electron transfer and proton translocation mechanism in the bc_1 complex.

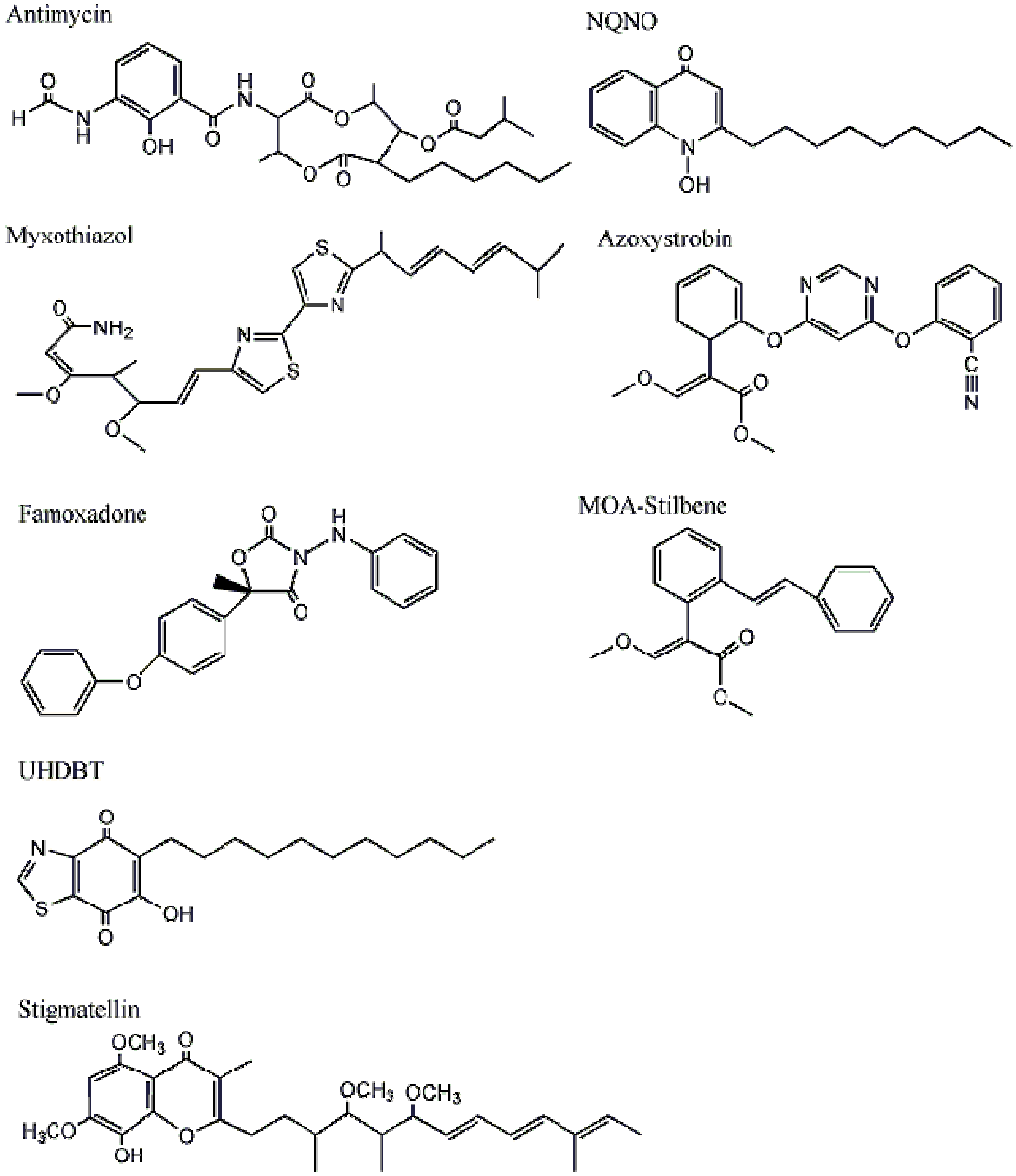

Figure 4. Chemical structures of some cytochrome *bc*$_1$ inhibitors. NQNO, heptylhydroxyquinoline-N-oxide; MOA, methyloxyacrylate; UHDBT, 5-undecyl-6-hydroxy-4,7-dioxobenzothiazole.

Three Dimensional Structure of the Cytochrome bc_1 Complex--The Q-cycle mechanism is supported by current X-ray structural information, which was obtained primarily from crystallographic studies of eukaryotic mitochondrial bc_1. The three dimensional (3D) structure of bovine heart mitochondrial cytochrome bc_1 complex was first determined by our group in collaboration with Dr. Deisenhofer's group at 2.9 Å resolution (81). Since then, crystallographic structures of bc_1 complexes from chicken (69) and yeast (82) have become available. The cytochrome b_6f is a complex analogous to the cytochrome bc_1 complex. Recently, its structure has also been established for the thermophilic cyanobacterium *Mastigocladus laminosus* (83) and the algae *Chlamydomonas reinhardtii* (83,84), at 3.0 Å and 3.1 Å respectively. In bovine $I4_122$ crystal structure, the bc_1 complex contains 4330 amino acid residues with a total molecular mass of 496 kDa. The complex exists as a pear-shaped, intertwined homodimeric, multi-subunit membrane protein with a maximal diameter of 130 Å and a height of 155 Å (see Figure 5). Each monomer contains three catalytic subunits and eight supernumerary subunits. The complex can be divided into three regions: matrix, trans-membrane helix, and inter-membrane space. More than one-half of the molecular mass is located in the matrix region, extending 75 Å from the transmembrane helices. This region contains subunits I, II, VI, part of subunit VII, the C-terminal portion of ISP, and subunit IX. The transmembrane (TM) region is about 42 Å thick, consisting of 13 transmembrane helices in each monomer, eight belonging to cytochrome *b*, and one each to cytochrome c_1, ISP, subunits VII, X and XI. The inter-membrane space region, which extends 38 Å into intermembrane space from the membrane surface, houses the functional domains of cytochrome c_1 and ISP, as well as subunit VIII (69).

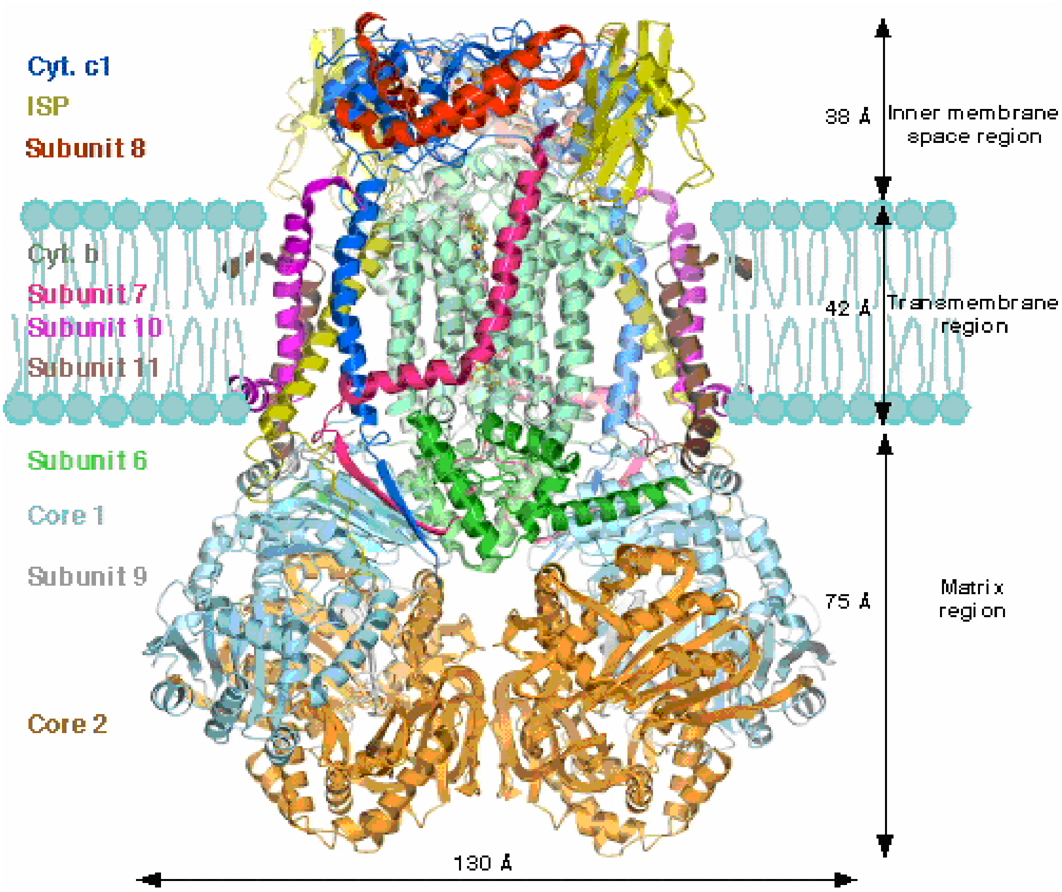

Figure 5. The 3-D structure of the mitochondrial cytochrome *bc*$_1$ complex from bovine heart (69). Colors identifying the subunits are given in the left margin. The top of the diagram is in the mitochondrial intermembrane space and the bottom in the mitochondrial matrix space.

The cytochrome *b* subunit has 379 amino acid residues and consists of eight membrane-spanning helices named sequentially from A to H with both the N and C terminus located in the mitochondrial matrix (79-81,85) (see Figure 6). The eight helices are arranged in two helical bundles, one consisting of helices A to E and the other of helices F to H. The first helical bundle incorporates the hemes b_L and b_H that are coordinated by conserved histidine residues (His-83 and His-182 for the heme b_L, His-97 and His-196 for the heme b_H). Prominent extra-membrane features include the AB, CD, DE, and EF loops. The DE loop with no secondary structure element is the only one located on the matrix side. The AB loop contains one helix, namely the ab, whereas the CD loop includes two helices, cd1 and cd2, in a hairpin-like arrangement, providing a "lid" for the Qo site and contributing residues to the docking site in the ISP crater for interaction with ISP (see Figure 6). The EF loop (residues 247-288) bridges between the two helical bundles as well as takes part in the formation of the ISP interaction site. Toward the end of the EF loop, there is a 12-residue helix, named ef, situated in a central position inside the Qo pocket. The PEWY motif (270-273 in bovine), conserved in all organisms, is found at the beginning of the ef helix. The two helical bundles contact each other at the matrix side of the membrane, but diverge towards the inter-membrane space side to form the Qo pocket between the b_L heme and the 2Fe-2S cluster of ISP (80). The Q_i pocket of the substrate and inhibitor bound structures were determined and defined by the structures of bovine mitochondrial bc_1 in the presence or absence of bound substrate ubiquinone and with the bound antimycin A (80). Residues from transmembrane helices A (Trp-31, Asn-32, Gly-34, Ser-35), D (Ala-193, Met-194, Leu-197, His-201), and E (Tyr-224, Lys-227, Asp-228); the amphipathic surface helix a (Phe-18); the A loop (Ile-

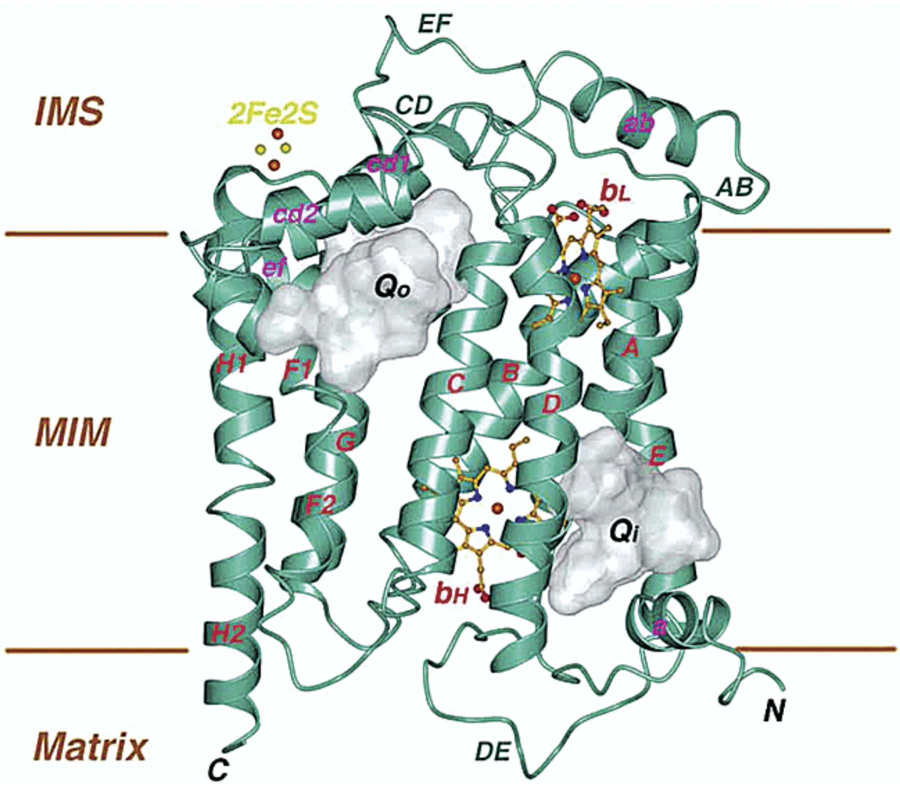

Figure 6. Ribbon presentation of the cytochrome *b* subunit in the bovine cytochrome $\boldsymbol{bc_1}$ (80). The subunit is oriented with the matrix side at the bottom of the figure and the intermembrane space (IMS) on the top. The mitochondrial inner membrane (MIM) is roughly delineated with the two parallel lines in brown. The eight TM helices are labeled A-H. Four prominent surface loops are labeled as AB, CD, DE, and EF. The helices within the surface loops are labeled as ab, cd1, cd2, and ef. Two active sites in the cyt *b* are labeled: one is the ubiquinone reduction site (Q_i) and the other is the ubiquinol oxidation site (Q_o). The two intercalating hemes, b_L and b_H, are rendered as the ball-and-stick models with carbon atoms in yellow, nitrogen in blue, oxygen in red, and iron in orange. The [2Fe-2S] cluster from subunit ISP is shown as balls with sulfur in yellow and iron in orange.

27); the DE loop (Ser-205, Phe-220); and some atoms from the high-potential heme b_H form the Qi pocket (80).

Cytochrome c_1 consists of an extramembrane domain in the intermembrane space along with a single transmembrane helix. Heme c_1 is ligated with residues Cys-37 and Cys-40. The carboxy group of one of the propionates of the heme c_1 forms a salt bridge with Arg-120, while the other propionate of the heme c_1 extends toward ISP. A methyl group on the porphyrin ring is solvent-exposed, likely near the binding site for cytochrome *c* (56). The exposed heme CD edge of cytochrome c_1 on the cytoplasmic surface of the membrane is surrounded by acidic residues that could form a docking site for cytochrome *c* (81). Tian *et al.*(86) found that the acidic residues (Glu-74, Glu-101, Asp-102, Glu-104, Asp-109, Glu-162, Glu-163, and Glu-168) on the surface of cytochrome c_1 of *Rhodobacter* (*R.*) *sphaeroides* cytochrome bc_1 complex were involved in binding positively charged cytochrome *c*. These acidic residues on opposite sides of the heme crevice of cytochrome c_1 direct the diffusion and binding of cytochrome *c* from the intramembrane space.

ISP contains a transmembrane helix and a hydrophilic domain in the intermembrane space and it can be divided into three domains: the membrane spanning N-terminal domain (tail domain, residues 1-62), the flexible linking domain (neck domain, residues 63-72), and the soluble C-terminal domain (head domain, residues 73-196) (87,88). ISPs extend across the interface between the two monomers, with the transmembrane helix in one monomer and the extramembrane domain within the other, thus resulting in an intertwining structure. In ISP, the [2Fe-2S] cluster positions at the tip of the head domain, bound by Cys-139, His-141, Cys-158, and His-161 (see Figure 7). A comparison of the reported crystal structures has shown that the position of [2Fe-2S] cluster changes in the presence of various Qo site inhibitors (69,79-81,89). These suggest that the mobility of the head domain of the ISP occurs during *bc*$_1$ catalysis.

By using site-directed mutagenesis in *R. sphaeroides bc*$_1$, Tian *et al*.(90) demonstrated that increasing the rigidity of the ISP neck region by generating a double-proline substitution at Ala-46 and Ala-48 (ALA-PLP) or a triple-proline substitution at residues 42-44 (ADV-PPP) decreases the activity and increases the activation energy. In addition, formation of a disulfide bond from a pair of cysteines substituted at Ala-42 and Val-44 (ADV-CDC) or at Pro-40 and Ala-42 (PSA-CSC), in the neck region of ISP, drastically reduces electron transfer activity (91). The activity can be restored by cleavage of the disulfide bond through the reduction with β-mercaptoethanol (β-ME). These results clearly demonstrated a need for neck flexibility for movement of the head domain of ISP during *bc*$_1$ catalysis. In 2000, Xiao *et al*. (92) further established the involvement of head domain movement of the ISP during *bc*$_1$ catalysis by generation and characterization of mutants with a pair of cysteines substituted (one cysteine each) at the interface between cytochrome *b* and the head domain of ISP in *R. sphaeroides bc*$_1$. The A185C(cyt*b*)/K70C(ISP) mutant *bc*$_1$ complex spontaneously forms a disulfide bond between ISP and cytochrome *b*. Formation of the disulfide bond is concurrent with the loss of the *bc*$_1$ activity and reduction of this disulfide bond by β-ME restored the activity.

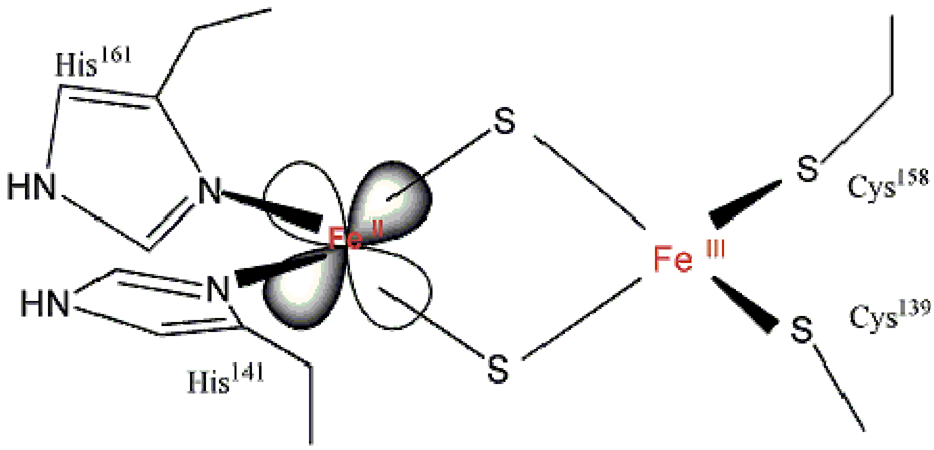

Figure 7. The ligands for the [2Fe-2S] cluster in ISP.

Cytochrome bc_1 Complex Functioning as a Dimer--The structural information suggests that the cytochrome bc_1 complex is functioning as a dimer (81) (see Figure 8). This suggestion stems from the following structural data:

(i) The presence of two non-communicating cavities in the dimeric complex, each connecting the Q_o pocket of one monomer to the Q_i pocket of the other monomer (see Fig. 8A). This makes it possible for a ubiquinone molecule reduced at the Q_i site of one monomer to be oxidized at the nearby Q_o site of the other monomer without leaving the bc_1 complex or diffusing into the membrane milieu.

(ii) The two ISP subunits span both monomers in an intertwined arrangement such that the head domain of ISP in one monomer is physically close to the cytochrome *b* and cytochrome c_1 in the 2-fold symmetry-related other monomer (see Fig. 8B).

To confirm that the cytochrome bc_1 complex exists as a dimer with intertwining ISPs not only in crystal but also in solution, two *R. sphaeroides* mutants expressing bc_1 complexes containing two pairs of cysteine substitutions, one at cytochrome *b* and the head domain of ISP and the other at cytochrome *b* and the tail domain of ISP, were generated and characterized by Xiao *et al*. (93). These mutants are: K70C(ISP)/A185C(cyt*b*)//P33C(ISP)/G89C(cyt*b*) and K70C(ISP)/A185C(cyt*b*)//N36C(ISP)/G89C(cyt*b*). An adduct protein with an apparent molecular mass of 128 kDa containing two cytochrome *b*s and ISPs was detected on SDS-PAGE as both mutant complexes were not treated by β-ME. This confirms that the bc_1 complex exists as a dimer with intertwining ISPs.

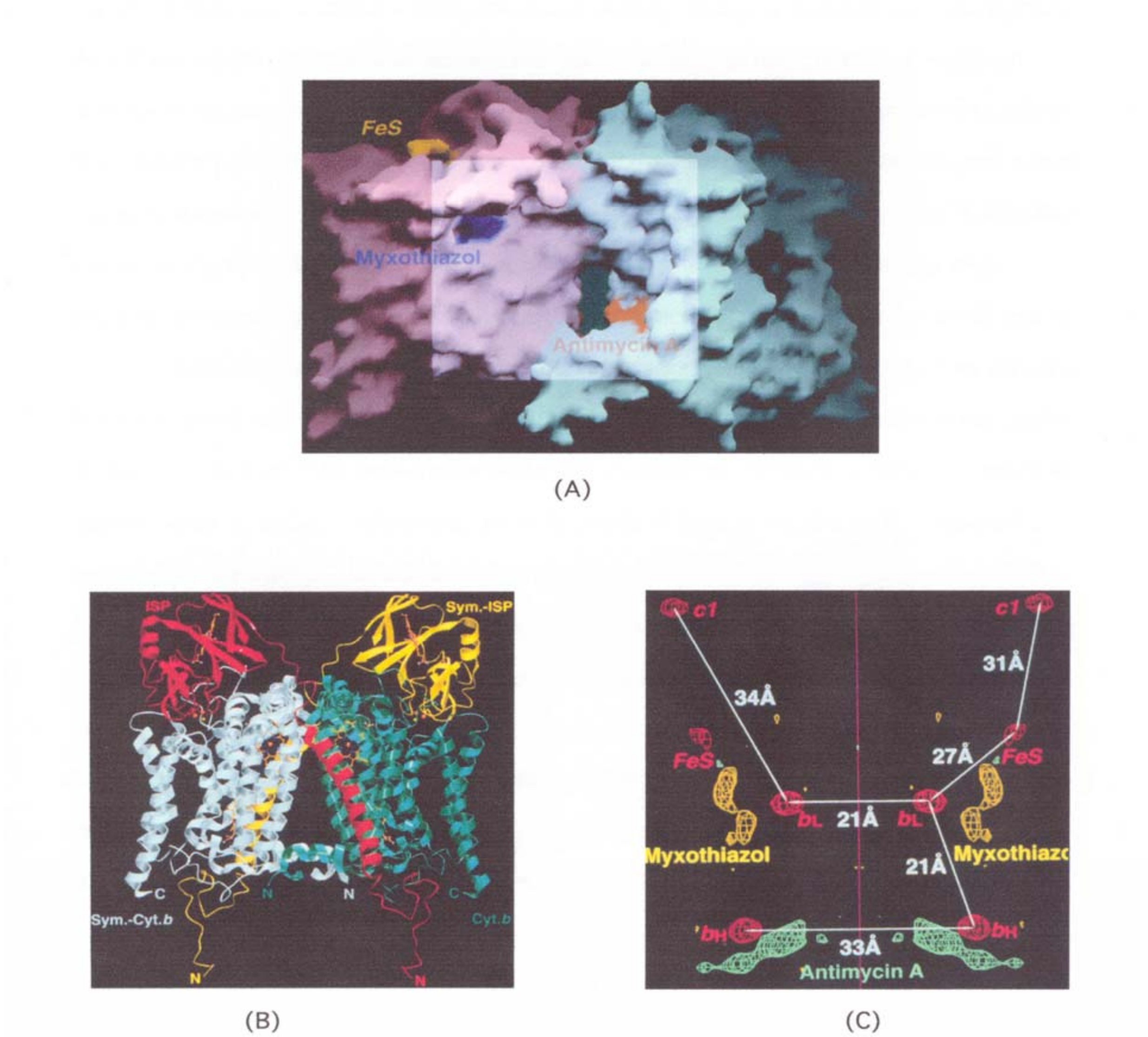

Figure 8. Structural data suggesting the cytochrome bc_1 complex functioning as a dimer. (A) The presence of two non-communicating cavities, each connecting the Qo pocket of one monomer to the Qi pocket of the other monomer. (B) The cross interaction between two cytochrome *b* subunits and two ISP subunits related by a molecular 2-fold symmetry. (C) Distance between iron centers of heme and [2Fe-2S] cluster.

(iii) The distance of 21 Å between the Fe atoms of the two hemes b_L is approximately the same as that between heme b_L and b_H within one monomer (see Fig. 8C). The short distance between the two hemes b_L and the presence of several aromatic amino acid residues at the interface of the two cytochrome *b* proteins has promoted investigators to speculate the existence of electron transfer or equilibrating between the two hemes b_L in the two symmetry-related monomers (72,81,94,95).

In 2002, Dr. Trumpower's group (96) demonstrated that stigmatellin and MOAS, two inhibitors that block ubiquinol oxidation at Qo site, inhibit the yeast bc_1 complex with a stoichiometry of 0.5 per one monomer. These data indicate that one molecule of inhibitor is sufficient to fully inhibit the dimeric enzyme and imply anti-cooperative interaction between the ubiquinol oxidation sites in the dimer.

To investigate the interaction between monomers of dimeric cytochrome bc_1 complex, Covian *et al*. (94) analyzed the pre-steady and steady state activities of the isolated yeast bc_1 complex in the presence of antimycin at pH 8.8 for wild type and pH 7.0 for ISP mutant Y185F. The redox potential of ISP in this mutant has value of 215 mV at pH 7.0, almost the same as that of the ISP in wild type at pH 8.8. At pH 8.8, the redox potential of wild type ISP is about 70 mV lower than that of cytochrome c_1. Under these conditions, the first turnover of ubiquinol oxidation can be observable in cytochrome c_1 reduction. The amount of cytochrome c_1 reduced by several equivalents of decyl-ubiquinol in the presence of antimycin is corresponded to only half of that present in the bc_1 complex. Similar experiments in the presence of several equivalents of cytochrome *c* also showed only half of the bc_1 complex participating in quinol oxidation. The extent of cytochrome *b* reduced corresponded to two b_H hemes undergoing reduction through one

Qo site per dimer, indicating electron transfer between the two cytochrome *b* subunits. The stimulation of steady state catalysis by low concentrations of antimycin requires both monomers to use only one Qi for Q reduction (94). These suggest that a second turnover through the only active Qo in the dimer reduced the b_H heme in the adjacent monomer by hemes b_L to b_L transfer.

Recently, it was reported that replacing one pair of the aromatic residues located between the two b_L hemes with alanine in *R. sphaeroides* cytochrome *b* decreased slightly the steady state activity and increased the production of superoxide radicals at Qo site several-fold (97). These indicate that this mutation interferes with electron transfer between the two hemes b_L in the dimeric bc_1 complex. The details will be presented in Chapter III of this thesis.

Most recently, Covian and Trumpower (95) analyzed the pre-steady state kinetics of reduction of cytochrome *b* by ubiquinol in the presence of variable concentrations of antimycin. The results demonstrated that electron equilibration between cytochrome *b* subunits through the b_L hemes of the dimeric bc_1 complex is the only model consistent with the experimental data, *i.e.*, electron equilibration must occur following the route QH_2 (monomer A)$\rightarrow$ b_H (monomer A)$\rightarrow$ b_L (monomer A) $\rightarrow$ b_L (monomer B) $\rightarrow$ b_H (monomer B) $\rightarrow$ Q (monomer B).

All of these results show that the dimeric structure of the bc_1 complex not only has a structural role in stabilizing this multisubunit enzyme but also is an essential part of its energy conserving mechanism. The possible function of the inter-monomer electron communication is to use the stabilization of SQ at the Qi site to maintain the b_H hemes in the oxidized state, ensuring a maximal rate of QH_2 oxidation at the Qo site (72,95).

Production of Superoxide Radicals by the Cytochrome *bc*$_1$ Complex--Respiration is linked to the generation of reactive oxygen species, which have been implicated in the aging process as well as in a variety of pathological conditions (98,99). Mitochondria are the major cellular source of reactive oxygen free radicals (100,101). The superoxide radical ($O_2^{\cdot-}$) is the first species in the univalent pathway of oxygen reduction. Two sites of the electron transfer chain were identified to be responsible for $O_2^{\cdot-}$ generation in mitochondria (102). One is located in complex I. At this site, $O_2^{\cdot-}$ is probably produced through autoxidation of the flavin semiquinone of NADH dehydrogenase (103). The other site is located in cytochrome *bc*$_1$ complex (103).

During electron transfer through cytochrome *bc*$_1$ complex, the second electron of QH_2 can shift from the low potential chain of the Q cycle electron transfer pathway and react with molecular oxygen to produce $O_2^{\cdot-}$. The electron leakage site is thought to be located at the ubisemiquinone of the Qo site or reduced cytochrome b_L (69,97,104-108). The amount of electron leakage is believed to be proportional to the concentration of reduced cytochrome b_L or ubisemiquinone at the Qo site (97).

Conveniently, the rate of $O_2^{\cdot-}$ production is measured by the superoxide dismutase (SOD)-sensitive reduction of cytochrome *c* (106-108). By this method, the rate of $O_2^{\cdot-}$ production by the cytochrome *bc*$_1$ complex can be determined by measuring the decrease in rate of cytochrome *c* reduction in the presence of superoxide dismutase under conditions of continuous turnover of the *bc*$_1$ complex (106-108). However, its relatively low sensitivity compromises the accuracy of this method.

An alternative method to measure $O_2^{\cdot-}$ formation is to follow the chemiluminescence of the methyl-6-(4-methoxyphenyl)-3,7-dihydroimidazol [1,2-

α]pyrazin-3-one hydrochloride (MCLA)- $O_2^{\cdot-}$ adduct (69,109). This MCLA chemiluminescence method is 95 times more sensitive than the cytochrome *c* reduction method (110). During continuing turnover of the bc_1 complex (in the presence of ubiquinol and cytochrome *c*), a high background rate of $O_2^{\cdot-}$ production resulting from the non-enzymatic oxidation of ubiquinol by cytochrome *c* makes it difficult to unambiguously compare rates of $O_2^{\cdot-}$ generation in complement and mutant complexes. To overcome this difficulty, the chemiluminescence of the MCLA-$O_2^{\cdot-}$ adduct during a single turnover of bc_1 complex is measured using the Applied Photophysics stopped-flow reaction analyzer SX.18 MV (97). By leaving the excitation light source off, the chemiluminescence of MCLA-$O_2^{\cdot-}$, generated when cytochrome bc_1 complex is mixed with ubiquinol and MCLA, is registered in light emission. Since the system contains no cytochrome *c*, chemiluminescence of MCLA-$O_2^{\cdot-}$, resulting from non-enzymatic oxidation of ubiquinol by cytochrome *c,* is eliminated. This method enables us to accurately evaluate changes in the rate of $O_2^{\cdot-}$ generation by various bc_1 complexes.

The Cytochrome bc_1 Complex from *R. sphaeroides*--*R. sphaeroides* has been used in our group as a model system to successfully study mitochondrial cytochrome bc_1 complex for a number of years (57,90-93,97,111,112). This organism can be grown aerobically, or anaerobically in the dark in the presence of electron acceptors (DMSO), or photosynthetically (113). The bc_1 complex has a dual role in *R. sphaeroides*. When the cells are grown photosynthetically, the bc_1 complex is present in the intracytoplasmic membrane (ICM) and is a critical component of the cyclic electron transport system (see Fig. 9A). When the cells are grown in the dark in the presence of oxygen, the same bc_1

complex is a necessary component of the cytochrome c_2-dependent respiratory chain (see Fig. 9B, left).

A very important feature and advantage of *R. sphaeroides* as a model for bc_1 complex study is that the bc_1 complex is not essential for its aerobic growth, since the electron from ubiquinol can be transferred to oxygen via a quinol oxidase as an alternative electron transfer pathway (see Fig. 9B, right). Therefore, *R. sphaeroides* mutants with severely defective bc_1 complexes are still able to survive and grow aerobically using the quinol oxidase. However, for preparation of bc_1 complex, the bacteria are grown under "semi-aerobic dark" conditions in order to have ICM where most of the photosynthetic machinery of *R. sphaeroides* is located (114-116). ICM can be analyzed by biophysical and biochemical methods to assess the basis of the defect.

Bacteria are much easier to handle experimentally than animals, plants and even unicellular eukaryote like yeast, especially for mutagenesis studies. Since *R. sphaeroides* bc_1 complex is believed similar in its structure and function as the much more complicated complex from mitochondria (53), the mutagenesis results from the bacteria can be applied to the mitochondrial complex. Efficient molecular engineering protocols for *R. sphaeroides* bc_1 complex are well established, and the genes of all its subunits have been cloned and sequenced (113,117).

Tian *et al.* (90) tagged the *R. sphaeroides* bc_1 complexes with six consecutive histidine residues on the c-terminus of the cytochrome c_1 subunits, which greatly facilitated the purification of the bc_1 complexes from cells using the nickel-nitrilotriacetic acid (Ni-NTA) agarose column. The purity, activity and cytochrome content of these

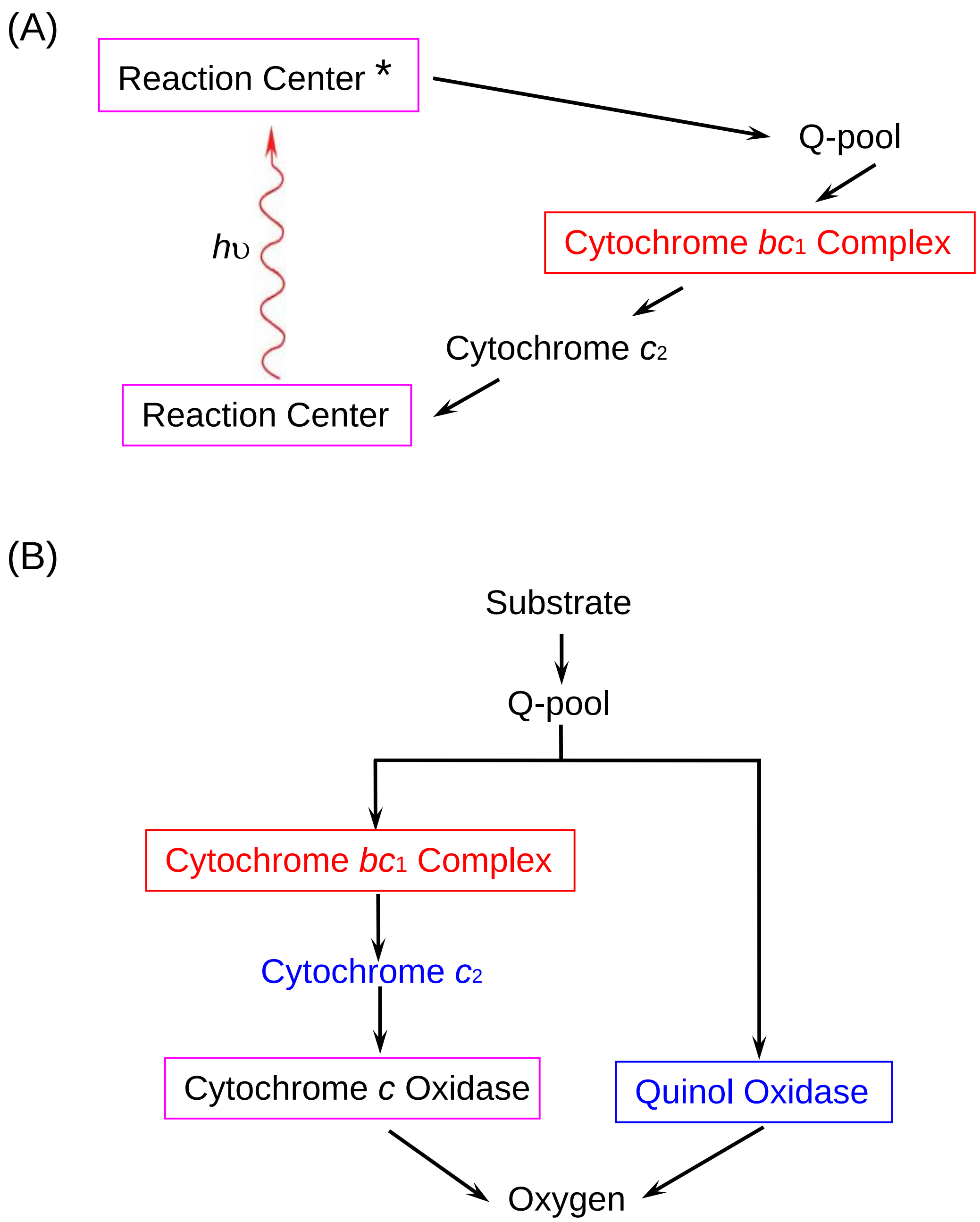

Figure 9. Electron-transport system of *R. sphaeroides* involved in anaerobic photosynthesis (A), cytochrome c_2-dependent aerobic respiration (B, left), and quinol oxidase-dependent aerobic respiration (B, right). Enzymes are indicated by boxes. Abbreviations: hν, light; Q-pool, ubiquinone pool; cytochrome *c* oxidase, aa_3- and cbb_3-type cytochrome *c* oxidase.

histidine-tagged bc_1 complexes are similar to those of the un-tagged ones. Such genetic system has been used extensively to study site-directed mutants and proven to be extremely valuable for our knowledge of the cytochrome bc_1 complexes (90-93,97,118-123).

Extra Fragments of Cytochrome bc_1 Complex from *R. sphaeroides*--The core subunits in bacterial complexes are generally bigger than their counter parts in the mitochondrial complexes. Sequence alignment of bacterial cytochrome *b*, cytochrome c_1, and ISP with their counterparts in the mitochondrial complexes reveals four extra fragments in bacterial cytochrome *b*, and one each in cytochrome c_1 and ISP (111). In the structure model of *R. sphaeroides* cytochrome bc_1 complex, these four extra fragments of cytochrome *b* are located at the N-terminus (residues 2-12, extra fragment 1), the connecting loop between helices D and E (residues 232 to 239, extra fragment 2), the connecting loop between *ef* and F (residues 309-326, extra fragment 3) and the C terminus (residues 421-445, extra fragment 4). The extra fragment of cytochrome c_1 (residues 141-161) is located at the long loop after helix α-3; and the extra fragment of ISP (residues 96-107) is located at the near middle portion of the ISP with an α-helical structure. The recently available, low resolution X-ray crystal structure of *R. capsulatus* bc_1 complex reveals that the positions of these extra fragments are at the same positions as those of *R. sphaeroides* (88). Unfortunately, the diffraction densities at these fragments are very poor and no detailed structural information can be revealed.

Are these extra fragments required for bc_1 complex? One effective way to answer this question is by site-directed mutagenesis of residues in these extra fragments followed by stability and functional assay of mutant complexes. By using this approach, the cytochrome c_1 extra fragment and the N-terminus extra fragment of cytochrome *b* from *R. sphaeroides* are found to be nonessential. The ISP extra fragment is required for structural stability of ISP in the complex (124), and the C-terminus extra fragment of cytochrome *b* (residues 421-445) is essential for maintaining structural integrity of the complex (125). However, the knowledge of the role of the second and third extra fragments of cytochrome *b* in *R. sphaeroides* bc_1 complex is still lacking.

As a continuous work, the role of the third extra fragment (residues 309 to 326) of *R. sphaeroides* cytochrome *b*, is studied in Chapter IV of this thesis (see Figure 10). This extra fragment is located between the *ef* amphipathic helix and the transmembrane helix F, and is in close proximity to the Qo site.

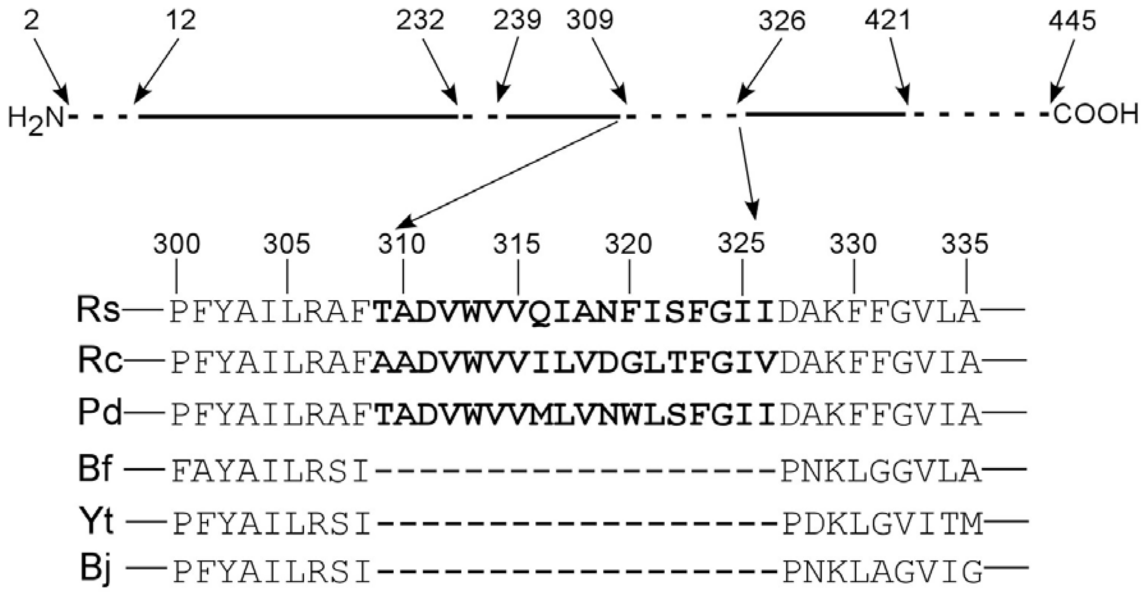

Figure10. Partial sequence comparison in an extra fragment (resides 309-326) of various cytochrome *b*s. Sequence alignment of cytochrome *b* in bacterial complexes with their counterparts in mitochondrial complexes reveals four extra fragments in bacterial cytochrome *b*. They are indicated in red lines at the top of the figure. The abbreviations used are: RS, *Rhodobacter sphaeroides*; RC, *Rhodobacter capsulatus*; Pd, *Paracoccus denitrificans*; Bf, beef; Yt, yeast; Bj, *Bradyrhizobium japonicum*.

References

1. Hatefi, Y. (1985) *Annu. Rev. Biochem.* **54**, 1015-1069
2. Zhang, L., Li, Z., Quinn, B., Yu, L., and Yu, C. A. (2002) *Biochim. Biophys. Acta* **1556**, 226-232
3. Mitchell, P. (1961) *Nature* **191**, 144-148
4. Yagi, T., and Matsuno-Yagi, A. (2003) *Biochemistry* **42**, 2266-2274
5. Arizmendi, J. M., Runswick, M. J., Skehel, J. M., and Walker, J. E. (1992) *FEBS Lett.* **301**, 237-242
6. Yagi, T., Yano, T., Di Bernardo, S., and Matsuno-Yagi, A. (1998) *Biochim. Biophys. Acta* **1364**, 125-133
7. Carroll, J., Shannon, R. J., Fearnley, I. M., Walker, J. E., and Hirst, J. (2002) *J. Biol. Chem.* **277**, 50311-50317
8. Chomyn, A., Cleeter, M. W., Ragan, C. I., Riley, M., Doolittle, R. F., and Attardi, G. (1986) *Science* **234**, 614-618
9. Anderson, S., de Bruijn, M. H., Coulson, A. R., Eperon, I. C., Sanger, F., and Young, I. G. (1982) *J. Mol. Biol.* **156**, 683-717
10. Walker, J. E. (1992) *Q Rev Biophys* **25**, 253-324
11. Guenebaut, V., Schlitt, A., Weiss, H., Leonard, K., and Friedrich, T. (1998) *J. Mol. Biol.* **276**, 105-112
12. Carroll, J., Fearnley, I. M., Shannon, R. J., Hirst, J., and Walker, J. E. (2003) *Mol. Cell Proteomics* **2**, 117-126
13. Leonard, K., Haiker, H., and Weiss, H. (1987) *J. Mol. Biol.* **194**, 277-286
14. Hofhaus, G., Weiss, H., and Leonard, K. (1991) *J. Mol. Biol.* **221**, 1027-1043
15. Djafarzadeh, R., Kerscher, S., Zwicker, K., Radermacher, M., Lindahl, M., Schagger, H., and Brandt, U. (2000) *Biochim. Biophys. Acta* **1459**, 230-238
16. Grigorieff, N. (1998) *J. Mol. Biol.* **277**, 1033-1046
17. Guenebaut, V., Vincentelli, R., Mills, D., Weiss, H., and Leonard, K. R. (1997) *J. Mol. Biol.* **265**, 409-418
18. Peng, G., Fritzsch, G., Zickermann, V., Schagger, H., Mentele, R., Lottspeich, F., Bostina, M., Radermacher, M., Huber, R., Stetter, K. O., and Michel, H. (2003) *Biochemistry* **42**, 3032-3039

19. Bottcher, B., Scheide, D., Hesterberg, M., Nagel-Steger, L., and Friedrich, T. (2002) *J. Biol. Chem.* **277**, 17970-17977
20. Sazanov, L. A., Peak-Chew, S. Y., Fearnley, I. M., and Walker, J. E. (2000) *Biochemistry* **39**, 7229-7235
21. Uhlmann, M., and Friedrich, T. (2005) *Biochemistry* **44**, 1653-1658
22. Galante, Y. M., and Hatefi, Y. (1979) *Arch. Biochem. Biophys.* **192**, 559-568
23. Leif, H., Sled, V. D., Ohnishi, T., Weiss, H., and Friedrich, T. (1995) *Eur. J. Biochem.* **230**, 538-548
24. Chen, S., and Guillory, R. J. (1981) *J. Biol. Chem.* **256**, 8318-8323
25. Rasmussen, T., Scheide, D., Brors, B., Kintscher, L., Weiss, H., and Friedrich, T. (2001) *Biochemistry* **40**, 6124-6131
26. Sazanov, L. A., and Walker, J. E. (2000) *J. Mol. Biol.* **302**, 455-464
27. Holt, P. J., Morgan, D. J., and Sazanov, L. A. (2003) *J. Biol. Chem.* **278**, 43114-43120
28. Gong, X., Xie, T., Yu, L., Hesterberg, M., Scheide, D., Friedrich, T., and Yu, C. A. (2003) *J. Biol. Chem.* **278**, 25731-25737
29. Magnitsky, S., Toulokhonova, L., Yano, T., Sled, V. D., Hagerhall, C., Grivennikova, V. G., Burbaev, D. S., Vinogradov, A. D., and Ohnishi, T. (2002) *J. Bioenerg. Biomembr.* **34**, 193-208
30. Ohnishi, T., Johnson, J. E., Jr., Yano, T., Lobrutto, R., and Widger, W. R. (2005) *FEBS Lett.* **579**, 500-506
31. Brandt, U. (1997) *Biochim. Biophys. Acta* **1318**, 79-91
32. Earley, F. G., and Ragan, C. I. (1984) *Biochem. J.* **224**, 525-534
33. Earley, F. G., Patel, S. D., Ragan, I., and Attardi, G. (1987) *FEBS Lett.* **219**, 108-112
34. Schuler, F., Yano, T., Di Bernardo, S., Yagi, T., Yankovskaya, V., Singer, T. P., and Casida, J. E. (1999) *Proc. Natl. Acad. Sci. U S A* **96**, 4149-4153
35. Ohnishi, T. (1998) *Biochim. Biophys. Acta* **1364**, 186-206
36. Miyoshi, H. (1998) *Biochim. Biophys. Acta* **1364**, 236-244
37. Schuler, F., and Casida, J. E. (2001) *Biochim. Biophys. Acta* **1506**, 79-87

38. Nakamaru-Ogiso, E., Sakamoto, K., Matsuno-Yagi, A., Miyoshi, H., and Yagi, T. (2003) *Biochemistry* **42**, 746-754
39. Fisher, N., and Rich, P. R. (2000) *J. Mol. Biol.* **296**, 1153-1162
40. Degli Esposti, M., Carelli, V., Ghelli, A., Ratta, M., Crimi, M., Sangiorgi, S., Montagna, P., Lenaz, G., Lugaresi, E., and Cortelli, P. (1994) *FEBS Lett.* **352**, 375-379
41. Majander, A., Finel, M., Savontaus, M. L., Nikoskelainen, E., and Wikstrom, M. (1996) *Eur. J. Biochem.* **239**, 201-207
42. Lunardi, J., Darrouzet, E., Dupuis, A., and Issartel, J. P. (1998) *Biochim. Biophys. Acta* **1407**, 114-124
43. Hofhaus, G., and Attardi, G. (1993) *EMBO J.* **12**, 3043-3048
44. Hofhaus, G., and Attardi, G. (1995) *Mol. Cell. Biol.* **15**, 964-974
45. Darrouzet, E., Issartel, J. P., Lunardi, J., and Dupuis, A. (1998) *FEBS Lett.* **431**, 34-38
46. Ohshima, M., Miyoshi, H., Sakamoto, K., Takegami, K., Iwata, J., Kuwabara, K., Iwamura, H., and Yagi, T. (1998) *Biochemistry* **37**, 6436-6445
47. Videira, A. (1998) *Biochim. Biophys. Acta* **1364**, 89-100
48. Videir, A., and Duarte, M. (2001) *J. Bioenerg. Biomembr.* **33**, 197-203
49. Schulte, U., Haupt, V., Abelmann, A., Fecke, W., Brors, B., Rasmussen, T., Friedrich, T., and Weiss, H. (1999) *J. Mol. Biol.* **292**, 569-580
50. Yamaguchi, M., Belogrudov, G. I., Matsuno-Yagi, A., and Hatefi, Y. (2000) *Eur. J. Biochem.* **267**, 329-336
51. Yadava, N., Potluri, P., Smith, E. N., Bisevac, A., and Scheffler, I. E. (2002) *J. Biol. Chem.* **277**, 21221-21230
52. Hatefi, Y., Haavik, A. G., and Griffiths, D. E. (1962) *J. Biol. Chem.* **237**, 1681-1685
53. Snyder, C., and Trumpower, B. L. (1998) *Biochim. Biophys. Acta* **1365**, 125-134
54. Yu, C. A., and Yu, L. (1993) *J. Bioenerg. Biomembr.* **25**, 259-273
55. Yu, C. A., Xia, J. Z., Kachurin, A. M., Yu, L., Xia, D., Kim, H., and Deisenhofer, J. (1996) *Biochim. Biophys. Acta* **1275**, 47-53

56. Yu, C. A., Tian, H., Zhang, L., Deng, K. P., Shenoy, S. K., Yu, L., Xia, D., Kim, H., and Deisenhofer, J. (1999) *J. Bioenerg. Biomembr.* **31**, 191-199
57. Chen, Y. R., Yu, C. A., and Yu, L. (1996) *J. Biol. Chem.* **271**, 2057-2062
58. Tzagoloff, A., Wu, M. A., and Crivellone, M. (1986) *J. Biol. Chem.* **261**, 17163-17169
59. Oudshoorn, P., Van Steeg, H., Swinkels, B. W., Schoppink, P., and Grivell, L. A. (1987) *Eur. J. Biochem.* **163**, 97-103
60. Schoppink, P. J., Hemrika, W., and Berden, J. A. (1989) *Biochim. Biophys. Acta* **974**, 192-201
61. Schmitt, M. E., and Trumpower, B. L. (1990) *J. Biol. Chem.* **265**, 17005-17011
62. Maarse, A. C., De Haan, M., Schoppink, P. J., Berden, J. A., and Grivell, L. A. (1988) *Eur. J. Biochem.* **172**, 179-184
63. Phillips, J. D., Schmitt, M. E., Brown, T. A., Beckmann, J. D., and Trumpower, B. L. (1990) *J. Biol. Chem.* **265**, 20813-20821
64. Dudkina, N. V., Eubel, H., Keegstra, W., Boekema, E. J., and Braun, H. P. (2005) *Proc. Natl. Acad. Sci. U S A* **102**, 3225-3229
65. Deng, K., Zhang, L., Kachurin, A. M., Yu, L., Xia, D., Kim, H., Deisenhofer, J., and Yu, C. A. (1998) *J. Biol. Chem.* **273**, 20752-20757
66. Mitchell, P. (1976) *J. Theor. Biol.* **62**, 327-367
67. Crofts, A. R., and Meinhardt, S. W. (1982) *Biochem. Soc. Trans.* **10**, 201-203
68. Brandt, U. (1996) *Biochim. Biophys. Acta* **1275**, 41-46
69. Zhang, Z., Huang, L., Shulmeister, V. M., Chi, Y. I., Kim, K. K., Hung, L. W., Crofts, A. R., Berry, E. A., and Kim, S. H. (1998) *Nature* **392**, 677-684
70. Link, T. A. (1997) *FEBS Lett.* **412**, 257-264
71. Junemann, S., Heathcote, P., and Rich, P. R. (1998) *J. Biol. Chem.* **273**, 21603-21607
72. Osyczka, A., Moser, C. C., Daldal, F., and Dutton, P. L. (2004) *Nature* **427**, 607-612
73. De Vries, S., Albracht, S. P., Berden, J. A., and Slater, E. C. (1982) *Biochim. Biophys. Acta* **681**, 41-53
74. Orii, Y., and Miki, T. (1997) *J. Biol. Chem.* **272**, 17594-17604

75. Brandt, U. (1998) *Biochim. Biophys. Acta* **1365**, 261-268

76. Crofts, A. R. (2004) *Biochim. Biophys. Acta.* **1665**, 77-92

77. Crofts, A. R., Guergova-Kuras, M., Kuras, R., Ugulava, N., Li, J., and Hong, S. (2000) *Biochim. Biophys. Acta* **1459**, 456-466

78. von Jagow, G., and Link, T. (1988) *Methods in Enzymology* **126**, 253-271

79. Gao, X., Wen, X., Yu, C., Esser, L., Tsao, S., Quinn, B., Zhang, L., Yu, L., and Xia, D. (2002) *Biochemistry* **41**, 11692-11702

80. Gao, X., Wen, X., Esser, L., Quinn, B., Yu, L., Yu, C. A., and Xia, D. (2003) *Biochemistry* **42**, 9067-9080

81. Xia, D., Yu, C. A., Kim, H., Xia, J. Z., Kachurin, A. M., Zhang, L., Yu, L., and Deisenhofer, J. (1997) *Science* **277**, 60-66

82. Hunte, C., Koepke, J., Lange, C., Rossmanith, T., and Michel, H. (2000) *Structure Fold Des.* **8**, 669-684

83. Kurisu, G., Zhang, H., Smith, J. L., and Cramer, W. A. (2003) *Science* **302**, 1009-1014

84. Stroebel, D., Choquet, Y., Popot, J. L., and Picot, D. (2003) *Nature* **426**, 413-418

85. Esser, L., Quinn, B., Li, Y. F., Zhang, M., Elberry, M., Yu, L., Yu, C. A., and Xia, D. (2004) *J. Mol. Biol.* **341**, 281-302

86. Tian, H., Sadoski, R., Zhang, L., Yu, C. A., Yu, L., Durham, B., and Millett, F. (2000) *J. Biol. Chem.* **275**, 9587-9595

87. Iwata, S., Saynovits, M., Link, T. A., and Michel, H. (1996) *Structure* **4**, 567-579

88. Link, T. A., Saynovits, M., Assmann, C., Iwata, S., Ohnishi, T., and von Jagow, G. (1996) *Eur. J. Biochem.* **237**, 71-75

89. Iwata, S., Lee, J. W., Okada, K., Lee, J. K., Iwata, M., Rasmussen, B., Link, T. A., Ramaswamy, S., and Jap, B. K. (1998) *Science* **281**, 64-71

90. Tian, H., Yu, L., Mather, M. W., and Yu, C. A. (1998) *J. Biol. Chem.* **273**, 27953-27959

91. Tian, H., White, S., Yu, L., and Yu, C. A. (1999) *J. Biol. Chem.* **274**, 7146-7152

92. Xiao, K., Yu, L., and Yu, C. A. (2000) *J. Biol. Chem.* **275**, 38597-38604

93. Xiao, K., Chandrasekaran, A., Yu, L., and Yu, C. A. (2001) *J. Biol. Chem.* **276**, 46125-46131

94. Covian, R., Gutierrez-Cirlos, E. B., and Trumpower, B. L. (2004) *J. Biol. Chem.* **279**, 15040-15049
95. Covian, R., and Trumpower, B. L. (2005) *J. Biol. Chem.* **280**, 22732-22740
96. Gutierrez-Cirlos, E. B., and Trumpower, B. L. (2002) *J. Biol. Chem.* **277**, 1195-1202
97. Gong, X., Yu, L., Xia, D., and Yu, C. A. (2005) *J. Biol. Chem.* **280**, 9251-9257
98. Fridovich, I. (1978) *Science* **201**, 875-880
99. Stadtman, E. R. (1992) *Science* **257**, 1220-1224
100. Raha, S., and Robinson, B. H. (2000) *Trends Biochem. Sci.* **25**, 502-508
101. Turrens, J. F. (2003) *J. Physiol.* **552**, 335-344
102. Cadenas, E., Boveris, A., Ragan, C. I., and Stoppani, A. O. (1977) *Arch. Biochem. Biophys.* **180**, 248-257
103. Turrens, J. F., and Boveris, A. (1980) *Biochem. J.* **191**, 421-427
104. Turrens, J. F., Alexandre, A., and Lehninger, A. L. (1985) *Arch. Biochem. Biophys.* **237**, 408-414
105. Nohl, H., and Jordan, W. (1986) *Biochem. Biophys. Res. Commun.* **138**, 533-539
106. Muller, F., Crofts, A. R., and Kramer, D. M. (2002) *Biochemistry* **41**, 7866-7874
107. Muller, F. L., Roberts, A. G., Bowman, M. K., and Kramer, D. M. (2003) *Biochemistry* **42**, 6493-6499
108. Sun, J., and Trumpower, B. L. (2003) *Arch. Biochem. Biophys.* **419**, 198-206
109. Kishimoto, W., Nakao, A., Nakano, M., Takahashi, A., Inaba, H., and Takagi, H. (1995) *Pancreas* **11**, 122-126
110. Nakano, M. (1990) *Methods Enzymol.* **186**, 227-232
111. Yu, L., Tso, S. C., Shenoy, S. K., Quinn, B. N., and Xia, D. (1999) *J. Bioenerg. Biomembr.* **31**, 251-257
112. Guner, S., Robertson, D. E., Yu, L., Qiu, Z. H., Yu, C. A., and Knaff, D. B. (1991) *Biochim. Biophys. Acta* **1058**, 269-279
113. Yun, C. H., Beci, R., Crofts, A. R., Kaplan, S., and Gennis, R. B. (1990) *Eur. J. Biochem.* **194**, 399-411
114. Knaff, D. B. (1990) *Trends Biochem. Sci.* **15**, 289-291

115. Gennis, R. B., Barquera, B., Hacker, B., Van Doren, S. R., Arnaud, S., Crofts, A. R., Davidson, E., Gray, K. A., and Daldal, F. (1993) *J. Bioenerg. Biomembr.* **25**, 195-209
116. Thony-Meyer, L. (1997) *Microbiol. Mol. Biol. Rev.* **61**, 337-376
117. Usui, S., and Yu, L. (1991) *J. Biol. Chem.* **266**, 15644-15649
118. Engstrom, G., Xiao, K., Yu, C. A., Yu, L., Durham, B., and Millett, F. (2002) *J. Biol. Chem.* **277**, 31072-31078
119. Xiao, K., Engstrom, G., Rajagukguk, S., Yu, C. A., Yu, L., Durham, B., and Millett, F. (2003) *J. Biol. Chem.* **278**, 11419-11426
120. Engstrom, G., Rajagukguk, R., Saunders, A. J., Patel, C. N., Rajagukguk, S., Merbitz-Zahradnik, T., Xiao, K., Pielak, G. J., Trumpower, B., Yu, C. A., Yu, L., Durham, B., and Millett, F. (2003) *Biochemistry* **42**, 2816-2824
121. Xiao, K., Liu, X., Yu, C. A., and Yu, L. (2004) *Biochemistry* **43**, 1488-1495
122. Muller, F. L., Liu, Y., and Van Remmen, H. (2004) *J. Biol. Chem.* **279**, 49064-49073
123. Gurung, B., Yu, L., Xia, D., and Yu, C. A. (2005) *J. Biol. Chem.* **280**, 24895-24902
124. Berry, E. A., Huang L. S., Saechao, L. K., Pon,N. G., Valkova-Valchanova, M., and Daldal, F. (2004) *Photosynthesis Res.* **81**, 251-275

CHAPTER II

THE UBIQUINONE-BINDING SITE IN NADH:UBIQUINONE OXIDOREDUCTASE FROM *ESCHERICHIA COLI*

Abstract

An azido-ubiquinone derivative, 3-azido-2-methyl-5-methoxy[^{3}H]-6-decyl-1,4-benzoquinone ([^{3}H]azido-Q) was used to study the ubiquinone-protein interaction and to identify the ubiquinone-binding site in *E. coli* NADH:ubiquinone oxidoreductase (complex I). The purified complex I showed no loss of activity after incubation with a 20-fold molar excess of [^{3}H]azido-Q in the dark. Illumination of the incubated sample with long wavelength UV light for 10 min at 0 °C caused a 40 % decrease of NADH:ubiquinone oxidoreductase activity. Sodium dodecyl sulfate-polyacrylamide gel electrophoresis of the complex labeled with [^{3}H]azido-Q followed by analysis of the radioactivity distribution among the subunits revealed that subunit NuoM was heavily labeled, suggesting that this protein houses the Q-binding site. When the [^{3}H]-azido-Q-labeled NuoM was purified from the labeled reductase by means of preparative SDS-PAGE, an azido-Q-linked peptide, with a retention time of 41.4 min, was obtained by high performance liquid chromatography of the protease K digest of the labeled subunit. This peptide had a partial N-terminal amino acid sequence of NH_2-VMLIAILALV-, which

corresponds to amino acid residues 184-193 of NuoM. The secondary structure prediction of NuoM using the Toppred hydropathy analysis showed that the Q-binding peptide overlaps with a proposed Q-binding motif located in the middle of the transmembrane helice 5 toward the cytoplasmic side of the membrane. Using the PHDhtm hydropathy plot, the labeled peptide is located in the transmembrane helix 4 toward the periplasmic side of the membrane.

Introduction

The *E. coli* NADH-Q oxidoreductase catalyzes electron transfer from NADH to ubiquinone and concomitantly translocates protons across the membrane to generate a membrane potential and proton gradient for ATP synthesis (1, 2). Whereas the mitochondrial enzyme contains up to 46 different subunits (3), this bacterial enzyme is made up of only 13 subunits encoded by the *nuo*-genes (4), and thus is used as a model for structural and functional studies of mitochondrial complex I.

The mechanism of electron transfer and its coupling to proton translocation in complex I is poorly understood. Ubiquinone is the final electron acceptor in NADH-Q oxidoreductase, and may take part in electron recycling and/or proton transport processes. Knowledge of ubiquinone binding is essential for mechanistic studies of this complex. To unambigously identify the Q-binding site(s) in complex I, we use a photoactivatable azido-Q derivative, 3-azido-2-methyl-5-methoxy[^{3}H]-6-decyl-1,4-benzoquinone, which has partial electron acceptor activity for complex I, to study the Q/protein interaction in *E. coli* complex I. Herein, we report conditions for photoaffinity labeling of complex I with azido-Q derivatives and a detailed isolation procedure for the Q-binding peptide.

Experimental Procedures

Materials--Sodium cholate was obtained from Sigma and re-crystallized from methanol. Dodecyl maltoside (DM) was from Anatrace. Insta-Gel liquid scintillation mixture was from ICN. Other chemicals were of the highest purity commercially available. The ubiquinone derivatives, 2, 3-dimethoxy-5-methyl-6-isoprenoyl-1, 4-benzoquinone (Q_1), 2, 3-dimethoxy-5-methyl-6-(10-bromodecyl)-1, 4-benzoquinone ($Q_0C_{10}Br$), 3-azido-2-methyl-5-methoxy- and 3-azido-2-methyl-5-methoxy[^{3}H]-6-decyl-1,4-benzoquinone (azido-Q and [^{3}H]azido-Q), 5-azido-2, 3-dimethoxy[^{3}H]-6-decyl-1, 4-benzoquinone (5-azido-Q) were synthesized by methods reported previously (5), and their chemical structures are shown in Figure 11.

Enzyme Preparations and Assays--*E. coli* complex I was prepared and assayed essentially as previously reported (6). Complex I, azido-Q treated or untreated, was mixed with asolectin at a ratio of 1:20 (by weight), incubated at 4 °C for 15 min before assaying for activity. The reaction mixture (1ml) contained 50 mM Tris-Cl buffer, pH 7.5, 5 mM NaN_3, 0.15 % dodecyl-maltoside, 100 μM NADH, and 60 μM Q_1. The reaction was started by addition of an appropriate amount of azido-Q treated- or untreated- complex I. The oxidation of NADH was followed by measuring the absorption decrease at 340 nm, using a millimolar extinction coefficient of $\varepsilon_{340\ nm} = 6.22\ mM^{-1}\ cm^{-1}$.

Identification of Endogenous Quinone in *E. coli* Complex I--Quinones were extracted from purified *E. coli* complex I with hexane as previously reported (7). The concentration of quinone was determined by the method of Redfearn (7). A millimolar extinction coefficient of 12.25 $mM^{-1}cm^{-1}$ was used as the difference in absorption of the oxidized and reduced forms of Q at 275 nm. Quinone identity was determined by

Qn

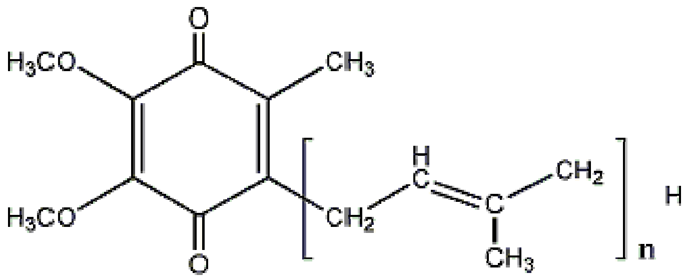

$Q_0C_{10}Br$

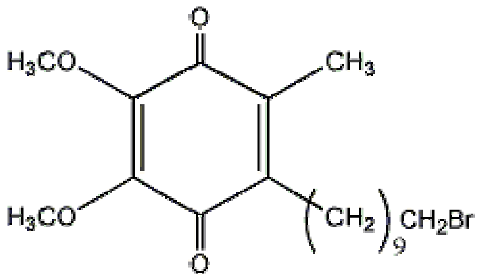

[^{3}H] azido-Q

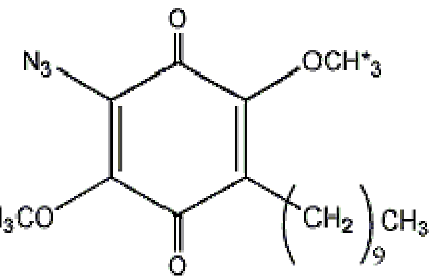

Figure 11. Chemical structures of the ubiquinone derivatives used in this study.

matching the retention time of quinone obtained from complex I with those of reference quinones, Q_2, Q_6, Q_8, and $Q_{10,}$ in a HPLC system using a Nova-Pak® reverse phase column (C18, 3.9 × 150 mm) from Waters, eluting with a linear gradient of methanol, from 90 to 100 % (v/v) in 20 ml at a flow rate of 0.8 ml/min.

Photoaffinity Labeling of *E. coli* Complex I with [^{3}H]Azido-Q--The dodecyl maltoside present in purified complex I was replaced with sodium cholate by repeated dilution-concentration using centriprep-30 as previously described (8). Complex I as prepared (specific activity, 0.301 mol NADH oxidized/min/mg protein) was in 50 mM NaCl, 0.15 % dodecyl maltoside, 50 mM MES/NaOH, pH 6.0. This complex was diluted with 1 % sodium cholate to a protein concentration of 1 mg/ml in 50 mM K^+/Na^+ phosphate buffer, pH 7.5 and concentrated to 10 mg/ml by centrifugation for 30 min at 3,000 rpm, using a JS-42 rotor in a Beckman centrifuge J6-HC. The concentrated complex I was diluted again with the same buffer containing 1 % sodium cholate and concentrated again to 10 mg/ml. This process was repeated eight times. The complex (specific activity, 0.267 mol NADH oxidized/min/mg protein) was then adjusted to a protein concentration of 4 mg/ml in the same buffer, containing 1 % of sodium cholate. 300 µl of this solution was mixed with 5 µl of [^{3}H]azido-Q (9.0 mM in 95% ethanol) and incubated at 0 °C for 30 min in the dark. The specific radioactivity of [^{3}H]-azido-Q used was 9.7×10^3 cpm/nmol in 95% ethanol and 3.6×10^3 cpm/nmol in the 50 mM K^+/Na^+ phosphate buffer, pH 7.5, containing 1.0 % sodium cholate in the presence of *E. coli* complex I. This mixture was transferred to a 2-mm light path quartz cuvette which was sealed with paraffin film and mounted on an illuminating apparatus. This assembly was immersed in ice water in a container with a quartz window and illuminated with long wavelength UV light

(Spectroline EN-14, 365 nm long wavelength, 23 watts) for 10 minutes at a distance of 4 cm from the light source. NADH-Q oxidoreductase activity was assayed, after reconstitution with asolectin, before and after the illumination.

To determine the amount of [^{3}H]azido-Q incorporated into complex I, illuminated samples were spotted on Whatman filter paper in the dark, and kept in the dark until all the desired samples were collected. The paper was then developed with a solvent system of chloroform and methanol (2:1, v/v). Under these conditions, proteins were denatured and retained on the original spots and non-protein bound [^{3}H]azido-Q moved upward. After the paper was air-dried, the origin spots was cut into small pieces and subjected to liquid scintillation counting in a Packard Tri-Carb 1900CA scintillation analyzer.

Determination of the Distribution of [^{3}H] Radioactivity among the Subunits of *E. coli* Complex I--The illuminated, [^{3}H]-azido-Q treated sample was digested with 1 % SDS and 0.4 % β-mercaptoethanol at 37 °C for 2 hrs before being subjected to SDS-PAGE. The SDS-polyacrylamide gel was prepared according to Schägger & von Jagow (9) except that bisacrylamide was substituted for the cleavable cross-linker, N, N'-diallyltartardiamide (DATA). Electrophoresis was run at 30 V for 2 hrs and then at 80 V for another 6 hrs. After electrophoresis, the gel was stained and destained (9). Gels were sliced according to the stained protein bands. The portion containing no protein was also sliced to the same size as that of the protein bands. Gel slices were completely dissolved by incubation in 0.3 ml of 3 % periodic acid at room temperature for 1 hr. 5 ml of Insta-Gel counting fluid was added and radioactivity determined.

Isolation of [^{3}H]Azido-Q-labeled NuoM--Part of the digest (see above) was subjected to preparative SDS-PAGE. A small portion (10 %) of the SDS-digested protein solution was treated with fluorescamine (100 fold molar excess) for 10 min at 37 °C and placed in the reference wells, located on both edges and the middle of the gel. The SDS-PAGE gel and electrophoresis conditions were as described in the preceding section. The protein bands were visualized by the UV fluorescence in the reference lanes. The SDS-PAGE pattern of the fluorescamine-treated sample was identical to that of the untreated sample, as established by Coomassie Blue staining. The NuoM protein band was excised from the SDS-PAGE gel. The protein was eluted from the combined gel slices with an electro-eluter from Bio-Rad.

Protease K Digestion of [^{3}H]Azido-Q-Labeled NuoM--Purified [^{3}H]azido-Q labeled NuoM obtained by electro-elution was subjected to a repeated dilution and concentration process using centriprep-30 with a dilution buffer of 30 mM Tris-Cl, pH 7.5, to remove SDS. The final protein concentration was about 1 mg/ml, with the SDS concentration around 0.5 %. Protein was then digested with protease K at 37 °C for 6 hrs using a protease K:NuoM ratio of 1:50 (w/w).

Isolation of Ubiquinone-binding Peptides--100 μl aliquots of the protease K-digested NuoM were separated by high performance liquid chromatography (HPLC) on a Supelcosil LC-308 column (C8, 5 μm particles, 300 Å pores, 4.6 mm ID, 25 cm length) using a gradient formed from 0.1 % trifluoroacetic acid and 90 % acetonitrile containing 0.1 % trifluoroacetic acid with a flow rate of 0.8 ml/min. 0.8 ml fractions were collected. For each fraction the absorbance, from 200 nm to 400 nm, was recorded with a Waters 996 Diode Array Detector and radioactivity was measured. Peaks with high specific radioactivity were collected, dried, and subjected to peptide sequence analysis.

Amino Acid Sequence Determination--Amino acid sequence analyses were done at the Molecular Biology Resource Facility, Saint Francis Hospital of Tulsa Medical Research Institute, University of Oklahoma Health Sciences Center, under the supervision of Dr. Ken Jackson.

Effect of Cofactors on the Labeling--Aliquots of 0.94 nmol NADH-Q oxidoreductase from *E. coli* in 50 mM K^+/Na^+ phosphate buffer, pH 7.5, containing 1.0 % sodium cholate were incubated with [^{3}H]azido-Q (18.7 nmol) for 30 min at 0 ^{0}C in the dark, then NADH, NAD or ATP (400 μM final concentration) plus 1 mM sodium pyruvate were added for activation, and the incubation was continued for 30 min. Residual NADH was oxidized by L-lactate dehydrogenase (type II, from rabbit muscles) to NAD shortly before photoirradiation as it would quench the UV light responsible for photoactivation of [^{3}H]azido-Q. Then, the mixtures were illuminated under UV for 10 min at 0 ^{0}C as described above.

Results and Discussion

Preparation of NADH-Q oxidoreductase--NADH-Q oxidoreductase, prepared according to the procedure described (6), contains 0.5 moles of bound coenzyme Q-8 (ubiquinone-40) per mol protein. When this preparation is titrated with exogenous Q_0C_{10}Br, no Q-binding is observed, suggesting that the vacant Q-binding site(s) are masked by the detergent dodecyl maltoside or phospholipids and the binding affinity of Q_0C_{10}Br is weaker than that of endogenous Q, phospholipid and detergent used. Since the binding affinity of azido-Q derivatives to the Q-binding sites of several Q-binding proteins was reported to be weaker than that of Q_0C_{10} or Q_0C_{10}Br (16, 21-23), study of the

Q:protein interaction in NADH-Q oxidoreductase, using azido-Q derivatives, requires prior removal of endogenous Q from the complex and an unmasking of the Q-binding sites.

When NADH-Q oxidoreductase is subjected to a repeated dilution-centrifugation/concentration process described in 'Experimental Procedures'; endogenous Q_8 is partially removed (from 0.5 mol/mol down to 0.3 mol/mol protein), and the Q-binding site is unmasked. That unmasking occurs during detergent exchange is evident from the binding of 0.7 mole of exogenous $Q_0C_{10}Br$ to one mol of NADH-Q oxidoreductase. The binding of exogenous $Q_0C_{10}Br$ was determined by titration according to the reported method (8). The SDS-PAGE gel electrophoretic pattern of the cholate containing NADH-Q oxidoreductase is similar to that of dodecyl maltoside containing enzyme except that a protein band with apparent molecular weight of 75 kDa becomes more apparent (see Figure 12). This protein band was identified by partial N-terminal amino acid sequence analysis as a proteolytic digestion product of subunit NuoG. Since sodium cholate replaced NADH-Q oxidoreductase has its Q-binding site unmasked, it is, therefore, suitable for use in photoaffinity labeling studies.

When the purified and cholate-containing NADH-Q oxidoreductase is incubated with a 20 fold molar excess of 3-azido-2-methyl-5-methoxy-6-decyl-1, 4-benzoquinone (azido-Q) or 5-azido-2, 3-dimethoxy-6-decyl-1, 4-benzoquinone (5-azido-Q) for 30 min at 0 °C in the dark and then illuminated with long wavelength UV light for 10 min, only the azido-Q treated sample shows inactivation and radioactivity uptaken by protein, indicating that azido-Q is suitable for studying the Q/protein interaction in this complex.

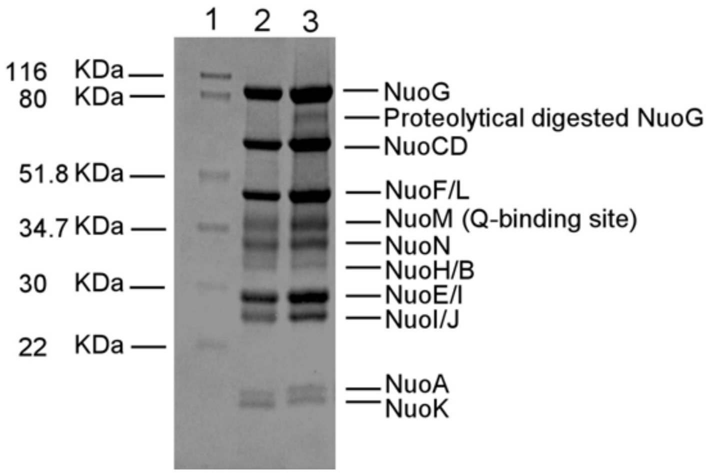

Figure 12. SDS-PAGE patterns of NADH-Q oxidoreductases before and after detergent exchange. Lane 1, protein standard; lane 2, purified NADH-Q oxidoreductase in dodecyl maltoside; and lane 3, purified NADH-Q oxidoreductase in sodium cholate.

This azido-Q derivative was previously used to identify the Q-binding sites in succinate-Q oxidoreductases (10-13) and cytochrome bc_1 complexes (5) from several sources.

Azido-Q Concentration-dependent Inactivation of NADH-Q Oxidoreductase--Figure 13 shows that when NADH-Q oxidoreductase is incubated with various concentrations of azido-Q and illuminated, activity decreases as the concentration of azido-Q is increased. Maximum inactivation of 40 % is obtained when 20 mol of azido-Q per mol of NADH-Q oxidoreductase is used. Inactivation is not due to the inhibition of NADH-Q oxidoreductase by photolyzed products of azido-Q, because when azido-Q is photolyzed in the absence of NADH-Q oxidoreductase and then mixed with the enzyme, no inhibition is observed. Inactivation is also not due to protein damage by UV radiation, because when the enzyme alone is illuminated, no activity loss is observed. Since the activity of the azido-Q treated NADH-Q oxidoreductase, after illumination, is assayed in the presence of excess Q_1 (60 μM), the extent of inactivation should be proportional to the fraction of the Q-binding sites covalently linked to azido-Q.

Correlation between [^{3}H]Azido-Q Incorporation and Inactivation of NADH-Q Oxidoreductase--To further confirm that the inactivation observed results from covalent linkage of azido-Q to protein in the complex, [^{3}H]azido-Q uptake and the extent of inactivation were determined for different periods of illumination. As shown in Figure 14, when the complex is treated with 20 molar excess of [^{3}H]azido-Q and illuminated for different time periods, activity decreases as illumination time increases; maximum inactivation (40 %) is reached at 10 min. Moreover, the amount of [^{3}H]azido-Q incorporated into protein parallels the extent of inactivation, until the maximum is reached, suggesting that inactivation results from binding of [^{3}H]azido-Q to the Q-

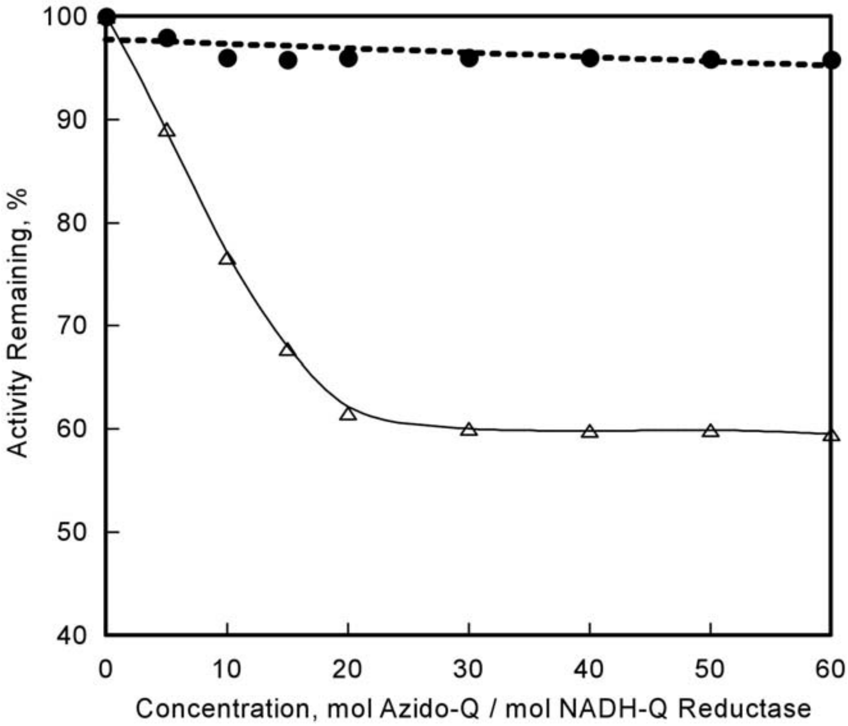

Figure 13. Effect of azido-Q concentration on NADH-Q oxidoreductase activity after illumination. Aliquots (0.1 ml) of NADH-Q oxidoreductase, 1 mg/ml, in 50 mM K^+/Na^+ phosphate buffer, pH 7.5, and 1 % sodium cholate were mixed with 2 µl of an alcoholic solution containing the indicated concentrations of azido-Q derivative in the dark. After incubation at 0 °C for 30 min the samples were illuminated for 10 min at 0 °C. NADH-Q_1 oxidoreductase activity was assayed, before (solid circles) and after (open triangles) illumination, after reconstitution with asolectin. 100 % activity is that of untreated NADH-Q oxidoreductase, which equals 0.301 µmol NADH oxidized per minute per mg protein in dodecyl maltoside and 0.267 µmol NADH oxidized per minute per mg protein in sodium cholate at 23 °C.

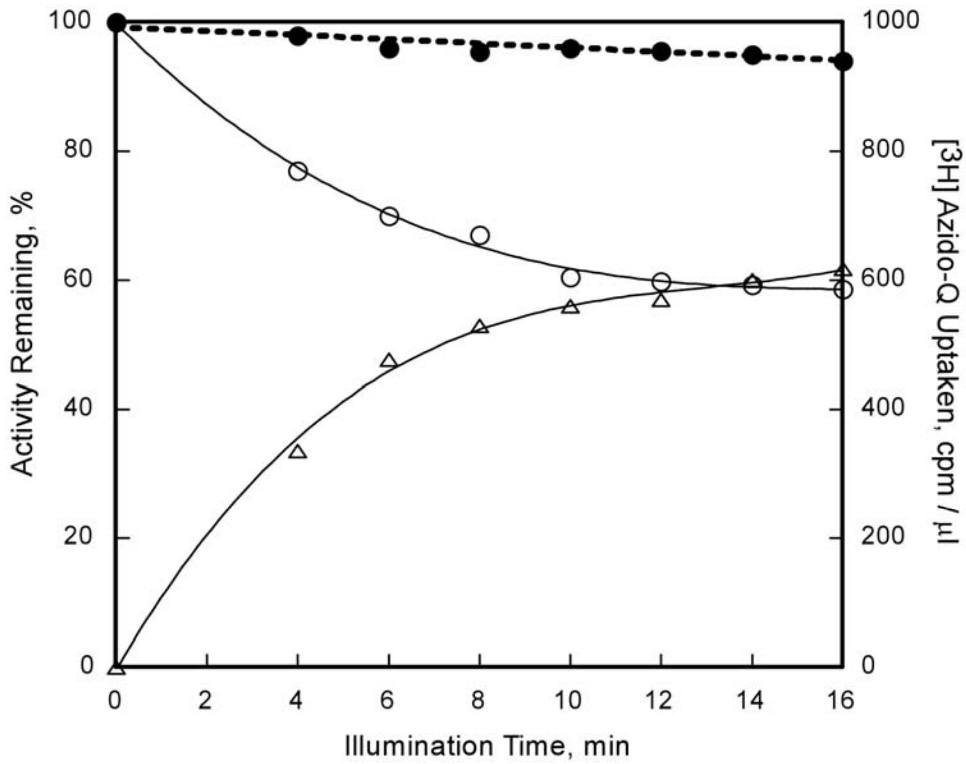

Figure 14. Effect of illumination time on azido-Q uptake and inactivation of NADH-Q oxidoreductase. The NADH-Q oxidoreductase, 1 mg/ml, in 50 mM K^+/Na^+ phosphate buffer, pH 7.5 containing 1 % sodium cholate was incubated with [^{3}H]azido-Q in ethanol (open circles, open triangles) or ethanol only (solid circles) for 30 min at 0 °C in the dark. The samples were then illuminated with long wavelength UV light for the indicated times at 0 °C. The determination of activity (open circles, solid circles) and radioactivity (open triangles) were performed as described in "Experimental Procedures".

binding site. Although illumination for longer than 10 min causes no further decrease in activity, [^{3}H]azido-Q uptake continues, but at a slower rate, indicating that this incorporation is due to nonspecific binding of [^{3}H]azido-Q to protein. It should be mentioned that a control sample containing the same amount of ethanol, illuminated under identical conditions, shows little (<5 %) activity loss over the time periods studied.

Identification of Q-binding Subunit in NADH-Q Oxidoreductase by Photoaffinity labeling with [^{3}H]Azido-Q Derivatives--Since the uptake of [^{3}H]azido-Q derivative by NADH-Q oxidoreductase upon illumination is correlated to the enzymatic inactivation, it is reasonable to assume that the azido-Q derivative is bound specifically to the Q-binding site(s). Thus, the distribution of the covalently bound azido-Q among subunits of NADH-Q oxidoreductase after SDS-PAGE indicates the specific Q-binding protein in this enzyme complex. Figure 15 shows the ^{3}H-radioactivity distribution among subunits of NADH-Q oxidoreductase. The advantage of using the acrylamide/DATA gel system, rather than the commonly used acrylamide/bisacrylamide system is that the gel slices can be completely dissolved in 3 % periodic acid and this solution can be used directly for radioactivity determination. The acrylamide/DATA gel system has been used to identify Q-binding proteins in a bacterial reaction center (14) and in mitochondrial ubiquinol-cytochrome *c* reductase (5). The electrophoretic pattern of illuminated, azido-Q treated NADH-Q oxidoreductase obtained with the acrylamide/DATA gel system is similar to that obtained from the acrylamide/bisacrylamide gel system; 11 major protein bands are observed in each (by Coomassie Blue staining). Radioactivity is found in the protein band 5, suggesting that this subunit provides the Q-binding site. No radioactivity is found in slices from a gel loaded with illuminated buffer containing [^{3}H]azido-Q and 1% sodium

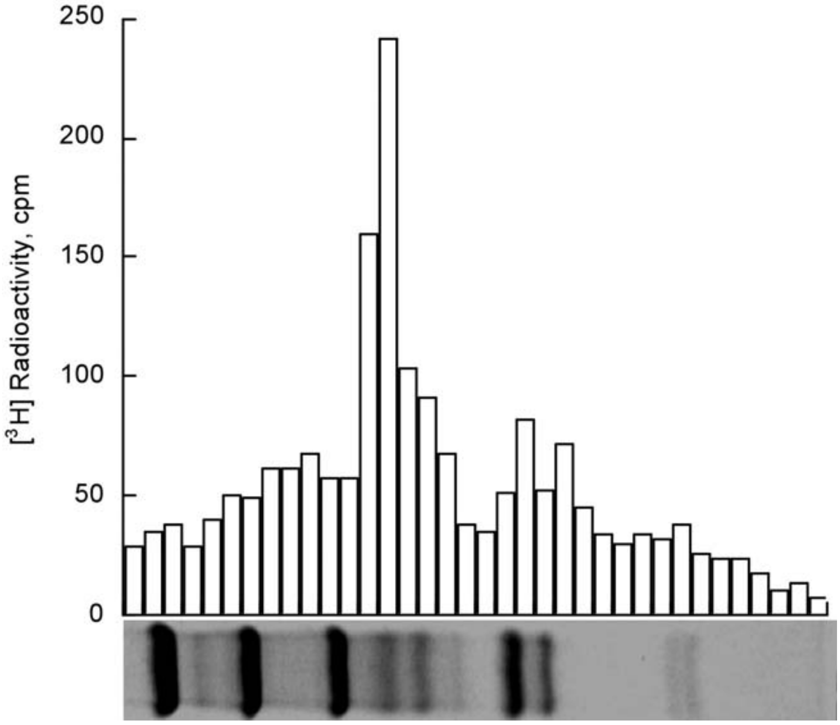

Figure 15. [^{3}H]Radioactivity distribution among subunits of NADH-Q oxidoreductase. Purified NADH-Q oxidoreductase was treated with a 20-fold molar excess of [^{3}H]azido-Q in the dark for 30 min, and illuminated for 10 min at 0 °C, and digested with 1 % SDS and 0.4 % β-mercaptoethanol at 37 °C for 2 hrs before being applied to a SDS-PAGE gel. The electrophoretic conditions are described in “Experimental Procedures.” Protein bands were visualized by Coomassie Brilliant Blue, after staining and destaining, and sliced. The portion containing no protein was also sliced, to the same size as that of the protein bands. The gel slices were dissolved with 3 % periodic acid and mixed with 5 ml of Insta-Gel, and the radioactivity was determined.

cholate. Since the amount of radioactivity in band 5 was directly proportional to the extent of inactivation of the oxidoreductase, participation of this protein in Q-binding is established.

This radioactive protein band in SDS-PAGE of the illuminated [^{3}H]azido-Q-treated NADH-Q oxidoreductase is identified as NuoM, based on the identification of two NuoM peptides in the protease K digest of the labeled protein. Peptide peaks with retention times of 29.9 min and 45.8 min obtained from HPLC separation of protease K digested labeled protein have the partial N-terminal amino acid sequence of NH_2-SAAGLFI- and NH_2-LPDAH- corresponding to residues 351 to 357 and 244 to 248 of NuoM subunit, respectively.

The identification of NuoM as the ubiquinone binding subunit of NADH-Q oxidoreductase is consistent with the report (15) that human complex I lacking the mtDNA-encoded subunit ND4, due to a frameshift mutation in the gene, has no NADH:Q_1 oxidoreductase activity but with normal NADH:$Fe(CN)_6$ oxidoreductase activity. ND4 of human complex I is the counterpart of NuoM of *E coli* enzyme (16).

<u>Isolation and Characterization of Ubiquinone-binding Peptides of NuoM</u>--In order to identify the Q-binding domain in NuoM through isolation and sequencing of an azido-Q-linked peptide, it is absolutely necessary that the isolated azido-Q labeled NuoM has to be free from contamination with unbound azido-Q and completely susceptible to proteolytic enzyme digestion. [^{3}H]Azido-Q-labeled NuoM was isolated from illuminated, [^{3}H]azido-Q-treated NADH-Q oxidoreductase by a procedure involving preparative SDS-PAGE, electrophoretic elution, and repeated dilution/concentration with centriprep-30. The SDS-PAGE step removes non-protein-bound azido-Q adducts. The SDS concentration

in the final purification step is about 0.5 %, while the concentration of [^{3}H]azido-Q labeled NuoM is about 1 mg/ml. Isolated [^{3}H]azido-Q-labeled NuoM shows only one band, in SDS-PAGE, which corresponds to the fifth subunit of NADH-Q oxidoreductase (data not shown). About 40 % of the NuoM protein present in NADH-Q oxidoreductase is recovered in the final purification step, assuming a molecular mass of 535 kDa for the *E. coli* NADH-Q oxidoreductase and that it contains 1 mol of NuoM/mol enzyme. This low yield of NuoM is probably due to our very small slicing of the NuoM band, in order to avoid contamination with neighboring proteins.

When SDS present in purified [^{3}H]azido-Q-labeled NuoM was removed by the commonly used cold acetone precipitation method, the resulting protein is highly aggregated and resistant to proteolytic enzyme digestion. Inclusion of 0.1 % SDS and 2 M urea in the digestion mixture does not increase proteolysis. Since the SDS-free, [^{3}H]azido-Q labeled NuoM is not digested by proteolytic enzymes, we needed a protease that is active when SDS concentration is higher than 0.5 %. Since of the commercially available proteolytic enzymes only protease K was reported to be active in 0.5 % SDS and 1 M urea, isolated [^{3}H]azido-Q labeled NuoM was subjected to protease K digestion at 37 °C using a protease K:NuoM ratio of 1:50 (w/w). To obtain the optimal digestion time 100 μl aliquots were withdrawn from the digestion mixture at different time intervals, subjected to HPLC separation, and analyzed for peptide patterns and radioactivity recovery on HPLC chromatograms. At 37 °C, a 6 hrs digestion time was found to be optimal. Figure 16 shows the ^{3}H radioactivity distribution on HPLC chromatogram of [^{3}H]azido-Q-labeled NuoM digested with protease K. Most of the radioactivity was found in one fraction with the retention time of 41.4 min (P42). The radioactivity recovery is about 72 % based on what was applied to the HPLC column.

The partial NH_2-teminal amino acid sequence of P42 was found to be NH_2-VMLIAILALV-, corresponding to amino acid residues 184-193 of NuoM. By mass spectral analysis, we determined the size of this Q-binding peptide to be 2906.4, suggesting that the Q-labeled peptide is composed of 23 amino acid residues, from V184 to N206.In the Toppred hydropathy analysis (17) of NuoM, this Q-binding peptide overlaps with the proposed Q-binding motif (L-X_3-H-X_3-T/S) (18) located in the middle of transmembrane helix 5 toward the cytoplasmic side of the membrane (see Figure 17a). If the PHDhtm hydropathy plot (19) is used (see Figure 17b), the Q-binding peptide is located in transmembrane helix 4, toward the periplasmic side of the membrane. It should be noted that the Q-binding domain identified in this study differs from that identified for rotenone binding in NADH-Q oxidoreductase (20, 21). Although only one Q-binding peptide is identified in the this study, one cannot rule out the possibility of more than one Q-binding site, because inhibition of the azido-Q treated sample is less than 50 % and a substantial amount of endogenous Q_8 (0.3 mole per mole protein) remains in the Q-deficient complex. The residual Q_8 would render a portion of the Q-binding site or a different Q-binding site inaccessible to azido-Q.

Recently, Nakumara-Ogiso *et al*. (22) have identified subunit ND5 (NuoL in *E.coli*) as Q-binding site based on the photoaffinity labeling study of submitochondrial particles using analogue of fenpyroximate, a specific inhibitor of complex I. Although the assumption that this inhibitor binds directly at the Q-binding site is difficult to establish, especially with inhibitors whose chemical structures have little resemblance to Q,

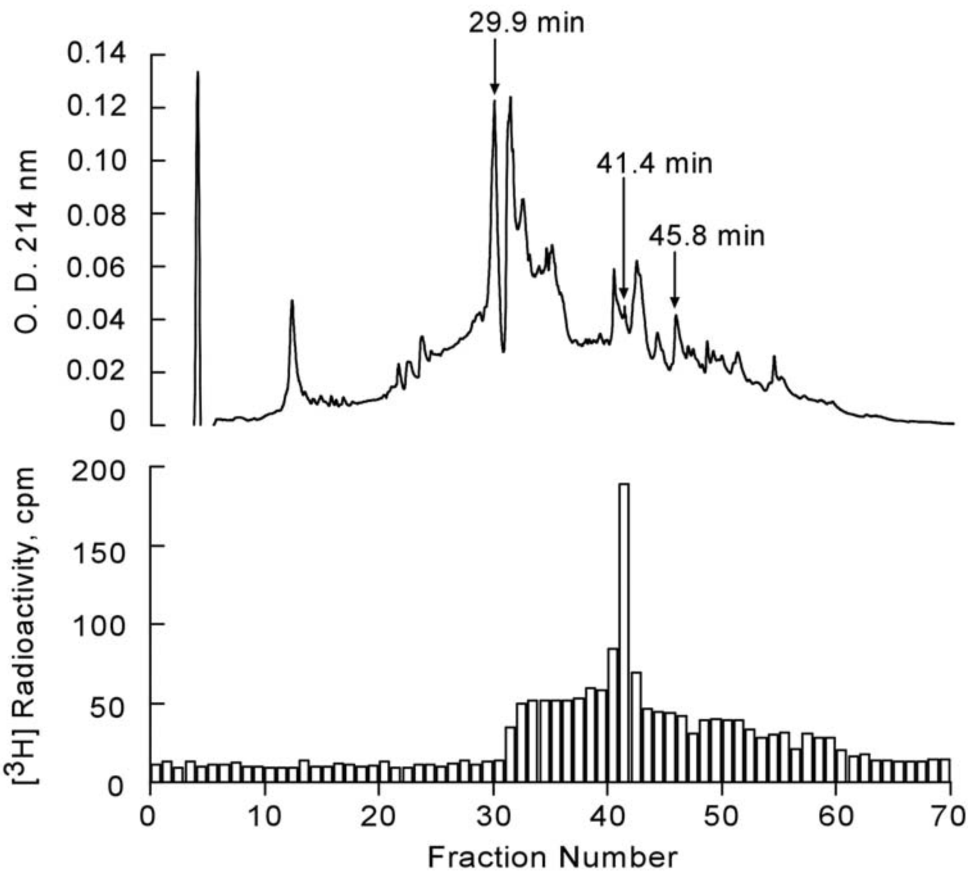

Figure 16. [^{3}H] Radioactivity distribution in an HPLC chromatogram of a protease K-digest of [^{3}H]azido-Q- labeled NuoM protein. The labeled protein (1 mg/ml, 1×10^5 cpm/mg) was digested, fractionated and assay for radioactivity as described under "Experimental Procedures".

(a)

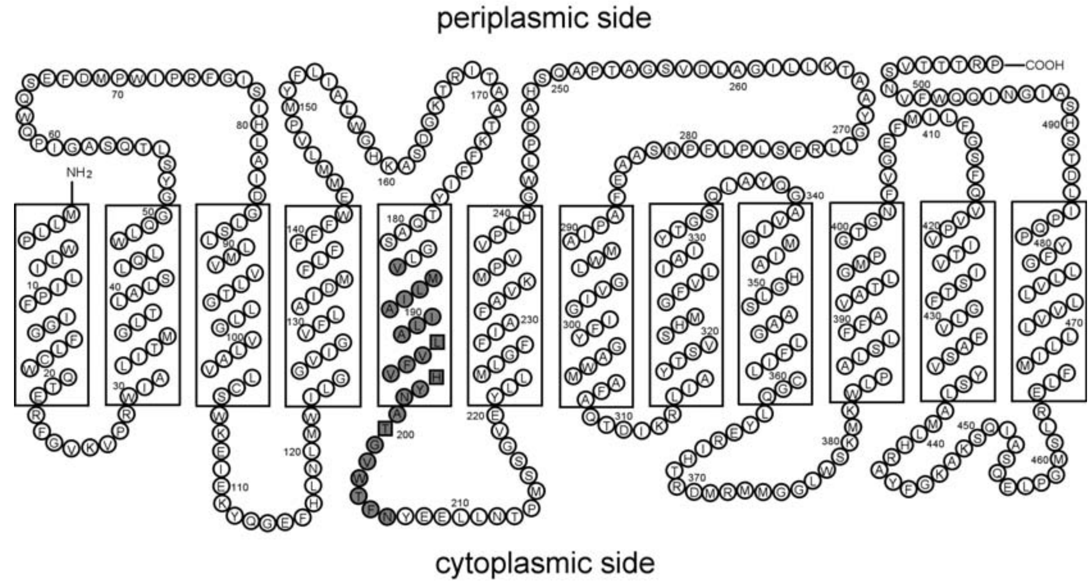

(b)

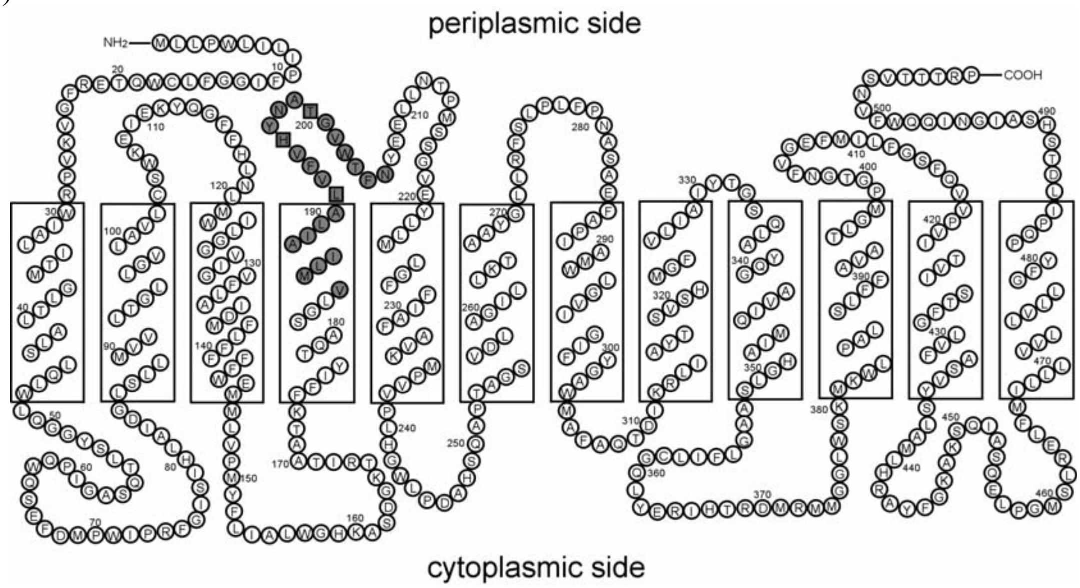

Figure 17. Putative Q-binding domain in the proposed structure of NuoM. The proposed secondary structure of NuoM of *E. coli* NADH-Q oxidoreductase was constructed from on the hydropathy plots of its amino acid sequence using Toppred hydropathy analysis (a) and the program of PHD (b). The shaded area indicates the Q-binding peptide identified in this report. The Q-binding motif (L-X_3-H-X_3-T) in complex I predicted by Fisher and Rich (18) is shown by squares.

identification of ND5 as one of the subunits possibly involved in quinone binding is very interesting as ND5 also contains a Q-binding motif, A-X_3-H-X_2-T. ND5 is composed of 14 transmembrane helices in the Toppred hydropathy plot, the Q-binding motif is located at the connecting loop of transmembrane helices 8 and 9 on the periplasmic side of the membrane. In the similar plot, Q-binding motif of NuoM, L-X_3-H-X_3-T, is located the end of transmembrane helix 5 toward the cytoplasmic side of the membrane. This would indicate that the Q-binding site in ND5 is not a part of the Q-binding site loacted in ND4. On the other hand, if PHDhtm hydropathy plots are compared then the Q-binding motif in ND5 could be a part of Q-binding site in ND4, as the motif of ND5 is located on the end of the transmembrane helix 9 toward periplasmic side of the membrane, which is spatially similar to Q-binding motif of NuoM locating at the connecting loop of transmembrane helices 4 and 5 on the periplasmic side of the membrane. In this context it is noteworthy to mention that ND4 and ND5 have evolved from a common ancestor (23) and might share related but not identical functions in NADH-Q oxidoreductase (24).

Effects of Cofactors on the Labeling of NuoM by [^{3}H]azido-Q--Table 3 shows the effects of 400 μM of NADH, NAD and ATP on [^{3}H]azido-Q labeling of NuoM. NAD and ATP had essentially no effect, which is consistent with the data recently reported by Nakamaru-Ogiso *et al*. (22) during photoaffinity labeling of inhibitor/quinone probes in complex I when isolated submitochondrial particles were used. [^{3}H]azido-Q labeling of NuoM subunit was not influenced by prior NADH incubation, even though NADH has been reported to stimulate the labeling of inhibitor/quinone probes in mitochondrial complex I (22, 25). Similar data was also obtained with a [^{3}H]pyridaben analogue labeling of Nqo6 (PSST in mitochondria) subunit from *Paracoccus denitrificans* (22).

Table 3: Effects of cofactors on the labeling of NuoM by [^{3}H]azido-Q

Additions	Relative amount of radioactivity incorporated by protein (%)
Control	100[a]
NADH (400 mM)	99
NAD (400 mM)	98
ATP (400 mM)	99

[a] 100% indicates 5,626 cpm/nmol of protein.

Activation of NADH-Q oxidoreductase by NADH has solely been demonstrated for the mitochondrial but not for the bacterial enzyme. The *E. coli* NADH-Q oxidoreductase shows no activity with NADPH as substrate and addition of NADPH has consequently no effect on the labeling of NuoM. These data suggest that activation of NADH-Q oxidoreductase by NADH has an effect on the binding of inhibitors, most likely due to conformational changes, but that binding of quinone itself is not influenced. This is another indication that at least the Q-binding site identified in this report is not identical to the inhibitor binding sites described in the literature.

<u>Effects of Inhibitors of *E. coli* NADH-Q oxidoreductase on [^{3}H]azido-Q labeling of NuoM</u>--We also examined the effects of various complex I inhibitors on the labeling with [^{3}H]azido-Q (see Figure 18). Rotenone was excluded in this series as it has only a very minor effect on the activity of the *E. coli* NADH-Q oxidoreductase (26). A 20-35% decrease in labeling of NuoM with [^{3}H]azido-Q was observed when dihydrocapsaicin (10 nmol/mg protein), pyridaben (1.0 nmol/mg protein), rolliniastatin-1 (0.2 nmol/mg protein), piericidin A (0.6 nmol/mg protein) and fenazaquin (1.0 nmol/mg protein) were used. At the concentrations given each inhibitor shows complete inhibition of NADH oxidoreductase activity. Similar phenomena were reported with the highly potent and specific inhibitor trifluromethyldiazirinyl[^{3}H]pyridaben labeling of the PSST subunit in isolated submitochondrial particles (25). Again, these results suggest that the binding sites of these inhibitors may not overlap with that of [^{3}H]azido-Q. The minor effect observed upon addition of inhibitors is probably due to a conformational change in NADH-Q oxidoreductase induced by binding of inhibitors. Alternatively, the minor effect of

inhibitors on [^{3}H]azido-Q labeling of NuoM could be explained by a partially overlapping a common binding site of inhibitors with [^{3}H]azido-Q binding site.

The location of the Q-binding site(s) in complex I is still under debate. So far, inhibitor labeling was set out for the identification of this site(s). Using various, structurally different inhibitors ND5 (NuoL) (31), PSST (NuoB) (27), and ND1 (NuoH) (21) have been indicated as the possible candidates representing this site. The 49 kDa (NuoD) was proposed to be involved in Q-binding due to inhibitor resistance conferred by a point mutation in this subunit (28). Thus, the Q-binding site is most likely located at the interface of the hydrophilic and hydrophobic part of the enzyme. NuoB, D, H, and either NuoM or NuoL seem to be in close spatial proximity as all these subunits are part of the evolutionary conserved hydrogenase module complex (29). As NuoM and L are related to each other it is hard to decide which of these two subunits is part of the hydrogenase module (29). Electron microscopic experiments indicate that NuoL is located at a distant position to NuoM (30). Therefore, it is most likely that NuoB, D, H, and NuoM are involved in building the Q-binding site of the complex. Contrary to the experiments carried out so far, we used a labeled quinone derivative for direct identification of ND4 (NuoM) as Q-binding site. This fits well with the proposed proximity of this subunit with NuoB, D, and H (30). Because the binding of the various inhibitors is affected by the presence of other inhibitors it was concluded that these binding sites partially overlap (31). Here, we have shown that the binding of [^{3}H]azido-Q is not influenced by addition of inhibitors indicating that the inhibitor binding site(s) may not be identical to the quinone binding site(s).

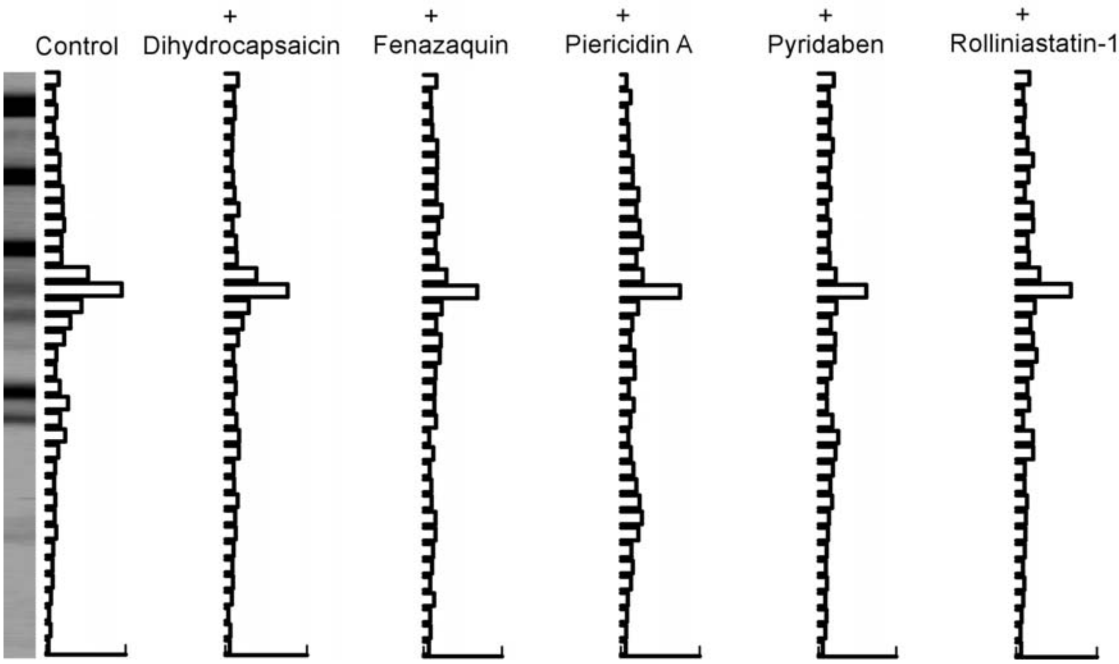

Figure 18. Effects of various complex I inhibitors on [^{3}H] azido-Q labeling of NuoM. NADH-Q oxidoreductase from *E. coli* (0.94 nmol protein in 50 mM K^+/Na^+ phosphate buffer, pH 7.5, containing 1.0 % sodium cholate) were treated with each inhibitor for 30 min on ice and incubated with [^{3}H]azido-Q (18.7 nmol) for 30 min at 0 ^{o}C in the dark. Then, the mixture was illuminated under UV for 10 min at 0 ^{0}C as described in "Experimental Procedures". Each calibration bar at the bottom designates 5.63 x 10^3 cpm/nmol of protein.

References

1. Anraku, Y., and Gennis, R. B. (1987) *Trends Biochem. Sci*. **12**, 262-266.
2. Walker, J. E. (1992) *Quarterly Rev. Biophys.* **25**, 253-324.
3. Carroll, J., Fearnley, I. M., Shannon, R. J., Hirst, J., and Walker, J. E. (2003) Molec. Cell. *Proteomics*, **2**, 117-126.
4. Weidner, U., Geier, S., Ptock, A., Friedrich, T., Leif, H., and Weiss, H. (1993) *J. Mol. Biol.* **233**, 109-122.
5. Yu, L., Yang, F.D., and Yu, C. A. (1985) *J. Biol. Chem*. **260**, 963-973.
6. Spehr, V., Schlitt, A., Scheide, D., and Friedrich, T. (1999) *Biochemistry* **38**, 16216-16267.
7. Redfearn, E. R. (1967) *Methods Enzymol*. **10**, 381-384.

8 Bader, M. W., Xie, T., Yu, C. A., and Bardwell, J. C. (2000) *J. Biol. Chem*. **275**, 26082-26088.

9. Schägger, H., and von Jagow G. (1987) *Anal. Biochem.* **166**, 368-379.
10. Lee, G. Y., He, D. Y., Yu, L., and Yu, C. A. (1995) *J. Biol. Chem*. **270**, 6193-6198.
11. Yang, X., Yu, L., He, D.Y., and Yu, C. A. (1998) *J. Biol. Chem.* **273**, 31916-3192.
12. Xie, T., Yu, L., Bader, M. W., Bardwell, J. C., and Yu, C. A. (2002) *J. Biol. Chem*. **277**, 1649-1652.
13. Shenoy, S. K., Yu, L., and Yu, C. A. (1997) *J. Biol. Chem*. **272**, 17867-17872.
14. Marinetti, T. D., Okamura, M. Y., and Feher, G. (1979) *Biochemistry,* **18**, 3126-3133.
15. Hofhaus, G. and Attardi, G. (1993) *The EMBO J*. **12**, 3043-3048.
16. Yagi, T., and Matsuno-Yagi, A. (2003) *Biochemistry*, **42**, 2266-2274.
17. von Heijne, G. (1992) *J. Mol. Biol.* **225**, 487-494.
18. Fisher, N., and Rich, P. R. (2000) *J. Mol. Biol.* **296**, 1153-1162.
19. Rost, B., Casadio, R., Fariselli, P., and Sander, C. (1995) *Prot. Science*. **4**, 521-533.
20. Earley, F. G. P., and Ragan, C. I. (1984) *Biochem. J.* **224**, 525-534.

21. Earley, F. G. P., Patel, S. D., Ragan, C. I., and Attardi, G. (1987) *FEBS Lett.* **219**, 108-112.

22. Nakamaru-Ogiso, E., Sakamoto, K., Matsuno-Yagi., Miyoshi, H., and Yagi, T., (2003) *Biochemistry*, **42**, 746-754.

23. Kikuno, R., and Miyata, T. (1985) *FEBS Lett.***189**, 85-88.

24. Friedrich, T.,and Weiss, H. (1997) *J. Theor. Biol.* **187**, 529-540.

25. Schuler, F., and Casida, J. E, (2001) *Biochim. Biophys. Acta*. **1506**, 79-87.

26. Friedrich, T., van Heek, P., Leif, H., Ohnishi, T., Forche, E., Kunze, B., Jansen, R., Trowitzsch-Kienast, W., Höfle, G. Reichenbach, H., and Weiss, H. (1994) *Eur. J. Biochem.* **219**, 691-698.

27. Schuler, F., Yano, T., DiBernardo, S., Yagi, T., Yankovskaya, V., Singer, T., and Casida, J.E. (1999). *Proc. Natl. Acad. Sci. USA* **96**, 4149-4153.

28. Darrouzet, E., Issartel, J. P., Lunardi, J., and Dupuis, A. (1998) *FEBS Lett*. **431**, 34-38.

29. Friedrich, T., and Scheide, D. (2000) *FEBS Lett.* **479**, 1-5.

30. Sazanov, L.A., and Walker, J.E. (2000) *J. Mol. Biol.* **302**, 455-464.

31. Ohshima, M., Miyoshi, H., Sakamoto, K., Takegami, K., Iwata, J., Kuwabara, K., Iwamura, H., and Yagi, T. (1998) *Biochemistry*, **37**, 6436-6445.

CHAPTER III

EVIDENCE FOR ELECTRON EQUILIBRIUM BETWEEN THE TWO HEMES b_L IN THE DIMERIC CYTOCHROME bc_1 COMPLEX

Abstract

The structural analysis of the dimeric mitochondrial cytochrome bc_1 complex suggests that electron transfer between inter-monomer hemes b_L-b_L may occur during bc_1 catalysis. Such electron transfer may be facilitated by the aromatic pairs present between the two b_L hemes in the two symmetry-related monomers. To test this hypothesis, *R. sphaeroides* mutants expressing His$_6$-tagged bc_1 complexes with mutations at three aromatic residues (F195, Y199, and F203), located between two b_L hemes, were generated and characterized. All three mutants grew photosynthetically at a rate comparable to that of wild-type cells. The bc_1 complexes prepared from mutants F195A, Y199A and F203A have, respectively, 78%, 100%, and 100% of ubiquinol-cytochrome *c* reductase activity found in the wild-type complex. Replacing the F195 of cytochrome *b* with Y, H, or W results in mutant complexes (F195Y, F195H, or F195W) having the same ubiquinol-cytochrome *c* reductase activity as the wild-type. These results indicate that the aromatic group at position195 of cytochrome *b* is involved in electron transfer reactions of the bc_1 complex. The rate of superoxide anion ($O_2^{-\cdot}$) generation, measured by the

chemiluminescence of 2-methyl-6-(p-methoxyphenyl)-3, 7-dihydroimidazo[1,2-α]pyrazin-3-one hydrochloride (MCLA)-$O_2^{\cdot-}$ adduct during oxidation of ubiquinol, is 3 times higher in the F195A complex than in the wild-type or mutant complexes Y199A or F203A. This supports the idea that the interruption of electron transfer between the two b_L hemes enhances electron leakage to oxygen and thus decreases the ubiquinol-cytochrome *c* reductase activity.

Introduction

The crystal of mitochondrial cytochrome bc_1 complex shows the distance between the Fe atoms of the two hemes b_L is only 21 Å, which is approximately the same as that between heme b_L and b_H in one monomer (1-4) (see Figure 19). The short distance between the two hemes b_L and the presence of several aromatic amino acid residues at the interface of the two cytochrome b proteins has promoted investigators to speculate the existence of electron transfer or equilibrating between the two hemes b_L (5-7). However, evidence for inter-monomer b_L-b_L electron transfer during bc_1 catalysis is still missing, due to the lack of a suitable assay method.

It has been reported that during electron transfer through the bc_1 complex, superoxide anion ($O_2^{\cdot-}$) is produced (8-14). This results from a leakage of the second electron of ubiquinol, from the "low-potential chain" of the Q cycle electron transfer pathway, to interact with molecular oxygen. The electron-leaking site is thought to be located at the reduced cytochrome b_{566} (b_L) or ubisemiquinone of the Qo site. The amount of electron leakage of the second electron of ubiquinol is believed to be proportional to

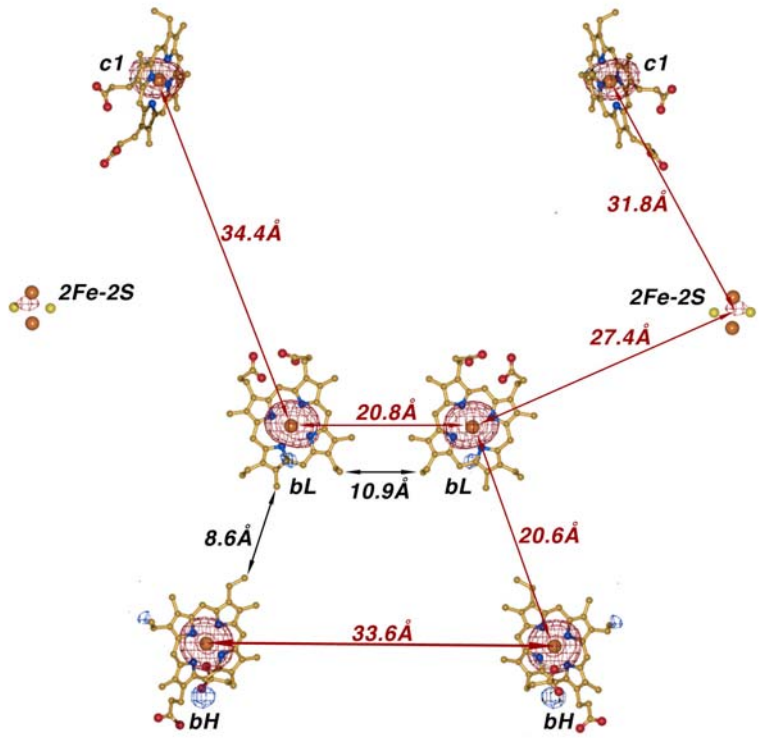

Figure19. Distances between redox centers in bovine dimeric cytochrome *bc*$_1$ complex. All distance measurements are made with native mitochondrial *bc*$_1$ complex, refined to 2.4 Å resolution. The center to center distances are indicated by red arrowed lines and are as labeled; the edge to edge distances of are shown with black arrowed lines and are as labeled.

the concentrations of reduced cytochrome b_L or ubisemiquinone at the Qo site. Thus, if the inter-monomer b_L-b_L electron transfer is interrupted, one should see an increase in the rate of $O_2^{\cdot -}$ generation because electrons that normally shuttle between the two b_L hemes will accumulate at the b_L heme of one monomer, thus enhancing the chance for leakage and reaction with oxygen.

In the 3-D structure of mitochondrial bc_1 complex, several pairs of aromatic residues are located at the dimer interface between the two hemes b_L (1). These aromatic pairs may facilitate the inter-monomer heme $b_L \rightarrow b_L$ electron transfer. If this is indeed the case the existence of inter-monomer heme b_L-b_L electron transfer in the bc_1 complex can be revealed by comparing the rates of $O_2^{\cdot -}$ generation by the wild-type bc_1 complex with those of mutant complexes having these aromatic pairs replaced with non-aromatic residues. An increase in $O_2^{\cdot -}$ generation, as a result of increasing the concentration of reduced b_L or ubisemiquinone at the Qo site, by the mutant bc_1 complex, would indicate inter-monomer heme b_L-b_L electron transfer, involving aromatic amino acid residues.

Herein we report procedures for generating *R. sphaeroides* mutants expressing His_6-tagged bc_1 complexes with mutations at three highly conserved aromatic residues (F195, Y199, and F203) located between the two b_L hemes of the dimeric complex. The rate of superoxide anion generation, the effect of oxygen on the activity and the EPR characteristics of the cytochromes b_L and b_H in purified complexes from wild type and mutant strains are examined and compared.

Experimental Procedures

Materials--Cytochrome *c* (horse heart, type III), hypoxanthine, and superoxide dismutase (SOD), and xanthine oxidase were purchased from Sigma Chemical Co. Dodecylmaltoside (DM) and octylglucoside (OG) were from Anatrace. Nickel nitrilotriacetic acid (Ni-NTA) gel and a Qiaprep spin Miniprep kit were from Qiagen. 2-Methyl-6-(4-methoxyphenyl)-3,7-dihydroimidazol [1,2-α]pyrazin-3-one, hydrochloride (MCLA) was from Molecular Probes, Inc. 2,3-Dimethoxy-5-methyl-6-(10-bromodecyl)-1,4-benzoquinol ($Q_0C_{10}BrH_2$) was prepared in our laboratory as previously reported (15). All other chemicals were of the highest purity commercially available.

Generation of *R. sphaeroides* Strains Expressing the His_6-Tagged Cytochrome bc_1 Complexes with Mutations of Aromatic Residues Located at the Dimer Interface between Two Hemes b_L--Mutations were constructed by the Quick Change site-directed mutagenesis kit from Stratagene using a supercoiled double-stranded pGEM7Zf(+)-*fbc*FB as template and a forward and a reverse primer for PCR amplification. The pGEM7Zf(+)-*fbc*FB plasmid (16) was constructed by ligating the *Eco*RI-*Xba*I fragment from pSELNB3503 into *Eco*RI and *Xba*I sites of the pGEM7Zf(+) plasmid. The primers used are given in Table 4.

The *Bst*EII-*Xba*I fragment from the pGEM7Zf(+)-*fbc*FB_m plasmid was ligated into the pRKD418-fbc$FB_{KmBX}C_HQ$ plasmid to generate the pRKD418-*fbc*FB_mC_HQ plasmid. A plate-mating procedure (17) was used to mobilize the pRKD418-*fbc*FB_mC_HQ plasmid in *E. coli* S17-1 cells into *R. sphaeroides* BC17 cells. The presence of engineered mutations were confirmed by DNA sequencing of the 962-base pair *Bst*EII-*Xba*I fragment before and after photosynthetic growth of the cells as previously reported (17). DNA sequencing and oligonucleotide syntheses were performed by the Recombinant DNA/Protein Core Facility at Oklahoma State University.

Table 4. Oligonucleotides used for site-directed mutagenesis (F and R in the parentheses denote forward and reverse primers, respectively)[a]

F195A (F)	5’-GCCACGCTCAACCGGTTCGCCTCGCTGCA CTACCTGCTGCCCTTC-3’
F195A (R)	5’-GAAGGGCAGCAGGTAGTGCAGCGAGGCG AACCGGTTGAGCGTGG-3’
F195Y (F)	5’-GCCACGCTCAACCGGTTCTACTCGCTGCA CTACCTGCTGCCCTTC-3’
F195Y (R)	5’-GAAGGGCAGCAGGTAGTGCAGCGAGTAG AACCGGTTGAGCGTGGC-3’
F195W (F)	5’-GCCACGCTCAACCGGTTCTGGTCGCTGCA CTACCTGCTGCCCTTC-3’
F195W (R)	5’-GAAGGGCAGCAGGTAGTGCAGCGACCAG AACCGGTTGAGCGTGGC-3’
F195H (F)	5’-GCCACGCTCAACCGGTTCCACTCGCTGCA CTACCTGCTGCCCTTC-3’
F195H (R)	5’-GAAGGGCAGCAGGTAGTGCAGCGAGTGG AACCGGTTGAGCGTGGC-3’
Y199A (F)	5’-CTCAACCGGTTCTTCTCGCTGCACGCCCT GCTGCCCTTCGTGATC-3’
Y199A (R)	5’-GATCACGAAGGGCAGCAGGGCGTGCAGC GAGAAGAACCGGTTGAG-3’
F203A (F)	5’-CGGTTCTTCTCGCTGCACTACCTGCTGCC CGCCGTGATCGCGGCC-3’
F203A (R)	5’-GGCCGCGATCACGGCGGGCAGCAGGTAG TGCAGCGAGAAGAACCG-3’
F195A/Y199A (F)	5’-CTCAACCGGTTCGCCTCGCTGCACGCCCT GCTGCCCTTCGTGATC-3’
F195A/Y199A (R)	5’-GATCACGAAGGGCAGCAGGGCGTGCAGC GAGGCGAACCGGTTGAG-3’

F195A/F203A (F)	5’-CTCAACCGGTTCGCCTCGCTGCACTACCTGCTGCCCGCCGTGATCGCG-3’
F195A/F203A (R)	5’-CGCGATCACGGCGGGCAGCAGGTAGTGCAGCGAGGCGAACCGGTTGAG-3’
Y199A/F203A (F)	5’-CGGTTCTTCTCGCTGCACGCCCTGCTGCCCGCCGTGATCGCGGCC-3’
Y199A/F203A (R)	5’-GGCCGCGATCACGGCGGGCAGCAGGGCGTGCAGCGAGAAGAACCG-3’
F195A/Y199A/F203A (F)	5’-CTCAACCGGTTCGCCTCGCTGCACGCCCTGCTGCCCGCCGTGATCGCG-3’
F195A/Y199A/F203A (R)	5’-CGCGATCACGGCGGGCAGCAGGGCGTGCAGCGAGGCGAACCGGTTGAG-3’

[a] The underlined bases correspond to the genetic codes for the amino acid(s) to be mutated.

Growth of Bacteria--*E. coli* cells were grown at 37 °C in LB medium (sodium chloride, SELECT peptone 140, and SELECT yeast extract, autolyzed low sodium). For photosynthetic growth of the plasmid-bearing *R. sphaeroides* BC17 cells an enriched Siström's medium containing 5 mM glutamate and 0.2% casamino acids was used. Photosynthetic growth conditions for *R. sphaeroides* were essentially as described previously (17). Cells harboring the mutated cytochrom*e b* gene on the pRKD418-*fbc*FB_mC_HQ plasmid were grown photosynthetically for one or two serial passages to minimize any pressure for reversion. The inoculation volumes used for photosynthetic cultures were at least 5% of the total volume. Antibiotics were added to the following concentrations: ampicillin (125 μg/ml), kanamycin sulfate (30 μg/ml), tetracycline (10 μg/ml for *E. coli* and 1 μg/ml for *R. sphaeroides*), and trimethoprim (100 μg/ml for *E. coli* and 30 μg/ml for *R. sphaeroides*). Cells were harvested with centrifugation at 3,500 x g for 30 min, when the turbidity (OD_{600nm}) of the cell culture reached 2.0. The harvested cells were then washed with 20 mM Tris-succinate buffer, pH 7.5, and stored at -20°C. About 5 grams of cells were routinely obtained from one liter of culture.

Enzyme Preparations and Activity Assay--Chromatophores were prepared as described previously (18). Frozen *R. sphaeroides* cells were suspended in 3 ml of 20 mM Tris-succinate (pH 7.5 at 4°C) in the presence of 1 mM sodium ethylenediamminetetraacetate (EDTA) per gram of cells, and passed twice through French press with 1,000 psi to break open the cells. During the suspension, a grain of DNase was added to digest the DNA, which will come out during cell's breakage and cause the tissue to be sticky thus giving incomplete solubilization of protein. Additionally, a protease inhibitor, phenylmethylsulfinyl fluoride (PMSF) freshly dissolved in dimethylsuloxide

(DMSO), was added to the cell suspension with the final concentration of 1 mM before passing through the French press, and was added to the same concentration two more times after each passage through the French press. The broken cells were centrifuged at 40,000 x g (19,000 rpm with JA-20 rotor) for 20 min to remove unbroken cells and cell debris. The supernatant was then subjected to centrifugation at 220,000 x g (49,000 rpm with rotor Ti-50.2 or 60,000 rpm with rotor Ti-70) for 150 min to separate the chromatophore fraction from the soluble protein fraction. The precipitate obtained was washed with buffer A (50 mM Tris/HCl, pH 8.0 at 4^{o}C, containing 1 mM $MgSO_4$) with 1 mM PMSF, and centrifuged at 220,000 x g for 90 min to recove the chromatophore in precipitate. The resulting chromatophores were suspended in buffer A in the presence of 1 mM PMSF and 20% glycerol, and stored at -80^{0}C, until use. To purify the His_6-tagged cytochrome bc_1 complex, the chromatophore suspensions were thawed and adjusted to a cytochrome *b* concentration of 25 μM with buffer A and 1 mM PMSF. DM solution (10%, w/v) was added to the chromatophore suspension to 0.56 mg/nmol of cytochrome *b*, and the mixture was stirred at 4 °C for 30 min. Then NaCl solution (4 M) was added to a final concentration of 0.1 M, and the suspension was stirred for 1 h at 4 °C. This mixture was centrifuged at 220,000 x g for 90 min. The supernatants were collected and diluted using the equivalent volume of BufferA following by passing through the Ni-NTA column (100 nmol of cytochrome *b*/ml of resin) equilibrated with buffer A at 4 °C. The column, absorbed with bc_1 complexes, was then subjected to a sequence of washings with TN buffer, which is 50 mM Tris-Cl (pH 8.0 at 4 °C) and 200 mM NaCl, containing 0.01% DM, TN buffer containing 5 mM histidine and 0.01% DM, and TN buffer containing 0.5% OG, and TN buffer with 5 mM histidine and 0.5% OG. The pure cytochrome bc_1 complex was eluted with TN buffer containing 200 mM histidine and 0.5% OG and concentrated using a Centriprep-30 concentrator to a final concentration of 300 μM cytochrome *b* or higher. The purified complex was stored at -80 °C in the presence of 20% glycerol. To assay cytochrome bc_1 complex activity, chromatophores or purified cytochrome bc_1 complexes were diluted with 50 mM Tris-Cl, pH 8.0, containing 200 mM NaCl and 0.01% DM to a final concentration of cytochrome *b* of 3 μM. Appropriate amounts of the diluted samples were added to 1 mL of assay mixture containing 100 mM Na^+/K^+ phosphate buffer, pH 7.4, 300 μM EDTA, 100 μM cytochrome *c*, and 25 μM $Q_0C_{10}BrH_2$. Activities were determined by measuring the reduction of cytochrome *c* (the increase of absorbance at 550 nm) in a Shimadzu UV 2101 PC spectrophotometer at 23 ^{0}C, using a millimolar extinction coefficient of 18.5 for calculation. The non-enzymatic oxidation of $Q_0C_{10}BrH_2$, determined under the same conditions in the absence of enzyme, was subtracted from the assay. To measure bc_1 activity in chromatophores, 30 μM potassium cyanide was added to the assay mixture to inhibit the trace of cytochrome *c* oxidase activity.

To measure the effect of oxygen on bc_1 activity, a Thunberg cuvette was used. 1 ml of assay mixture was placed in the main chamber, and a 10-μl aliquot of enzyme (5-10 pmol) was in the side arm. The cuvette was evacuated and flushed with argon 5 times. The reaction was started by mixing the bc_1 complex solution and the assay mixture.

Measurement of Superoxide Anion Generation--Superoxide anion generation by the cytochrome bc_1 complex was determined by measuring the chemiluminescence of MCLA-$O2^{-\cdot}$ adduct (19), in an Applied Photophysics stopped-flow reaction analyzer SX.18MV (Leatherhead, England), by leaving the excitation light off and registering light emission (20). Reactions were carried out at 23 °C by mixing 1:1 solutions A and B.

Solution A contains 100 mM Na^+/K^+ phosphate buffer, pH 7.4, 1 mM EDTA, 1 mM KCN, 1 mM NaN_3, 0.1% BSA, 0.01% DM and an appropriate amount of wild-type or mutant bc_1 complex. Solution B was the same as A with bc_1 complex being replaced with 50 μM $Q_0C_{10}BrH_2$ and 4 μM MCLA. $O_2^{\cdot -}$ generation is expressed in XO units. One XO unit is defined as chemiluminescence (maximum peak height of light intensity) generated by 1 unit of xanthine oxidase, which equals 2.71 V from an Applied Photophysics stopped-flow reaction analyzer SX.18MV, when solution A containing 100 mM Na^+/K^+ phosphate buffer, pH 7.4, 100 μM hypoxanthine, 4 μM MCLA, and 1 mM NaN_3 is mixed with solution B containing 100 mM Na^+/K^+ phosphate buffer, pH 7.4, 1 mM NaN_3, and 50 units/ml of xanthine oxidase.

Other Biochemical and Biophysical Techniques--Protein concentration was determined by the method of Lowry et al. (21). The protein sample was diluted to a concentration of 0.1-0.5 mg/ml. To 0.2 ml of the diluted sample, 1 ml of copper-alkali solution was added. The copper-alkali solution contained 0.01% of copper sulphate ($CuSO_4 \cdot 5H_2O$), 0.02% of sodium potassium tartrate, 0.1 M of sodium hydroxide and 2% of sodium carbonate. After mixing and incubating for 10 min, 0.05 ml of Folin-Ciocalteau's phenol reagent (Sigma F-9252) was added. The absorbance at 550 nm was read after 30 min incubation. Bovine serum albumin (BSA) was used as a standard to estimate the protein concentration of the sample. The content of cytochrome *b* was determined from the sodium dithionite reduced minus potassium ferricyanide spectrum using the extinction coefficient of 28.5 $mM^{-1}cm^{-1}$ for wavelength pair 560 and 576 nm (22) and the content of cytochrome c_1 was from the sodium ascorbate reduced minus potassium ferricyanide spectrum using 17.5 $mM^{-1}cm^{-1}$ as the extinction coefficient for wavelength pair 552 and 537 nm (23). SDS-PAGE was performed according to Laemmli (24) using a Bio-Rad Mini-Protean dual slab vertical cell. Samples were digested with 10 mM Tris-Cl buffer, pH 6.8, containing 1% SDS, and 3% glycerol in the presence of 0.4% β-mercaptoethanol for 2 h at 37 °C before being subjected to electrophoresis.

EPR spectra of *b* cytochromes were recorded at 8.5 K on a Bruker EMX EPR spectrometer equipped with an Air Products flow cryostat. The instrument settings are detailed in the figure legend. Refined coordinates for the crystal structure of native bovine mitochondrial bc_1 (25, PDB code 1NTM) were used for distance determination.

Results and Discussion

Involvement of the F195 of Cytochrome *b* in Electron Transfer Activity of the Cytochrome bc_1 Complex--Three aromatic amino acid residues in cytochrome *b*: F195, Y199, and F203, were selected for mutation to test the hypothesis that inter-monomer b_L-b_L electron transfer occurs during bc_1 catalysis and such electron transfer is facilitated by aromatic residues located between the two b_L hemes. Alignment of more than 40 sequences of cytochrome *b* reveals that F195 is fully conserved except in *R. virids* (in which F is replaced by Y); Y199 is highly conserved although it is replaced by F in many cases; and F203 is less conserved, being substituted with M, S, L and W in some species (26). The selection of these three residues was based on the three-dimensional structure of the four-subunit cytochrome bc_1 complex of *R. sphaeroides* (see Figure 20A) constructed by using coordinates from bovine cytochromes *b* and c_1, ISP, and subunit VII (27). The distances between the symmetry pairs of aromatic residues F195, Y199, or F203 are 4.5, 7.7, and 6.8 Å (see Figure 20B), respectively, when measured from edge to edge of the phenyl rings of the amino acid residues. They are, edge to edge, 3.8, 3.7, and 3.3 Å apart, respectively, in the corresponding residues in the bovine complex (F179, F183 and F187 in bovine). The distances from heme b_L to F195, Y199, or F203 are 8.8, 4.9. 10.3 Å, respectively, when measured from the iron center to the edges of the aromatic ring of the amino acid residues. They are 7.5, 8.6, and 10.2 Å, respectively, in the corresponding bovine enzyme. Recently a relative low resolution structure of cytochrome bc_1 complex from *Rhodobacter capsulatus* was reported (28). The distances obtained among these aromatic amino acids pairs are surprisingly close to those deduced from model of *R. sphaeroides'* complex.

When each of these three aromatic residues was replaced with alanine, the resulting mutants (F195A, Y199A, and F203A) grew photosynthetically at a rate comparable to that of the complement (wild-type) cells. Chromatophores prepared from these mutants have, respectively, 80, 100, and 100% of the bc_1 activity found in the complement chromatophores (see Table 5). When cytochrome bc_1 complexes prepared from these three mutant chromatophores were assayed for ubiquinol-cytochrome *c* reductase activity, the Y199A and F203 mutant complexes had the same activity as the complement complex and the F195 mutant complex had about 78% (see Table 5). These results indicate that F195 of cytochrome *b* is involved in inter-monomer electron transfer in the dimeric bc_1 complex, but residues Y199 or F203 are not.

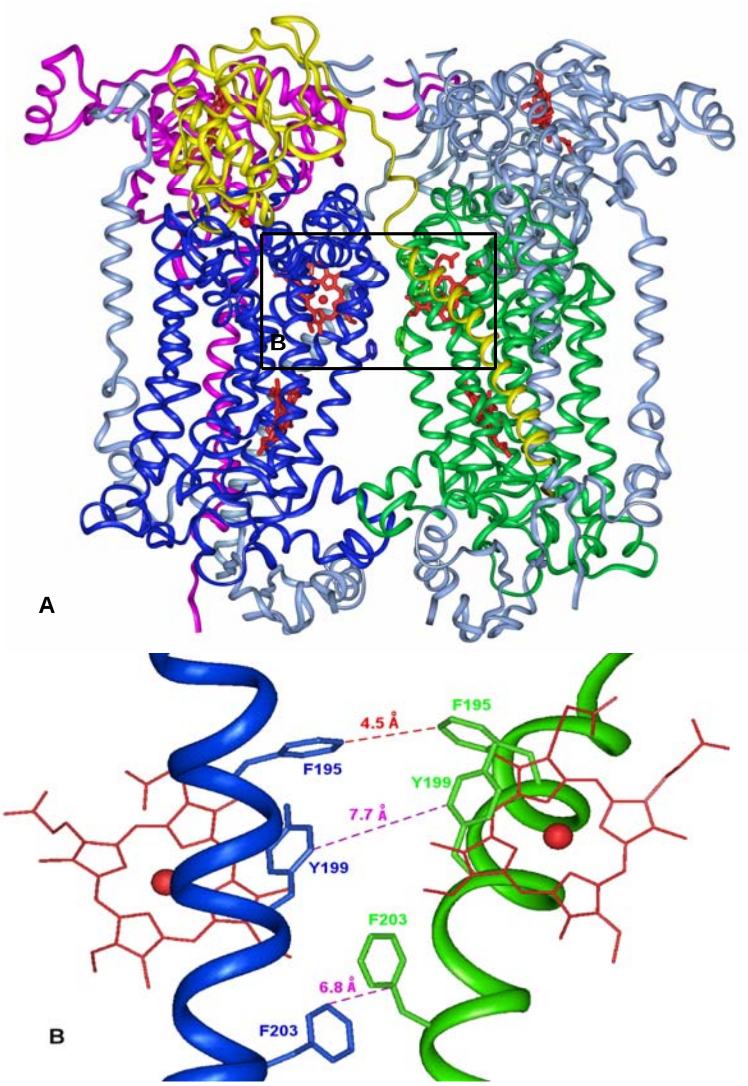

Figure 20. Location of mutated aromatic residues in the structural model of the *R. sphaeroides* *bc*$_1$ complex. In the upper panel (A), cytochrome *b* is shown in blue ribbon in one monomer and green in the symmetric monomer, ISP (from the symmetric monomer) is in yellow, and cytochrome c_1 from the same monomer is in pink. Both subunit IVs, ISP (from one monomer) and cytochrome c_1 (from the symmetric monomer) are shown in turquoise. All hemes are indicated by red sticks. The mutated aromatic residues are indicated by blue sticks in cytochrome *b* in one monomer and green sticks in the symmetric monomer. The lower panel (B) shows the residues located on the interface of two b_L hemes, and mutated to alanine, from different cytochrome *b*'s. Some peptide sequences have been omitted for clarity. The nearest edge to edge distances between aromatic residues from different monomers are indicated.

Mutants with double and triple alanine substitutions in these three aromatic residues of cytochrome *b* were also generated and characterized. These are: F195A/Y199A, F195A/ F203A, Y199A/F203A, and F195A/Y199A/F203A. All but theY199A/F203A mutant complex have about 78% of the activity found in the complement complex (see Table 5). The Y199A/F203A has the same activity as that of the complement complex. Since the extent of bc_1 activity decrease in the double or triple alanine substitution mutants containing the F195A mutation is the same as that observed for the F195A mutant complex, aromatic residues Y199 and F203 apparently play no complementary or auxiliary role to residue F195 in inter-monomer electron transfer.

Since the extent of activity change upon the replacement F195 with alanine is relatively small, 22% decrease, special attention was paid during data collection. The experiments were not only repeated three times but also repeated by different investigators. We are very confident that the difference in activity is real and not an experimental artifact. As matter of fact the small change in activity observed upon replacement of aromatic amino acid with an alanine at residue position 195 is expected, because the inter-monomer electron transfer is not in the main path of electron transfer.

Absorption spectral analysis of mutant complexes of F195A, F195A/Y199A, F195A/F203A, and F195A/Y199A/F203A indicates that the amounts and absorption properties of cytochromes *b* and c_1 in these mutant complexes are the same in the complement complex. Western blot analysis using antibodies against *R. sphaeroides* ISP and subunit IV also indicate that these mutant complexes have the same amount of ISP and subunit IV as does the complement complex. Thus the decrease in bc_1 activity in the

Table 5. Characterization of mutants in the cytochrome *b* of the bc_1 complex

Mutants	Photosynthetic growth	Activity	
		Chromatophore	bc_1 complex[a]
		S.A.[b]	S.A.[b]
Wild type	+ +[c]	2.21 ± 0.03	2.50 ± 0.01
F195A	+ +	1.76 ± 0.04	1.94 ± 0.02
Y199A	+ +	2.21 ± 0.03	2.52 ± 0.03
F203A	+ +	2.20 ± 0.03	2.51 ± 0.02
F195Y	+ +	2.22 ± 0.03	2.50 ± 0.01
F195W	+ +	2.20 ± 0.02	2.49 ± 0.03
F195H	+ +	2.21 ± 0.01	2.50 ± 0.02
F195A/Y199A	+ +	1.76 ± 0.02	1.95 ± 0.02
F195A/F203A	+ +	1.78 ± 0.01	1.93 ± 0.03
Y199A/F203A	+ +	2.20 ± 0.02	2.50 ± 0.02
F195A/Y199A/F203A	+ +	1.77 ± 0.01	1.96 ± 0.02

[a] The purified bc_1 complex was in 50 mM Tris-Cl, pH 8.0, containing 200 mM NaCl, 200 mM histidine, and 0.5% octyl glucoside.

[b] Specific activity (S.A.) is expressed as μmol cytochrome *c* reduced/min/nmol cytochrome *b* at room temperature.

[c] + +, cell growth rate is essentially the same as that of the wild type cells.

The data presented are mean values ± SD (standard deviation) from three experiments.

F195A mutant complex is not due to mutational effects on the assembly of the bc_1 protein subunits into the chromatophore membrane or to changes in the binding affinity of protein subunits in the complex.

Although the three pairs of aromatic residues are all located at the dimer interface of the cytochrome *b* subunits, they are not the only residues contributing to the stability of the dimer. As observed in the bovine complex, at least 23 residue pairs from a cytochrome *b* subunit make contact at the dimer interface, most are from the transmembrane (TM) helices of A and E, from the AB loop and from the N-terminal helix. In addition, the ISP TM helix and the head domain make substantial contributions to holding the dimer together. As the cytochrome *b* and ISP subunits are highly conserved, it is reasonable to believe that the interaction at the dimer interface would also be conserved. Since the structural effect of these mutations is probably creation of small cavities, it is not surprising to find that even the triple mutation does not disturb the structural integrity of the bc_1 dimer.

In bovine cytochrome *b* the three interfacial aromatic pairs display three entirely different contact geometries: the Phe179 pair (195 in *R. sphaeroides* bc_1) has an on-edge interaction with the two phenyl rings aligned roughly parallel to the membrane plane; with an angle between the two planes of 37°; the phenyl rings of the Phe183 pair (199 in *R. sphaeroides* bc_1) are stacked on top of each other with an angle of 0°; the Phe187 pair (203 in *R. sphaeroides* bc_1) is partially stacked and these two phenyl rings are normal to the membrane plane with an angle between the two rings of 34.7°. In biological electron transfer complexes such as the cytochrome bc_1 complex (1) and photosynthetic reaction centers (29), donors and receptors of electron transfer machines are always observed in an on-edge arrangement, as determined by x-ray crystallography. Presumably the on-edge interaction between partners provides more efficient electron transfer than other orientations. The observed on-edge interaction for the Phe179 pair in the bovine bc_1 structure strongly supports our mutational data indicating that this particular pair mediates lateral electron transport between bc_1 monomers. In addition, Phe179 has the shortest distance to the Qo site, which may also be advantageous for its role as an electron transfer mediator between monomers.

Essentiality of the Aromatic Group in the F195 of Cytochrome *b*--To establish that the loss of ubiquinol-cytochrome *c* reductase activity in the F195A mutant complex results from the loss of an aromatic ring at this position of cytochrome *b*, mutants with conservative substitution at F195 (F195Y, F195W, and F195H), were generated and characterized. These three mutants grew photosynthetically at a rate comparable to that of the complement cells and, in bc_1 complexes in chromatophore membranes or in the purified state, have the same ubiquinol-cytochrome *c* reductase activity as that of the complement complex (see Table 5). These results confirm the essentiality of an aromatic group at position 195 of cytochrome *b* in the electron transfer of the bc_1 complex. Since F195 is located between two b_L hemes in the dimeric bc_1 complex, and its role is to facilitate the lateral, inter-monomer b_L-b_L electron transfer; the essentiality of aromaticity in this residue is apparent.

Superoxide Anion Generation by Cytochrome bc_1 Complexes with the F195A Mutation--It has been reported that during electron transfer through the bc_1 complex, the second electron of ubiquinol can shift from the "low-potential" chain and react with molecular oxygen to produce superoxide anion ($O_2^{\cdot-}$). The electron leakage site has been identified as ubisemiquinone of the Qo site or reduced cytochrome b_L. If inter-monomer b_L-b_L electron transfer occurs in the bc_1 complex and the aromatic group in the F195 facilitates this lateral electron transfer, one would expect to see an increase in the rate of $O_2^{\cdot-}$ generation by the F195A mutant, compared to that by the complement complex, due to accumulation of electrons in the b_L heme of the mutant. This accumulation would increase the chance of leakage from the normal pathway, at reduced heme b_L or the ubisemiquinone of the Qo site, and reaction with oxygen to form $O_2^{\cdot-}$. Therefore, one way to confirm that the aromatic group in F195 participates in inter-monomer b_L-b_L electron transfer during bc_1 catalysis is to compare superoxide anion radical generation by the complement and F195A mutant complexes.

Although the rate of superoxide anion production by the cytochrome bc_1 complex can be determined by measuring the decrease in rate of cytochrome *c* reduction in the presence of superoxide dismutase under conditions of continuous turnover of the bc_1 complex, the small rate of superoxide anion formation, compared to the normal rate of cytochrome *c* reduction, compromises the accuracy of this method. MCLA has a high sensitivity for $O_2^{\cdot-}$ in the neutral pH range (30,31). The MCLA chemiluminescence method, which has been widely used to detect $O_2^{\cdot-}$ (10, 32-34), is 95 times more sensitive than the cytochrome *c* reduction method (35). However, use of the MCLA- $O_2^{\cdot-}$ chemiluminescence method to determine the rate of superoxide anion production during continuing turnover of the bc_1 complex (in the presence of ubiquinol and cytochrome *c*), encounters a high background rate of $O_2^{\cdot-}$ production resulting from the non-enzymatic oxidation of ubiquinol by cytochrome *c*, making it difficult to unambiguously compare rates of $O_2^{\cdot-}$ generation in complement and F195A mutant complexes. This difficulty has been overcome by measuring the chemiluminescence of the MCLA-$O_2^{\cdot-}$ adduct during a single turnover of bc_1 complex, using the Applied Photophysics stopped-flow reaction analyzer SX.18 MV. By leaving the excitation light source off, the chemiluminescence of MCLA-$O_2^{\cdot-}$, generated when cytochrome bc_1 complex is mixed with ubiquinol and MCLA, is registered in light emission. Since the system contains no cytochrome *c*, chemiluminescence of MCLA- $O_2^{\cdot-}$, resulting from non-enzymatic oxidation of ubiquinol by cytochrome *c,* is eliminated. This method enables us to accurately evaluate changes in the rate of superoxide anion generation by various bc_1 complexes.

Figure 21 shows actual tracings of superoxide generation by wild-type and F195A mutant bc_1 complexes. MCLA chemiluminescence induced by bc_1 complex reaches peak intensities after approximately 0.06 sec at room temperature and then decays. No detectable luminescence is detected when bc_1 complex is omitted from the enzyme-containing solution or $Q_0C_{10}BrH_2$ is omitted from the substrate-containing solution. Addition of superoxide dismutase to either the substrate or enzyme solution completely abolishes luminescence, indicating that $O_2^{\cdot-}$ is responsible for the luminescence observed. Maximum peak height induced by the F195A mutant complex (0.13 volts) is about three times higher than that reached by the wild-type complex.

Table 6 compares the rates of $O_2^{\cdot-}$ generation by the complement and mutant cytochrome bc_1 complexes. Oxidation of ubiquinol by complement and F195A mutant complexes produces 0.17 and 0.49 XO units of $O_2^{\cdot-}$ per mg protein, respectively. A similar increase in the rate of $O_2^{\cdot-}$ production is observed in mutant complexes of F195A/Y199A, F195A/F203A, and F195A/Y199A/F203A. However, the rates of $O_2^{\cdot-}$ production by mutant complexes Y199A, F203A, and Y199A/F203A are similar to that of the complement complex. These results support the idea that the decrease in bc_1 activity in the F195 mutant complex results from interruption of the inter-monomer b_L-b_L electron transfer, facilitated by the aromatic group in position F195.

Effect of Oxygen on Cytochrome *c* Reduction by Cytochrome bc_1 Complex--Table 7 shows the effect of oxygen on the cytochrome bc_1 activity in purified complexes from wild type and mutants F195A, Y199A and F203A. The complement, Y199A and F203A mutant complexes catalyzed electron transfer, from ubiquinol to cytochrome *c*, at a rate of 2.5 µmol cytochrome *c* reduced per min per nmol cytochrome *b* at 23 ˚C under aerobic conditions. Removal of oxygen from the assay system increases the activities of these four complexes by 4% (2.6 µmol cytochrome *c* reduced per min per nmol cytochrome *b*). It should be noted that this activity increase is not due to the inhibition of the contaminated cytochrome *c* oxidase in the bc_1 preparation, since addition of sodium azide to the assay mixture, under aerobic conditions, does not increase the rate of cytochrome *c* reduction. Addition of superoxide dismutase to the assay mixture causes a 5.2 % activity decrease in the complement, Y199A and F203A cytochrome bc_1 complexes. Apparently the $O_2^{\cdot -}$ generated from the electron leak at the Qo site is capable of reducing cytochrome *c* at a slightly lower rate than normal electron transfer through bc_1 complex. Addition of superoxide dismutase to the assay system converts the $O_2^{\cdot -}$ into hydrogen peroxide, which reduces cytochrome *c* very slowly, and thus decreases the rate of cytochrome *c* reduction. From the activity of cytochrome bc_1 complex, determined by reduction of cytochrome *c* in the presence or absence of oxygen, one can estimate the rate of cytochrome *c* reduction by $O_2^{\cdot -}$. It is about 3 quarters of the rate of cytochrome *c* reduction by bc_1 complex.

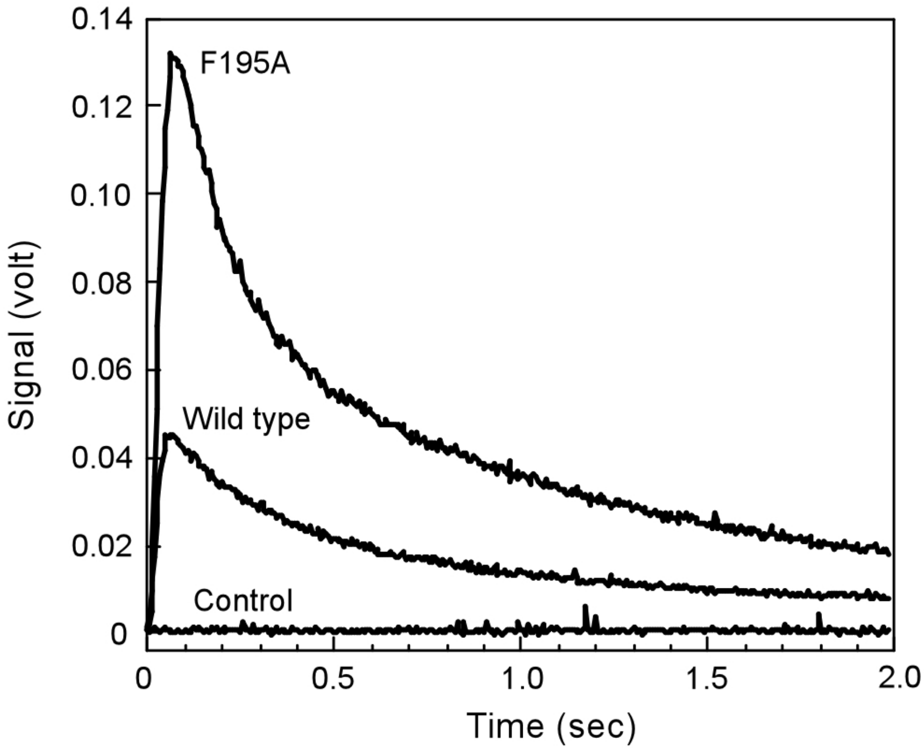

Figure 21. Tracings of superoxide generation in wild-type and mutant F195A cytochrome bc_1 complexes. To measure the superoxide anion production during the pre-steady state reaction of the reduction of the bc_1 complex by ubiquinol, stopped-flow assays were carried out at 23^0C in an Applied Photophysics stopped-flow reaction analyzer SX 18MV by mixing 1:1 solutions A and B. Solution A consisted of 100 mM Na^+/K^+ phosphate buffer, pH 7.4, containing 1 mM EDTA, 1 mM KCN, 1 mM NaN_3, 0.1% BSA, 0.01% DM and 9 μM bc_1 complexes. Solution B was the same as solution A except that the bc_1 complex was replaced with 50 μM $Q_0C_{10}BrH_2$ and 4 μM MCLA. For each sample, eight kinetic traces were averaged. For control, either bc_1 complexes or $Q_0C_{10}BrH_2$ were omitted from the above system, or 300 units/ml SOD was added to the system.

Table 6. Production of superoxide anion by purified wild-type and mutant complexes

Strains	Superoxide anion[a]
	XO units / mg protein
Wild type	0.17 ± 0.02
F195A	0.49 ± 0.01
Y199A	0.16 ± 0.02
F203A	0.17 ± 0.03
F195A/Y199A	0.47 ± 0.03
F195A/F203A	0.49 ± 0.02
Y199A/F203A	0.18 ± 0.02
F195A/Y199A/F203A	0.48 ± 0.01

[a] XO units are defined under "Experimental Procedures." For the experimental conditions, see the legend to Fig. 21. The data presented are mean values ± SD from five experiments.

Table 7. Effect of oxygen on the activity of cytochrome bc_1 complex purified from wild type and mutants

Preparations	Specific activity[a]	
	Aerobic	Anaerobic
	μmol cyt c red /min /nmol cyt b	
Wild type	2.50 ± 0.01	2.60 ± 0.03
F195A	1.94 ± 0.02	2.39 ± 0.04
Y199A	2.52 ± 0.02	2.60 ± 0.03
F203A	2.51 ± 0.03	2.61 ± 0.03

[a] To measure the effect of oxygen on bc_1 activity, 1 ml of assay mixture containing 100 mM Na^+/K^+ phosphate buffer, pH 7.4, 300 μM EDTA, 100 μM cytochrome *c*, and 25 μM $Q_0C_{10}BrH_2$ was placed in the main chamber, and a 10-μl aliquot of enzyme with cytochrome *b* of 1μM was in the side arm of a Thunberg cuvette. Complete anaerobic conditions were achieved by evacuating and flushing with argon five times. The reaction was started by tipping the bc_1 complex solution in the side arm into the main chamber. The measurement and calculation of activity were as described in "Experimental Procedures". The data presented are mean values ± SD from five experiments.

When bc_1 complex from mutant F195A was assayed in the presence and absence of oxygen, the activities were 1.93 and 2.39 μmol cytochrome *c* reduced per min per nmol cytochrome *b*, respectively. This amounts to a 24 % activity increase in the absence of oxygen. Under aerobic conditions, addition of superoxide dismutase to the assay mixture causes the activity of the F195A mutant complex to decrease from 1.93 to 1.70 μmol cytochrome *c* reduced per min per nmol cytochrome *b*. This indicates that 12 % of the observed activity (reduction of cytochrome *c*) is due to $O_2^{\cdot -}$. The disruption of electron transfer between the two b_L hemes in dimeric cytochrome bc_1 complex enhances (from 5.2 to 12%) the electron leakage and decreases (2.61 to 2.39 μmol cytochrome *c* reduced per min per nmol cytochrome *b*) the normal electron transfer rate during oxidation of ubiquinol and reduction of cytochrome *c*. Since under the anaerobic conditions the activity of F195A mutant complex is not restored to the level of the activity of the complement complex, activity loss due to disruption of electron transfer between the two hemes b_L can not attributed entirely to electron leak to oxygen. About half of the activity loss is due to disruption of electron transfer between the two hemes b_L. In the presence of inter-monomer electron transfer, the electron at Qo (either at b_L or ubisemiquinone) of one monomer can be oxidized by the two hemes b_H of the complex. When inter-monomer electron transfer is interrupted, as in the F195A mutant complex, the electron at heme b_L can only be oxidized by heme b_H of the same monomer; this accounts for a 9% decrease of activity. Another explanation for activity decrease in the F195A mutant complex is the relatively more oxidized state of hemes b_L in dimeric bc_1 complex with inter heme b_L electron transfer than in those without. This more oxidized state of heme b_L would facilitate electron transfer from ubisemiquinone at Qo site. The fact that disruption of electron transfer between two b_L hemes of dimeric complex causes a decrease of activity indicates that both monomers are not functioning independently, some sort of negative cooperativity does exist (6).

Effect of F195A on EPR Characteristics of the *b* Cytochrome--Although evidence presented above clearly demonstrates that the loss of bc_1 complex activity in mutants, F195A, F195A/Y199A, F195A/F203A, and F195A/Y199A/F203A, correlates with the leakage of electrons that normally shuttle between the two b_L hemes through F195, whether or not mutation F195A affects the microenvironments of the cytochromes *b* is unknown. To test this possibility, EPR characteristics of the *b* cytochromes in cytochrome *b* F195A and wild type were examined after samples were reduced with sodium ascorbate to eliminate the overlapping signal from cytochrome c_1. As shown in Figure 22, this mutant has EPR characteristics identical to those of the wild-type complex, with features at g = 3.53 and g = 3.77 previously assigned to cytochrome b_H and b_L, respectively, and a g = 4.29 signal thought to be due to nonspecifically bound iron (III) (36). These data indicate that substitution of F195 with alanine has no significant effect on the environments of cytochrome *b* heme. This mutation also has no effect on the midpoint potential of cytochromes *b*.

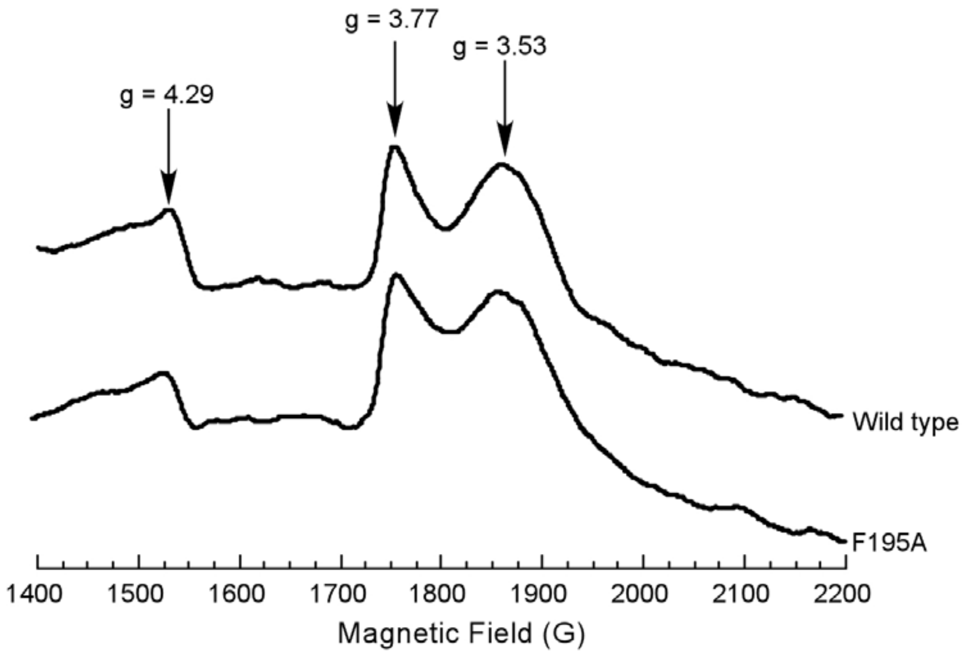

Figure 22. The EPR spectra of *b* cytochromes in purified complexes from wild type and cytochrome *b* F195A. Purified cytochrome bc_1 complexes (300 μM cytochrome *b*) were treated with just enough ascorbate solution to fully reduce cytochrome c_1 and frozen in liquid nitrogen. EPR spectra were recorded at 8.5 K on a Bruker EMX EPR spectrometer equipped with an Air Products flow cryostat with the following instrument settings: microwave frequency, 9.25 G; microwave power, 107.93 milliwatts; modulation amplitude, 20 G; modulation frequency, 100 KHz; time constant, 655 ms; sweep time, 167.8 s; conversion time, 163.8 ms.

References

1. Xia, D., Yu, C. A., Kim, H., Xia, J. Z., Kachurin, A. M., Zhang, L., Yu, L., and Deisenhofer, J. (1997) *Science* **277**, 60-66
2. Iwata, S., Lee, J. W., Okada, K., Lee, J. K., Iwata, M., Rasmussen, B., Link, T. A., Ramaswamy, S., and Jap, B. K. (1998) *Science* **281**, 64-71
3. Zhang, Z. L., Huang, L.-S., Shulmeister, V. M., Chi, Y.-I., Kim, K. K., Huang, L.-W., Crofts, A. R., Berry, E. A., and Kim, S.-H. (1998) *Nature* **392**, 677-684
4. Hunte, C., Koepke, J., Lange, C., Robmanith, T., and Michel, H. (2000) *Structure* **8**, 669-684
5. Soriano, G. M., Ponamarev, M. V., Carell, C. J., Xia, D., Smith, J., and Cramer, W. A. (1999) *J. Bioenerg. Biomembr*. 31, 201-213.
6. Covian, R., Gutierrez-Cirlos, E. B., and Trumpower, B. L. (2004) *J. Biol. Chem*. **279**, 15040-15049
7. Osyczka, A., Moser, C. C., Daldal, F. and Dutton, P. L. (2004) *Nature* 427, 607-612
8. Turrens, J. F., Alexandre, A., and Lehninger, A. L. (1985) *Arch. Biochem. Biophys.* **237**, 408-414
9. Nohl, H., and Jordan, W. (1986) *Biochem. Biophys. Res. Commun*. **138**, 533-539
10. Zhang, L., Yu, L., and Yu, C. A. (1998) *J. Biol. Chem*. **273**, 33972-33976
11. Muller, F., Crofts, A. R., and Kramer, D. M. (2002) *Biochemistry* **41**, 7866-7874
12. Staniek, K., Gille, L., Kozlov, A. V., Nohl, H. (2002) *Free Radic. Res.* **36**, 381-387
13. Muller, F., Roberts, A. G., Bowman, M. K., and Kramer, D. M. (2003) *Biochemistry* **42**, 6493-6499
14. Sun, J., and Trumpower, B. L. (2003) *Arch. Biochem. Biophys*. **419**, 198-206
15. Yu, C. A., and Yu, L. (1982) *Biochemistry* **21**, 4096-4101
16. Xiao, K., Liu, X., Yu, C. A., and Yu, L. (2004) *Biochemistry* **43**, 1488-1495
17. Mather, M. W., Yu, L., and Yu, C. A. (1995) *J. Biol. Chem*. **270**, 28668-28675
18. Tian, H., Yu, L., Mather, M. W., and Yu, C. A. (1998) *J. Biol. Chem*. **273**, 27953-27959
19. Nakano, M. (1990) *Methods Enzymol*. **186**, 585-591
20. Denicola, A., Souza, J. M., Gatti, R. M., Augusto, O., and Radi, R. (1995) *Free Radic. Biol. Med.* **19**, 11-19

21. Lowry, O. H., Rosebrough, N. J., Farr, A. L., and Randall, R. J. (1951) *J. Biol. Chem.* **193**, 265-275
22. Berden, J. A., and Slater, E. C. (1970) *Biochim. Biophys. Acta* **216**, 237-249
23. Yu, L., Dong, J. H., and Yu, C. A. (1986) *Biochim. Biophys. Acta* **852**, 203-211
24. Laemmli, U. K. (1970) *Nature* **227**, 680-685
25. Gao, X., Wen, X., Yu, C. A., Esser, L., Tso, S., Quinn, B., Zhang, L., Yu, L., and Xia, D. (2002) *Biochemistry* **41**, 11692-11702
26. Esposti, M. D., Vrits, S. D., Crimi, M., Gholli, A., Patarnello, T., and Meyer, A. (1993) *Biochim. Biophys. Acta.* **1143**, 243-271
27. Tso, S-C., Shenoy, S. K., Quinn, B., and Yu, L. (2000) *J. Biol. Chem*. **275**, 15287-15294
28. Berry, E. A., Huang, L.S., Saechao, L. K., Pon, N. G., Valkova-Valchanova, M. and Daldal, F. (2004) *Photosynthesis Research* **81**, 251-275.
29. Deisenhofer, J., and Michel, H. (1989) *Science* **245**, 1463-1473
30. Kambayashi, Y., and Ogino, K. (2003) *J. Toxicol. Sci*. **28**,139-148
31. Aoki, S., Ito-Kuwa, S., Nakamura, K., Nakamura, Y., Vidotto, V., and Takeo, K. (2002) *Med. Mycol.* **40**,13-19
32. Kishimoto, W., Nakao, A., Nakao, M., Takahashi, A., Inaba, H., and Takagi, H. (1995) *Pancreas* **11**, 122-126
33. Midorikawa, J., Maehara, K., Yaoita, H., Watanabe, T., Ohtani, H., Ushiroda, S., and Maruyama, Y. (2001) *Jpn Circ. J.* **65**, 207-212
34. Uehara, K., Maruyama, N., Huang, C. K., Nakano, M. (1993) *FEBS Lett*. **335**, 167-170
35. Nakano, M. (1990) in Methods in Enzymology (Packer, L. and Glazer, A. N. Eds.) Vol. 186, pp. 227-232. Academic Press, Inc. New York.
36. McCurley, J. P., Miki, T., Yu, L., and Yu, C. A. (1990) *Biochim. Biophys. Acta* **1020**, 176-186

CHAPTER IV

THE ROLE OF AN EXTRA FRAGMENT OF CYTOCHROME *b* (RESIDUES 309-326) IN THE CYTOCHROME *bc*$_1$ COMPLEX FROM *RHODOBACTER SPHAEROIDES*

Abstract

Sequence alignment of cytochrome *b* of the cytochrome *bc*$_1$ complex from various sources reveals that bacterial cytochrome *b* contains an extra fragment located between the amphipathic helix *ef* and the transmembrane helix F. To study the role of this fragment in bacterial cytochrome *bc*$_1$ complex, *Rhodobacter sphaeroides* mutants expressing His-tagged cytochrome *bc*$_1$ complexes with mutations at various positions of this fragment (residues 309-326) were generated and characterized. The cyt*b*-Δ(309-326) and cyt*b*-(309-326)A *bc*$_1$ complexes, in which all residues of this fragment are deleted or substituted with alanine, respectively, have about 20% of the *bc*$_1$ activity found in the complement complex. Mutant complexes of cyt*b*-(309-311)A, cyt*b*-(312-314)A, cyt*b*-(315-317)A, cyt*b*-(318-321)A, cyt*b*-(322-323)A, cyt*b*-(324-326)A, cyt*b*-(F323A), and cyt*b*-(S322A) have, respectively, 87, 85, 89, 100, 32, 90, 100 and 32% of the *bc*$_1$ activity detected in the complement complex, indicating that the S-322 of cytochrome *b* is critical. The g_x signal of the [2Fe-2S] cluster in the cyt*b*-(S322A) mutant complex becomes broadened and shifts

to g = 1.76. Replacing the Ser-322 of cytochrome *b* with Thr, Tyr, or Cys results in mutant complexes having the same bc_1 activity and EPR characteristics of the [2Fe-2S] cluster as the complement complex. The rate of superoxide anion ($O_2^{\cdot-}$) generation, measured during the oxidation of ubiquinol, is 4 times higher in the cyt*b*-(S322A) mutant complex than in the complement or mutant complexes of S322T, S322Y, or S322C. These support the idea that alanine substitution at S-322 of cytochrome *b* causes conformational changes of Q_o site by weakening the binding between cytochrome *b* and ISP through hydrogen bonding provided by the hydroxyl group of this residue. This change facilitates electron leakage from the Qo site to react with molecular oxygen to form superoxide anion thus decreasing the bc_1 activity.

Introduction

Study of cytochrome bc_1complex (Complex III) has advanced substantially as a result of molecular genetic manipulation of bacterial complex. Although bacterial enzymes have simpler subunit composition than their mammalian counter parts, the sizes of core subunits (cytochrome *b*, ISP and cytochrome c_1) are generally larger. Sequence alignment of bacterial cytochrome *b*, cytochrome c_1, and ISP with their counterparts in the mitochondrial complexes reveals four extra fragments in bacterial cytochrome *b*, one each in cytochrome c_1 and ISP (1).

Are these extra fragments required for bc_1 complex? One effective way to answer this question is by site-directed mutagenesis of residues in these extra fragments followed by stability and functional assay of mutant complexes. By using this approach, the cytochrome c_1 extra fragment and the N-terminus extra fragment of cytochrome *b* from *R.*

sphaeroides are found to be nonessential. The ISP extra fragment is required for structural stability of ISP in the complex (2), and the C-terminus extra fragment of cytochrome *b* is essential for maintaining structural integrity of the complex (3). However, the knowledge of the role of the second and third extra fragments of cytochrome *b* in *R. sphaeroides* bc_1 complex is still lacking.

The third extra fragment of cytochrome *b* (residues 309 to 326 in *R. sphaeriodes*) is in close proximity to the Qo site where electrons from ubiquinol are bifurcated according to the "proton-motive Q-cycle" mechanism (4). At the Qo site, the first electron of ubiquinol is transferred through the so-called "high-potential" chain consisting of [2Fe-2S] and heme c_1. The second electron of ubiquinol is passed through the "low-potential" chain including hemes b_L and b_H. It has been reported that, during the electron transfer through the bc_1 complex, the second electron of ubiquinol can shift from the low potential chain and react with molecular oxygen to form superoxide anion ($O_2^{\cdot-}$) (5-12). The electron leakage site has been thought to be located at the reduced cytochrome b_L or ubisemiquinone of the Qo site. Thus, studies the role of the third extra fragment in *R. sphaerodies* cytochrome *b* may help to understand structural elements involved in structural stability of the Qo site and thus lead to understand the bc_1 complex function.

Herein we report generation of *R. sphaeroides* mutants expressing His-tagged cytochrome bc_1 complexes with deletion or substitution at various positions in the third extra fragment of cytochrome *b* to investigate the role of this fragment in the bc_1 complex. The photosynthetic growth behavior, the bc_1 activity, and the amount of cytochrome *b*, cytochrome c_1, ISP and subuit IV in the chromatophore membrane and the purified state of the complement and mutants, were determined and compared to identify the critical amino acid residue(s). The effect of mutations on EPR spectra of ISP and on superoxide anion generation during ubiquinol oxidation by the complex is also examined.

Experimental Procedures

Materials--Cytochrome *c* (horse heart, type III), hypoxanthine, and superoxide dismutase (SOD), and xanthine oxidase were purchased from Sigma Chemical Co. Dodecylmaltoside (DM) and octylglucoside were from Anatrace. Nickel nitrilotriacetic acid (Ni-NTA) gel and a Qiaprep spin Miniprep kit were from Qiagen. 2-Methyl-6-(4-methoxyphenyl)-3,7-dihydroimidazol [1,2-α]pyrazin-3-one, hydrochloride (MCLA) was from Molecular Probes, Inc. 2,3-Dimethoxy-5-methyl-6-(10-bromodecyl)-1,4-benzoquinol ($Q_0C_{10}BrH_2$) was prepared in our laboratory as previously reported (13). All other chemicals were of the highest purity commercially available.

Growth of Bacteria--*E. coli* cells were grown at 37 °C in LB medium. Extra-rich media, *e.g.* TYP (1.6 g Bact-tryptone, 1.6 g Bacto-yeast extract, 0.5 g NaCl and 0.25 g K_2HPO_4 in 100 ml medium), were used in procedures for the rescue of single-stranded DNA or the purification of low copy number plasmids (14). For photosynthetic growth of the plasmid-bearing *R. sphaeroides* BC17 cells an enriched Siström's medium containing 5 mM glutamate and 0.2% casamino acids was used. Photosynthetic growth conditions for *R. sphaeroides* were essentially as described previously (15). Cells harboring the mutated cytochrome *b* gene on the pRKD418-*fbc*FB_mC_HQ plasmid were grown photosynthetically for one or two serial passages to minimize any pressure for reversion. The inoculation volumes used for photosynthetic cultures were at least 5% of the total volume. Antibiotics were added to the following concentrations: ampicillin (125 µg/ml), kanamycin sulfate

(30 μg/ml), tetracycline (10 μg/ml for *E. coli* and 1 μg/ml for *R. sphaeroides*), and trimethoprim (100 μg/ml for *E. coli* and 30 μg/ml for *R. sphaeroides*).

Generation of *R. sphaeroides* Strains Expressing the His_6-Tagged Cytochrome bc_1 Complexes with Mutations at the Extra Fragment of Cytochrome *b* (Residues 309-326)-- Mutations were constructed by site-directed mutagenesis using the Altered Sites II mutagenesis system from Promega or the QuikChange site-directed mutagenesis kit from Stratagene. The cyt*b*-(309-326)A mutant was constructed by the Altered Sites II mutagenesis method using single-stranded pSELNB3503 (16) as template and the following mutant oligonucleotide as the annealing primer, 5'-GCGATCCTGCGCGCC TTCGCCGCCGCCGCCGCCGCCGCCGCCGCCGCCGCCGCCGCCGCCGCCGCCGC CGCCGACGCCAAGTTCT-3'. The underlined bases correspond to the genetic codes for the target mutated amino acids. Other mutants were constructed by the QuikChange site-directed mutagenesis method, using a supercoiled double-stranded pGEM7Zf(+)-*fbc*FB as template and a forward and a reverse primer for PCR amplification. The pGEM7Zf(+)-*fbc*FB plasmid (2) was constructed by ligating the *Eco*RI-*Xba*I fragment from pSELNB3503 into *Eco*RI and *Xba*I sites of the pGEM7Zf(+) plasmid. The primers used are given in Table 8.

Following mutagenesis, a 962-base pair *BstE*II-*Xba*I fragment from pSELNB3503 or pGEM7Zf(+)-*fbc*FB plasmid containing the mutant cytochrome *b* gene was ligated into *BstE*II and *Xba*I sites of the low copy number plasmid, pRKD418-*fbc*FB_{KmBX}CHQ, to generate the pRKD418-*fbc*FB_mCHQ plasmid. Loss of kanamycin resistance was then used to screen for recombinant plasmids. The pRKD418-*fbc*FB_mCHQ plasmid in *E. coli* S17-1 cells were conjugated into *R. sphaeroides* BC17 cells by a plate-mating procedure (15).

The presence of engineered mutations and the absence of any additional changes in the template region were confirmed by DNA sequencing of the 962-base pair *Bst*EII-*Xba*I fragment before and after photosynthetic growth of the cells as previously reported (15). Expression plasmid pRKD418-*fbc*FB_mC_HQ was purified from an aliquot of a semi-aerobic and photosynthetic culture using the Qiagen Plasmid Mini Prep kit. Since *R. sphaeroides* cells contain four types of endogenous plasmids, the isolated plasmids lacked the purity and concentration needed for direct sequencing. Therefore, a 1,883-base pair DNA segment containing the mutation sequence was amplified from the isolated plasmids by PCR and purified by 1% agarose gel electrophoresis. The 1,883-base pair PCR product was recovered from the gel with an extraction kit from Qiagen. DNA sequencing and oligonucleotide syntheses were performed by the Recombinant DNA/Protein Core Facility at Oklahoma State University.

Enzyme Preparations and Activity Assay--Chromatophores were prepared, from which the His_6-tagged cytochrome bc_1 complexes were purified, as previously reported (16). Quantification of the bc_1 complexes was performed according to published methods using extinction coefficients of 28.5 $mM^{-1}cm^{-1}$ at 563-578 nm for cytochrome *b* (17), and 17.5 $mM^{-1}cm^{-1}$ at 553-539 nm for cytochrome c_1 (18). To assay ubiquinol-cytochrome *c* reductase activity, chromatophores or purified cytochrome bc_1 complexes were diluted with 50 mM Tris-Cl, pH 8.0, containing 200 mM NaCl and 0.01% DM to a final concentration of cytochrome *b* of 3 μM. Appropriate amounts of the diluted samples were added to 1 mL of assay mixture containing 100 mM Na^+/K^+ phosphate buffer, pH 7.4, 300 μM EDTA, 100 μM cytochrome *c*, and 25 μM $Q_0C_{10}BrH_2$. 30 μM potassium cyanide was added to the assay mixture when bc_1 activity in chromatophores was determined. For determination of apparent K_m for $Q_0C_{10}BrH_2$, various concentrations of $Q_0C_{10}BrH_2$ were used. Activities were determined by measuring the reduction of cytochrome *c* (the increase of absorbance at 550 nm) in a Shimadzu UV-2401 PC spectrophotometer at 23 ^{0}C, using a millimolar extinction coefficient of 18.5 for calculation. The non-enzymatic oxidation of $Q_0C_{10}BrH_2$, determined under the same conditions in the absence of enzyme, was subtracted from the assay.

Measurement of Superoxide Anion Generation--Superoxide anion generation by the cytochrome bc_1 complex was determined by measuring the chemiluminescence of MCLA-$O2^{-\cdot}$ adduct, in an Applied Photophysics stopped-flow reaction analyzer SX.18MV (Leatherhead, England), by leaving the excitation light off and registering light emission, as described previously (12). Reactions were carried out at 23 °C by rapid mixing 1:1 solutions A and B. Solution A contains 100 mM Na^+/K^+ phosphate buffer, pH 7.4, 1 mM EDTA, 1 mM KCN, 1 mM NaN_3, 0.1% BSA, 0.01% DM and an appropriate amount of wild-type or mutant bc_1 complex. Solution B was the same as A with bc_1 complex being replaced with 50 μM $Q_0C_{10}BrH_2$ and 4 μM MCLA. $O_2^{-\cdot}$generation is expressed in XO units. One XO unit is defined as chemiluminescence (maximum peak height of light intensity) generated by 1 unit of xanthine oxidase, which equals 2.71 V from an Applied Photophysics stopped-flow reaction analyzer SX.18MV, when solution A containing 100 mM Na^+/K^+ phosphate buffer, pH 7.4, 100 μM hypoxanthine, 4 μM MCLA, and 1 mM NaN_3 is mixed with solution B containing 100 mM Na^+/K^+ phosphate buffer, pH 7.4, 1 mM NaN_3, and 50 units/ml of xanthine oxidase.

Quantification of Endogenous Ubiquinone in Purified bc_1 Complexes--Ubiquinones were extracted from the purified bc_1 complexes with cyclohexane according to the procedure reported by Redfearn (19). A millimolar extinction coefficient of 12.25 $mM^{-1}cm^{-1}$ was used to as the difference in absorption of the oxidized and reduced forms of Q at 275 nm.

<u>Differential Scanning Calorimetry</u>--Calorimetric measurements were performed with a CSC 6100 NanoII DSC. The reference and sample solutions were carefully degassed under vacuum for 15 min prior to use. A 0.50-ml bc_1 solution, 2 mg/ml, in 50 mM K^+/Na^+ phosphate buffer, pH 7.4, containing 100 mM KCl and 0.002% DM, was placed in the sample capillary cell, and the same amount of buffer was placed in the reference capillary cell. All DSC scans reported in this study were run at a rate of 1^0C/min. After the first scan, the samples were cooled to the original temperature and rescanned. Since after the first scan the protein was completely and irreversibly denatured, no thermotransition peaks were observed in the second scan. Thus the second scan could be used as a baseline. All thermodynamic analyses were carried out according to the program known as CpCal from the Nano DSC program group.

<u>Other Biochemical and Biophysical Techniques</u>--Protein concentration was determined by the method of Lowry et al. (20). SDS-PAGE was performed according to Laemmli (21) using a Bio-Rad Mini-Protean dual slab vertical cell. Samples were digested with 10 mM Tris-Cl buffer, pH 6.8, containing 1% SDS, and 3% glycerol in the presence of 0.4% β-mercaptoethanol for 2 h at 37 °C before being subjected to electrophoresis. Western blotting was performed with rabbit polyclonal antibodies against ISP and subunit IV of the *R. sphaeroides* bc_1 complex (16). The polypeptides separated by SDS-PAGE gel were transferred to polyvinylidene difluoride membrane for immunoblotting. Goat anti-

rabbit IgG conjugated to alkaline phosphatase or protein A conjugated to horseradish peroxidase was used as the second antibody.

Redox titrations of cytochromes *b* and c_1 in complement and mutant bc_1 complexes were conducted potentionmetrically according to the previously published method (3,22,23), using a Shimadzu model UV-2410 spectrophotometer. 3-ml aliquots of the bc_1 complex (2 μM cytochrome *b*) in 0.1 M Na^+/K^+ phosphate buffer, pH 7.0, were used in the presence of 20 μM phenazine methosulfate (midpoint redox potential (E_m) +80 mV), 20 μM phenazine ethosulfate (E_m +55 mV), 20 μM phenazine (E_m -120 mV), 20 μM pyocyanine (E_m -34 mV), 25 μM 1,4-benzoquinone (E_m +293 mV), 25 μM 1,2-naphthoquinone (E_m +143 mV), 25 μM 1,4-naphthoquinone (E_m +36 mV), 50 μM duroquineone (E_m +5 mV), 70 μM 2,3,5,6-tetramethyl-*p*-phenylenediamine (E_m +260 mV), and 15 μM 2-hydroxy-1,4-naphthoquinone (E_m -145 mV) as mediators. Samples were poised at desired redox potentials (*E*h) using sodium dithionite or potassium ferricyanide solution.

Low temperature EPR spectra were recorded with a Bruker EMX EPR spectrometer equipped with an Air Products flow cryostat. The instrument setting details are provided in the legend of the relevant figure.

Table 8. Oligonucleotides used for site-directed mutagenesis (F and R in the parentheses denote forward and reverse primers, respectively)[a]

cyt*b*Δ-(309-326) (F)	5'-CCTTCTACGCGATCCTGCGCGCCTTCGACGCCAAGTTCTTCGGCGTG -3'
cyt*b*Δ-(309-326) (R)	5'-CACGCCGAAGAACTTGGCGTCGAAGGCGCGCAGGATCGCGTAGAAGG -3'
cyt*b*-(309-311)A (F)	5'-CTGCGCGCCTTCGCCGCCGCCGTCTGGGTGGTGCAGATCGCCAAC-3'
cyt*b*-(309-311)A (R)	5'-GTTGGCGATCTGCACCACCCAGACGGCGGCGGCGAAGGCGCGCAG-3'
cyt*b*-(312-314)A (F)	5'-GCCTTCACCGCCGACGCCGCGGCGGTGCAGATCGCCAAC-3'
cyt*b*-(312-314)A (R)	5'-GTTGGCGATCTGCACCGCCGCGGCGTCGGCGGTGAAGGC-3'
cyt*b*-(315-317)A (F)	5'-CCGCCGACGTCTGGGTGGCCGCCGCCGCCAACTTCATCAGCTTC-3'
cyt*b*-(315-317)A (R)	5'-GAAGCTGATGAAGTTGGCGGCGGCGGCCACCCAGACGTCGGCGG-3'
cyt*b*-(318-321)A (F)	5'-GGGTGGTGCAGATCGCCGCCGCCGCCAGCTTCGGCATC-3'
cyt*b*-(318-321)A (R)	5'-GATGCCGAAGCTGGCGGCGGCGGCGATCTGCACCACCC-3'
cyt*b*-(322-323)A (F)	5'-CGCCAACTTCATCGCCGCCGGCATCATCGACGCCAAGTTCTTC-3'
cyt*b*-(322-323)A (R)	5'-GAAGAACTTGGCGTCGATGATGCCGGCGGCGATGAAGTTGGCG-3'
cyt*b*-(324-326)A (F)	5'-GCCAACTTCATCAGCTTCGCCGCCGCCGACGCCAAGTTCTTC-3'
cyt*b*-(324-326)A (R)	5'-GAAGAACTTGGCGTCGGCGGCGGCGAAGCTGATGAAGTTGGC-3'

cyt*b*-(S322A) (F)	5'-CGCCAACTTCATCGCCTTCGGCATCATCG ACGCCAAG-3'
cyt*b*-(S322A) (R)	5'-CTTGGCGTCGATGATGCCGAAGGCGATGA AGTTGGCG-3'
cyt*b*-(F323A) (F)	5'-GCCAACTTCATCAGCGCCGGCATCATCGA CGCCAAG-3'
cyt*b*-(F323A) (R)	5'-CTTGGCGTCGATGATGCCGGCGCTGATGA AGTTGGC-3'
cyt*b*-(S322T) (F)	5'-CGCCAACTTCATCACCTTCGGCATCATCG ACGCCAAG -3'
cyt*b*-(S322T) (R)	5'-CTTGGCGTCGATGATGCCGAAGGTGATGA AGTTGGCG-3'
cyt*b*-(S322C) (F)	5'-CGCCAACTTCATCTGCTTCGGCATCATCG ACGCCAAG -3'
cyt*b*-(S322C) (R)	5'-CTTGGCGTCGATGATGCCGAAACGGATGA AGTTGGCG-3'
cyt*b*-(S322Y) (F)	5'-CGCCAACTTCATCTACTTCGGCATCATCG ACGCCAAG -3'
cyt*b*-(S322Y) (R)	5'-CTTGGCGTCGATGATGCCGAAATGGATGA AGTTGGCG-3'

[a] The underlined bases correspond to the genetic codes for the amino acid(s) to be mutated.

Results and Discussion

<u>The Requirement of an Extra Fragment of Cytochrome *b* (residues 309-326) for the Cytochrome *bc*$_1$ Complex</u>--*R. sphaeroides* cytochrome *b* has an extra fragment that corresponds to residues 309-326 with a sequence of –TADVWVVQIANFISFGII– (see Figure 10). This fragment is located between the amphipathic helix *ef*, a key structural component of the Qo site**,** and the transmembrane helix F of the cytochrome *b* sequence, in the modeled 3-D structure of *R. sphaeroides bc*$_1$ complex (see Figure 23) or in the low resolution 3-D structure of the *R. capulatus bc*$_1$ complex (24). To probe the role of this fragment, *R. sphaeroides* mutants expressing His$_6$-tagged *bc*$_1$ complexes with deletion or substitution at various positions of the extra fragment were generated and characterized.

When this extra fragment is deleted from the cytochrome *b* sequence, the resulting cells [cyt*b*-Δ(309-326)] after a long lag time (when the wild-type cells have grown to stationary phase under the same conditions) starts to grow photosynthetically at a rate comparable to that of the complement (wild-type) cells. Chromatophores prepared from this mutant have only 20% of the *bc*$_1$ activity found in the complement chromatophores (see Table 9). A similar electron transfer activity is found in the *bc*$_1$ complex purified from this mutant chromatophores (see Table 9). These results indicate that this region is required for *bc*$_1$ complex activity.

To further confirm that a decrease in *bc*$_1$ activity found in the [cyt*b*-Δ(309-326)] mutant complex results from the essentiality of this extra fragment for the *bc*$_1$ complex, and not from improper protein assembly or folding due to the large deletion, a mutant with this extra fragment substituted with alanine [cyt*b*-(309-326)A] was generated and

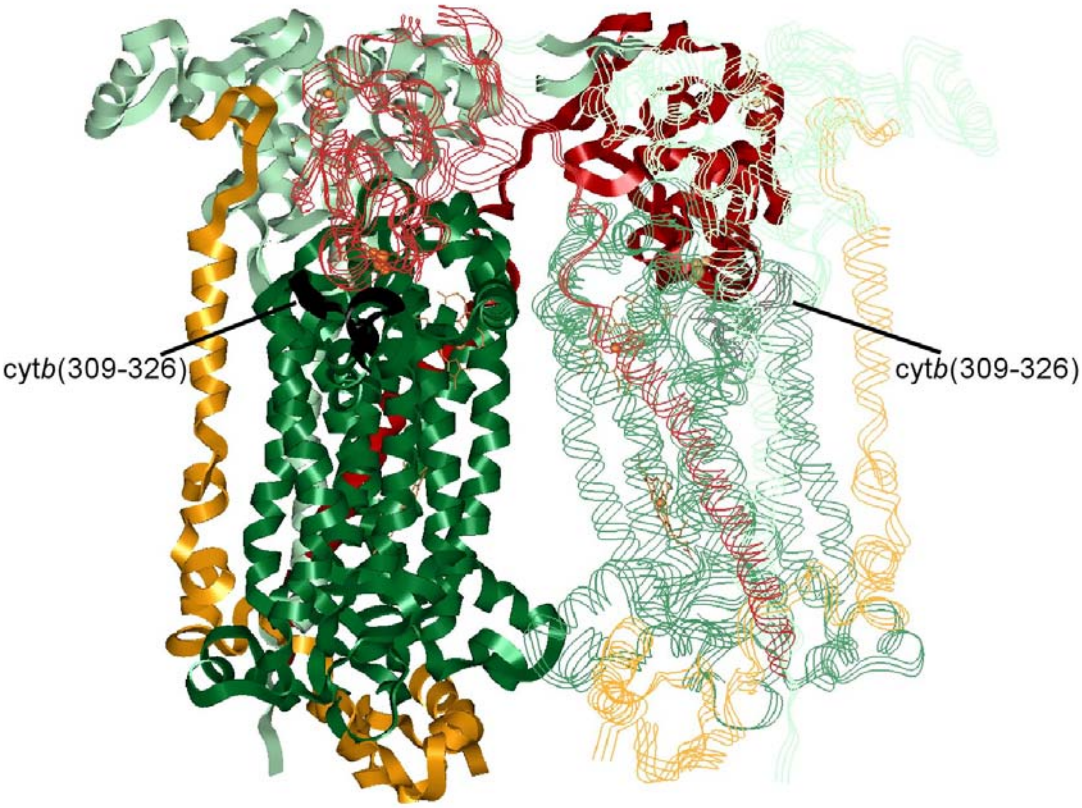

Figure 23. Location of an extra fragment of cytochrome *b* (residues 309-326) in the proposed structural model of *R. sphaeroides bc*$_1$ complex. One monomer *(left)* is displayed in solid ribbons, and the symmetric monomer *(right)* is displayed in three-tread-line ribbons. Cytochrome c_1 is *silver*; ISP is *brown*; subunit IV is *rust*; cytochrome *b* is *green*; and the extra fragment (residues 309-326) is colored in *black*.

Table 9. Characterization of mutants in the cytochrome *b* of the bc_1 complex

Mutants	Photosynthetic growth	The bc_1 complex activity	
		Chromatophore	Purified complex [a]
		S.A.[b]	S.A.[b]
Wild type	+ + [c]	2.21 (100%)	2.50 (100%)
cyt*b*-Δ(309-326)	+ [d]	0.44 (20%)	0.53 (21%)
cyt*b*-(309-326)A	+	0.46 (21%)	0.52 (21%)
cyt*b*-(309-311)A	+ +	1.90 (86%)	2.18 (87%)
cyt*b*-(312-314)A	+ +	1.96 (89%)	2.13 (85%)
cyt*b*-(315-317)A	+ +	2.06 (93%)	2.23 (89%)
cyt*b*-(318-321)A	+ +	2.21 (100%)	2.49 (100%)
cyt*b*-(322-323)A	+	0.69 (31%)	0.80 (32%)
cyt*b*-(324-326)A	+ +	2.01 (91%)	2.25 (90%)
cyt*b*-(S322A)	+	0.68 (31%)	0.81 (32%)
cyt*b*-(F323A)	+ +	2.22 (100%)	2.52 (100%)
cyt*b*-(S322T)	+ +	2.21 (100%)	2.51 (100%)
cyt*b*-(S322C)	+ +	2.10 (95%)	2.45 (98%)
cyt*b*-(S322Y)	+ +	2.08 (94%)	2.43 (97%)

[a] The purified bc_1 complex was in 50 mM Tris-Cl, pH 8.0, containing 200 mM NaCl, 200 mM histidine, and 0.5% octyl glucoside.

[b] Specific activity (S.A.) is expressed as μmol cytochrome *c* reduced/min/nmol cytochrome *b* at room temperature.

[c] + + , cell growth rate is essentially the same as that of the wild type cells.

[d] +, cells grow photosynthetically with a rate comparable to that of the wild type cells after a period of lag.

characterized. This mutant cell has photosynthetic growth behavior and bc_1 activity similar to those of the [cyt*b*-Δ(309-326)] mutant. These results support the requirement of this extra fragment of cytochrome *b* for the bacterial cytochrome bc_1 complex, and suggest that the amino acid residues, rather than the length of this fragment, are critical, since the alanine-substituted fragment should have the same length and structure as the wild-type fragment.

Serine-322 Is a Critical Residue in this Extra Fragment of Cytochrome *b*-- To identify critical amino acid residues in this extra fragment, we first located the critical regions. Residues in six portions of this fragment were replaced with alanine to generate six mutants, cyt*b*-(309-311)A, cyt*b*-(312-314)A, cyt*b*-(315-317)A, cyt*b*-(318-321)A, cyt*b*-(322-323)A, and cyt*b*-(324-326)A. When these mutants were subjected to photosynthetic growth conditions, mutants cyt*b*-(309-311)A, cyt*b*-(312-314)A, cyt*b*-(315-317)A, cyt*b*-(318-321)A, and cyt*b*-(324-326)A grow photosynthetically at a rate comparable with that of the complement cells. However, the cyt*b*-(322-323)A mutant requires a longer lag time (>12 hrs) before it starts to grow at a rate comparable to that of the wild-type cells. This growth behavoir is similar to that of mutants [cyt*b*-Δ(309-326)] and [cytb-(309-326)A]. Chromatophores prepared from mutants cyt*b*-(309-311)A, cyt*b*-(312-314)A, cyt*b*-(315-317)A, cyt*b*-(318-321)A, and cyt*b*-(324-326)A have, respectively, 86, 89, 93, 100, and 91% of bc_1 activity detected in the complement chromatophores. Similar activities are observed in bc_1 complexes purified from these mutant chromatphores (see Table 9). On the other hand, chromatophores and purified complex obtained from the cyt*b*-(322-323)A mutant has only 31% of bc_1 activity found in the complement chromatophores or bc_1

complex. These results indicate that either one or both residues 322-323 of cytochrome *b* are important.

Since residues 322 and 323 of cytochrome *b* are Ser and Phe, to see which of these two residues is essential, mutants cyt*b*-(S322A) and cyt*b*-(F323A) were generated and characterized. As shown in Table 9, chromatophores prepared from these two mutants have, respectively, 31 and 100% of the bc_1 activity found in the complement chromatophores, indicating that S-322 of cytochrome *b* is critical. The S-322 is highly conserved in bacterial cytochrome *bs.*

<u>Essentiality of the hydroxyl group in the Ser-322 of Cytochrome *b*</u>--Absorption spectral analysis reveals that the amounts and absorption properties of cytochromes *b* and c_1 in mutant complexes of cyt*b*-Δ(309-326), cyt*b*-(309-326)A, and cyt*b*-(S322A) are the same as those in the complement complex. Western blot analysis using antibodies against *R. sphaeroides* ISP and subunit IV also indicate that these mutant complexes have the same amount of ISP and subunit IV as does the complement complex. Redox potentials of cytochromes *b* and c_1 in these mutant complexes are also the same as those in the complement complex. Thus, the decrease in bc_1 activity in the cyt*b*-(S322A) mutant complex is not due to mutational effects on the assembly of the bc_1 protein subunits into the chromatophore membrane, to changes in the binding affinity of protein subunits in the complex, or to change the redox potential of cytochromes *b* and c_1 in the complex.

Since S-322 contains a hydroxyl group, it is possible that the loss of bc_1 activity in the cyt*b*-(S322A) mutant complex results from the mutation abolishing hydrogen bond forming ability of the residue at this position of cytochrome *b*. To confirm this possibility, mutants with S-322 substituted with the hydroxyl-containing residues [cyt*b*-(S322T) and cyt*b*-(S322Y)] and the SH-containing residue [cyt*b*-(S322C)] were generated and characterized. These three mutants grew photosynthetically at a rate comparable to that of the complement cells and, in bc_1 complexes in chromatophore membranes or in the purified state, have the same electron transfer activity as that of the complement complex (see Table 9). These results indicate that a hydrogen bond forming group at position 322 of cytochrome *b* is essential for the electron transfer activity of the bc_1 complex.

Effect of the Mutation at S322 of Cytochrome *b* on the Rieske Iron-Sulfur Cluster--Figure 24 compares EPR spectra of the Rieske iron-sulfur cluster in complement and mutant complexes. When the complement and cyt*b*-(S322A) mutant complexes were reduced by a small excess of ascorbate, the EPR signal of the [2Fe-2S] cluster in the complement complex is essentially the same as previously reported for the wild-type complex, with resonance at $g_x = 1.800$, $g_y = 1.898$, and $g_z = 2.026$. While the signatures of g_y and g_z of [2Fe-2S] in the cyt*b*-(S322A) mutant complex are the same as those detected in the complement complex, the g_x signature becomes broadened and shifts to $g = 1.768$, indicating that alanine substitution at S322 of cytochrome *b* perturbs the microenvironment of [2Fe-2S] cluster of ISP. As expected, the broadened, $g_x = 1.768$ signal is observed in mutant complexes of cyt*b*-Δ(309-326), cyt*b*-(309-326)A, and cyt*b*-(322-323)A (see Fig. 24), since these mutant complexes lack the essential hydrogen bonding forming hydroxyl group at residue 322 of cytochrome *b*.

Replacing S322 with T, Y, or C, the resulting mutant complexes have EPR characteristics of [2Fe-2S] cluster identical to those observed in the complement complex, indicating that the presence of a hydrogen bond forming residue at position 322 of cytochrome *b* is essential for maintaining proper microenvironments of the [2Fe-2S] cluster of ISP in the bacterial complex.

It has been reported that the g_x of bc_1 from *R. sphaeroides* is at $g = 1.800$ when ubiquinone is present but shifts to 1.750 and broadens when ubiquinol is present (3,25). When ubiquinone is extracted from chromatophore membranes, the g_x signal of the"depleted state" is at $g = 1.765$ and is considerably broader than those seen in the presence of either ubiquinone or ubiquinol (26). Although the broadened, $g_x = 1.768$ resonance observed in the cyt*b*-(S322A) mutant complex resembles the “reduced state” or the “depleted state” spectrum, it is not because of changes the redox state of Q or a decrease of Q content in the mutant complex, because the EPR spectrum of [2Fe-2S] cluster in this mutant complex is detected under the same redox conditions as that of the complement complex and the Q content in the cyt*b*-(S322A) mutant complex is the same as that in the complement complex.

The broadened, $g_x = 1.768$ signal observed in the cyt*b*-(S322A) mutant complex is also reminiscent of that observed for the substitution of Leu for Phe-144 (F144L) in the cytochrome *b* from *R. capsulatu*s (23) and of Ser for Thr-160 (T160S) in the cytochrome *b* from *R. sphaeroides* (15). The F144L bc_1 complex in *R. capsulatus* and the T160S mutant complex in *R. sphaeroides* chromatophores were reported to have a very low turnover rate with a broadened, redox state-insensitive, g_x value at 1.765. It was suggested that these properties of the F144L and T160S complexes resulted from a reduced affinity for quinone and quinol at the Q_o center of the mutated complexes. Since the K_ms for $Q_0C_{10}BrH_2$ determined with mutant complexes of cyt*b*-Δ(309-326) and cyt*b*-(S322A) are comparable with that of the complement complex, mutational effects observed in the

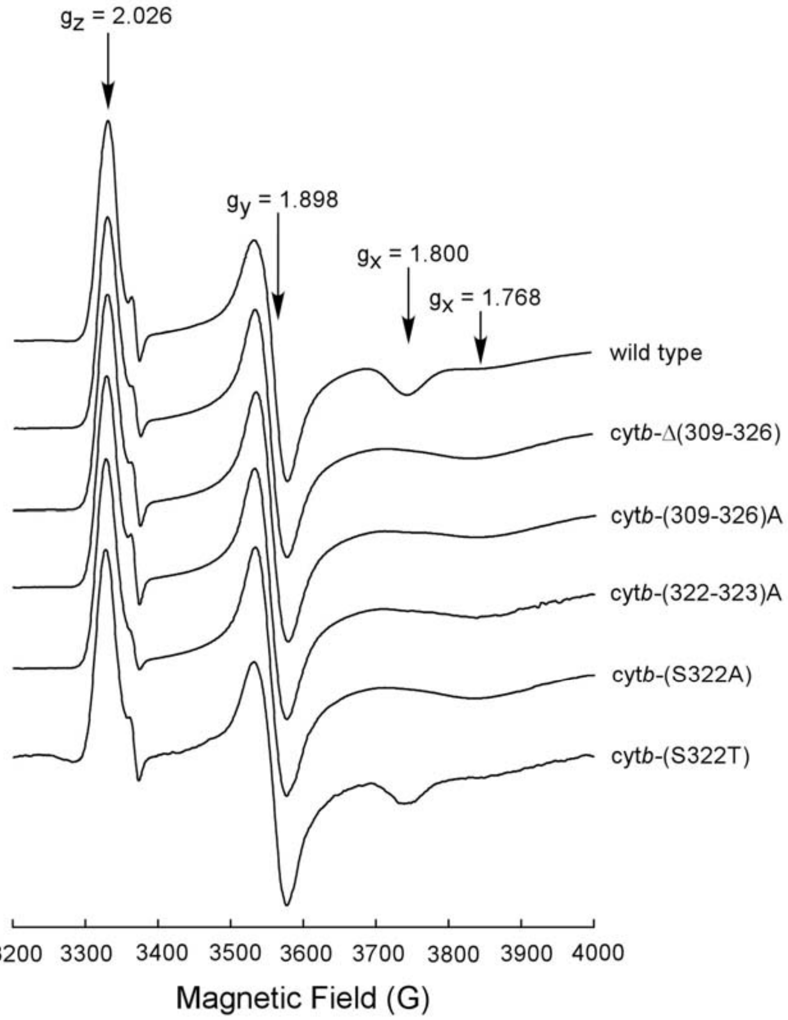

Figure 24. EPR spectra of the [2Fe-2S] cluster of the Rieske iron-sulfur protein in purified *bc*$_1$ complexes from the complement and mutants cyt*b*-Δ(309-326), cyt*b*-(309-326)A, cyt*b*-(322–323)A, cyt*b*-(S322A), and cyt*b*-(S322T). Purified complement and mutant *bc*$_1$ complexes were treated with a small excess of sodium ascorbate solution to fully reduce cytochrome c_1 and frozen in liquid nitrogen. EPR spectra were recorded EPR spectra were recorded at 11 K on a Bruker EMX EPR spectrometer equipped with an Air Products flow cryostat with the following instrument settings: microwave frequency, 9.3 GHz; microwave power, 2.2 milliwatts; modulation amplitudes, 6.3 G; modulation frequency, 100 kHz; time constant, 665.4 ms; sweep time: 167.8 s; conversion time, 163.8 ms.

cyt*b*-(S322A) mutant complex cannot be attributed to the decrease in quinol binding at the Qo site.

Since S322 is at the tip of this extra fragment of cytochrome *b* which is located between the amphipathic helix *ef*, a key structural component of the Qo site, and the transmembrane helix F, one possibility, which could account for the decreased turnover rate of the cyt*b*-(S322A) mutant complex and its reduced state or the high field shift of the g_x EPR singal is that alanine substitution at S322 causes conformational changes at the Q_o site, due to weakening putative interaction between ISP and cytochrome *b* through the loss of hydrogen bonding provided by the hydroxyl group of S322, to enhance the electron leakage thus decreasing the bc_1 activity.

<u>Superoxide Anion Generation by Cytochrome bc_1 Complexes with the S322A Mutation</u>--If the decrease in bc_1 activity observed in the cyt*b*-(S322A) mutant complex indeed results from the alteration of Q_o site to enhance electron leakage, one would expect to see an increase in the rate of $O_2^{\cdot-}$generation by the cyt*b*-(S322A) mutant complex, compared with that by the complement complex.

Figure 25 shows tracings of superoxide generation by complement and cyt*b*-(S322A) mutant bc_1 complexes. The rate of superoxide generation by bc_1 complex was measured by the chemiluminescence of the MCLA-$O_2^{\cdot-}$ adduct during a single turnover of bc_1 complex (in the absence of cytochrome *c*) using the Applied Photophysics stopped-flow reaction analyzer SX.18 MV. Since the system contains no cytochrome *c*, chemiluminescence of MCLA-$O_2^{\cdot-}$ resulting from non-enzymatic oxidation of ubiquinol by cytochrome *c*, is eliminated. MCLA chemiluminescence induced by bc_1 complex reaches peak intensities after approximately 0.06 sec at room temperature and then decays. No detectable luminescence is detected when bc_1 complex is omitted from the enzyme-containing solution or $Q_0C_{10}BrH_2$ is omitted from the substrate-containing solution. Addition of superoxide dismutase to either the substrate or enzyme solution completely abolishes luminescence, indicating that $O_2^{\cdot-}$ is responsible for the luminescence observed. Maximum peak height induced by the cyt*b*-(S322A) mutant complex is about four times higher than that reached by the wild-type complex.

Table 10 compares the rates of $O_2^{\cdot-}$ generation by the wild-type and mutant cytochrome bc_1 complexes. Oxidation of ubiquinol by complement and cyt*b*-(S322A) mutant complexes produces 0.19 and 0.72 XO units of $O_2^{\cdot-}$ per mg of protein, respectively. A similar increase in the rate of $O_2^{\cdot-}$ production is observed in mutant complexes of cyt*b*-Δ(309-326), cyt*b*-(309-326)A, and cyt*b*-(322-323)A. However, the rate of $Q_2^{\cdot-}$ production by mutant complexes of cyt*b*-(F323A) and cyt*b*-(S322T) are similar to that of the wild-type complex. These results support the idea that alanine substitution at S322 causes conformational changes at the Qo site, mainly through weakening the interaction between ISP and cytochrome *b* by replacing hydroxyl group at the position of 322, to facilitate electron leakage to react with molecular oxygen thus decreasing the bc_1 activity. Substituting S322 with threonine does not alter the putative hydrogen bounding and therefore has no effect on superoxide generation and the bc_1 activity.

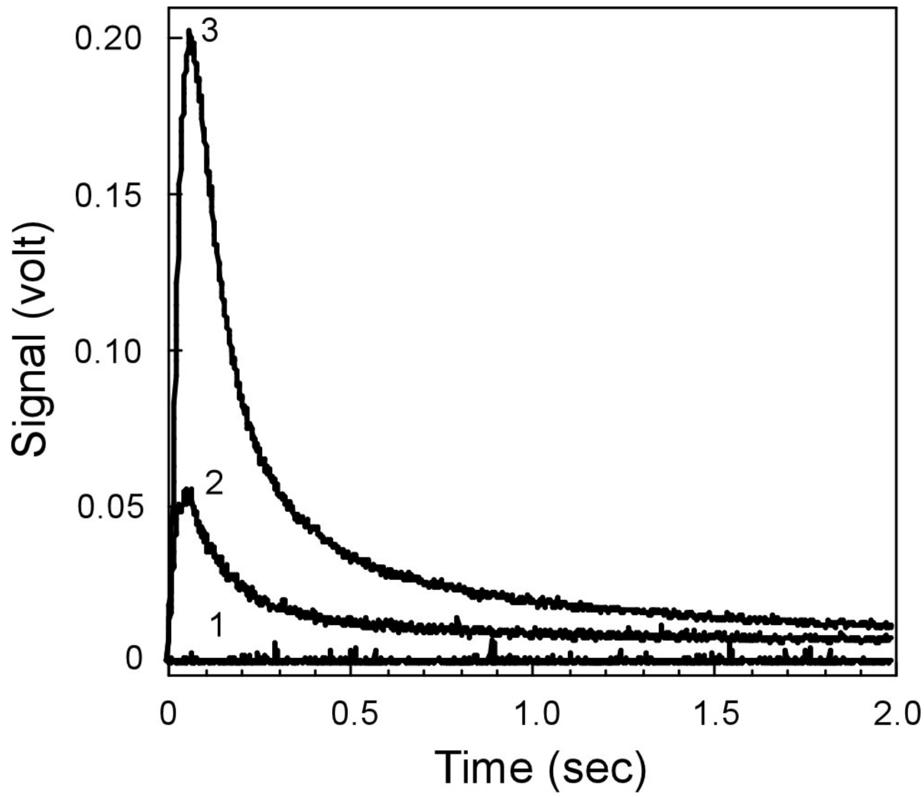

Figure 25. Tracings of superoxide generation in the cytochrome bc_1 complexes of wild-type and mutants in cytochrome *b*. To measure the superoxide anion production during the pre-steady state reaction of the reduction of the bc_1 complex by ubiquinol, stopped-flow assays were carried out at 23^{0}C in an Applied Photophysics stopped-flow reaction analyzer SX 18MV by mixing 1:1 solutions A and B. Solution A consisted of 100 mM Na^+/K^+ phosphate buffer, pH 7.4, containing 1 mM EDTA, 1 mM KCN, 1 mM NaN_3, 0.1% BSA, 0.01% DM and 9 µM bc_1 complexes. Solution B was the same as solution A except that the bc_1 complex was replaced with 50 µM $Q_0C_{10}BrH_2$ and 4 µM MCLA. For each sample, eight kinetic traces were averaged. For control, either bc_1 complexes or $Q_0C_{10}BrH_2$ were omitted from the above system, or 300 units/ml SOD was added to the system. Key: trace 1, control; trace 2, wild-type; trace 3, cyt*b*-(S322A).

Table 10. Production of superoxide anion by purified wild-type and mutant complexes

Strains	Superoxide anion[a]
	XO units / mg protein
Wild type	0.19 ± 0.02
cyt*b*-Δ(309-326)	0.73 ± 0.01
cyt*b*-(309-326)A	0.72 ± 0.03
cyt*b*-(322-323)A	0.72 ± 0.02
cyt*b*-(S322A)	0.72 ± 0.02
cyt*b*-(F323A)	0.19 ± 0.03
cyt*b*-(S322T)	0.18 ± 0.03

[a] XO units are defined under “Experimental Procedures.” For the experimental conditions, see the legend to Fig. 25. The data presented are mean values ± SD from five experiments.

Effect of Mutation on the Thermotropic Properties of Cytochrome *bc*$_1$ Complex-- Since it has been shown that alanine substitution at S322 of cytochrome *b* decreases the *bc*$_1$ complex activity, perturbs the microenvionment of ISP, and increases the rate of superoxide anion radical generation, it is of interest to see whether or not this mutation also affects structural stability of the *bc*$_1$ complex. Differential scanning calorimetry (DSC), a widely used method for determining protein structural stability, was employed to compare the stability of complement and mutant complexes. The lower T_m and ΔH of the mutant complex indicate that it is less stable than the complement complex.

When the thermotrophic properties of complement and mutant cyt*b*-(S322A) complexes were measured by DSC, the mutant complex exhibited a thermodenaturation temperature (T_m) of 44.1 ˚C with an enthalpy change (ΔH) of 74.0 kcal/mol whereas the complement complex showed a T_m of 46.3 ˚C with a ΔH of 96.7 kcal/mol. Under identical conditions, mutant complexes of cyt*b*-Δ(309-326), cyt*b*-(309-326)A, and cyt*b*-(S322T) showed, respectively, T_ms of 43.3, 43.3, and 46.2°C with ΔHs of 64.1, 63.6, and 95.6 kcal/mol. These results indicate that replacing the hydroxyl group bearing amino acid residue at the position 322 of cytochrome *b* with a non-hydroxyl amino acid causes not only a decrease in the electron transfer activity but also in the structural stability of the *bc*$_1$ complex.

References

1. Yu, L., Tso, S. C., Shenoy, S. K., Quinn, B. N., and Xia, D. (1999) *J. Bioenerg. Biomembr.* **31**, 251-257
2. Xiao, K., Liu, X., Yu, C. A., and Yu, L. (2004) *Biochemistry* **43**, 1488-1495
3. Liu, X., Yu, C. A., and Yu, L. (2004) *J. Biol. Chem.* **27**9, 47363-47371
4. Mitchell, P. (1976) *J. Theor. Biol.* **62**, 327-367
5. Turrens, J. F., Alexandre, A., and Lehninger, A. L. (1985) *Arch. Biochem. Biophys.* **237**, 408-414
6. Nohl, H., and Jordan, W. (1986) *Biochem. Biophys. Res. Commun.* **138**, 533-539
7. Zhang, L., Yu, L., and Yu, C. A. (1998) *J. Biol. Chem.* **273**, 33972-33976
8. Muller, F., Crofts, A. R., and Kramer, D. M. (2002) *Biochemistry* **41**, 7866-7874
9. Staniek, K., Gille, L., Kozlov, A. V., and Nohl, H. (2002) *Free Radic. Res.* **36**, 381-387
10. Muller, F. L., Roberts, A. G., Bowman, M. K., and Kramer, D. M. (2003) *Biochemistry* **42**, 6493-6499
11. Sun, J., and Trumpower, B. L. (2003) *Arch. Biochem. Biophys.* **419**, 198-206
12. Gong, X., Yu, L., Xia, D., and Yu, C. A. (2005) *J. Biol. Chem.* **280**, 9251-9257
13. Yu, C. A., and Yu, L. (1982) *Biochemistry* **21**, 4096-4101
14. Khosravi, M., Ryan, W., Webster, D. A., and Stark, B. C. (1990) *Plasmid* **23**, 138-143
15. Mather, M. W., Yu, L., and Yu, C. A. (1995) *J. Biol. Chem.* **270**, 28668-28675
16. Tian, H., Yu, L., Mather, M. W., and Yu, C. A. (1998) *J. Biol. Chem.* **273**, 27953-27959
17. Berden, J. A., and Slater, E. C. (1970) *Biochim. Biophys. Acta* **21**6, 237-249
18. Yu, L., Dong, J. H., and Yu, C. A. (1986) *Biochim. Biophys. Acta* **852**, 203-211
19. Redfearn, E. R. (1967) *Methods Enzymol.*__**10**__*,* 381-384
20. Lowry, O. H., Rosebrough, N. J., Farr, A. L., and Randall, R. J. (1951) *J. Biol. Chem.* **19**3, 265-275
21. Laemmli, U. K. (1970) *Nature* **227**, 680-685
22. Dutton, P. L. (1978) *Methods Enzymol.* **54**, 411-435

23. Guner, S., Robertson, D. E., Yu, L., Qiu, Z. H., Yu, C. A., and Knaff, D. Bj. (1991) *Biochim. Biophys. Acta* **1058**, 269-279
24. Esser, L., Quinn, B., Li, Y. F., Zhang, M., Elberry, M., Yu, L., Yu, C. A., and Xia, D. (2004) *J. Mol. Biol.* **341**, 281-302
25. Crofts, A. R., and Meinhardt, S. W. (1982) *Biochem. Soc. Trans.* **10**, 201-203
26. Ding, H., Robertson, D. E., Daldal, F., and Dutton, P. L. (1992) *Biochemistry* **31**, 3144-3158

CHAPTER V

SATURATION TRANSFER ELECTRON PARAMAGNETIC RESONANCE AND DIFFERENTIAL SCANNING CALORIMETRY STUDIES OF THE INTERACTION BETWEEN CYTOCHROME *caa*$_3$ AND F_1F_0-ATP SYNTHASE FROM ALKALIPHILIC *BACILLUS PSEUDOFIRMUS* OF4

Abstract

The interaction between cytochrome *caa*$_3$ and F_1F_0-ATP synthase from the alkaliphilic *Bacillus pseudofirmus* OF_4 was studied by differential scanning calorimetry (DSC) and by saturation transfer electron paramagnetic resonance (ST-EPR). When these two purified complexes are embedded in phospholipids vesicles individually [(*cca*$_3$) × PL, (F_1F_0) × PL)] or in combination [(*cca*$_3$+F_1F_0) × PL] and subjected to DSC analysis, they undergo exothermic thermodenaturation with transition temperatures at 69, 57, and 46/75 ˚C, respectively. The ΔH (-9.45 kcal/mol) of protein-phospholipid vesicles containing both cytochrome *caa*$_3$ and F_1F_0 is smaller than that (-12.3 kcal/mol) of a mixture of protein-phospholipid vesicles formed from each individual electron transfer complex [(*cca*$_3$ × PL) + (F_1F_0 × PL)]. These results suggest that a specific interaction between cytochrome *caa*$_3$ and F_1F_0 exists in the membrane. Further evidence for the interaction between these two complexes is provided by ST-EPR studies in which the rotational correlation time of spin-

labeled *caa*$_3$ (65 μs) increases significantly when the complex is mixed with F_1F_0 prior to being embedded in phospholipids vesicles (270 μs). From these results, it is concluded that at least a part of *caa*$_3$ and a part of F_1F_0 form a supermacromolecular complex in this bacterial membrane.

Introduction

The facultative alkaliphile, *Bacillus pseudofirmus* OF_4, grows well over a pH range extending from 7.5 to above 10.5 (1). The organism possesses a branched respiratory chain with at least two terminal oxidases, cytochrome *bd* and cytochrome *caa*$_3$ (2). Increased amounts of cytochrome *caa*$_3$ are associated with two distinct growth conditions where the bulk electrochemical proton gradient (Δp) is low: pH 10.5 (3) or pH 7.5 in the presence of protonophore carbonyl cyanide *m*-chlorophenylhydrazone (CCCP) (4). Additionally, a CCCP-resistant mutant strain was found to contain constitutively elevated levels of cytochrome *caa*$_3$ when grown at pH 7.5 (4).

Like mitochondria of eukaryotic organisms and most bacteria, alkaliphilic *Bacillus pseudofirmus* OF_4 synthesizes ATP using a proton-coupled F_1F_0-ATP synthase via oxidative phosphorylation (5). The widely confirmed chemiosmotic mechanism for ATP synthesis and other membrane-associated bioenergetic work requires establishment of Δp during respiration and photosynthesis. Coupling is achieved by the proton-translocating nature of the reversible F_1F_0-ATP synthase (6). Two properties of proton-coupled oxidative phosphorylation by alkaliphilic *Bacillus* species suggest that above pH 9.5, ATP synthesis utilizes a mechanism that depends upon the bulk transmembrane electrical potential, the $\Delta\Psi$, but also depends upon a sequestered transfer of protons from the respiratory chain to the ATP synthase. Firstly, the protonmotive driving force is very low at pH 10.5 and above, because the needs of pH homeostasis produce a large ΔpH, acid in. Nonetheless, the ATP synthesized, as reflected in the observed phosphorylation potential, is even greater than at pH 7.5, where the Δp is three times higher. Secondly, artificially imposed diffusion potentials fail to energize ATP synthesis at pH values above 9.5 (7).

We have hypothesized that robust alkaliphile oxidative phosphorylation at very alkaline pH values involves the required respiratory chain proton pumping to the bulk phase to establish a Δp and also involves use of one or more specific respiratory chain complexes to transfer protons to F_0 sector of the F_1F_0 ATP-synthase during dynamic protein-protein interactions (7). In this way, the proton-translocating F_1F_0-ATPase accesses protons that have not completely equilibrated with the alkaline medium, accounting for greater synthesis than anticipated from the measured bulk Δp and for the inefficacy of an imposed bulk potential. The *caa*$_3$ terminal oxidase is the best candidate for that interacting partner both because of its alkali-dependent expression and because of the observation that small mutational decreases in the level of this oxidase lead to a non-alkaliphilic phenotype on non-fermentative substrates (3,8). An alternative hypothesis that would not involve protein-protein interactions between a respiratory chain complex and the ATP synthase is that alkaliphile oxidative phosphorylation at high pH utilizes protons that are sequestered near the membrane surface in some trapped, delocalized manner (9), but such hypotheses have not been experimentlly supported and do not account from the requirement of specific features of the alkaliphile F_1F_0-ATPase for ATP synthesis at high pH (10).

Using methods of differential scanning calorimetry (DSC) and saturation transfer electron paramagnetic resonance (ST-EPR), we had earlier been able to detect protein-protein interactions between the bovine heart mitochondrial cytochrome *c* oxidase and F_1F_0-ATP synthase in the native membrane state (11). Recently, we used these methods to study the interaction between cytochrome *caa*$_3$ and ATP synthase from alkaliphilic *Bacillus pseudofirmus* OF_4 in an attempt to test the hypothesis that protein-protein interactions are involved in ATP synthesis. If the assays supported such interactions, they could then be used to assess the role of specific features of the ATP synthase and oxidase. The DSC study is based on the assumption that if two lipoprotein complexes exist separately in a phospholipid vesicle, no difference in thermotropic properties will be observed between protein-phospholipid vesicles formed from a mixture of two complexes and a mixture of protein-phospholipid vesicles formed individually from each complex. Differences in the thermodenaturation temperatures and enthalpy changes would suggest formation of a physical complex between cytochrome *caa*$_3$ and ATP synthase. In the ST-EPR study, the formation of a physical complex between cytochrome *caa*$_3$ and ATP synthase will be indicated by an increase of rotational correlation time of spin-labeled cytochrome *caa*$_3$. Herein, we report experimental details and results of DSC and ST-EPR studies with cytochrome *caa*$_3$ and ATP synthase embedded in phospholipid vesicles. The results of DSC and ST-EPR indicate that cytochrome *caa*$_3$ does indeed interact directly with the ATP synthase in phospholipid vesicles.

Experimental Procedures

Materials--4-Maleimide-2,2,6,6-tetramethyl-1-piperidinyl-N-oxyl (MSL), Cytochrome c (horse heart, type III) and sodium cholate were from Sigma. Dodecyl maltoside (DM) and octyl glucoside were from Anatrace. Asolection was obtained from Associated Concentrates, Inc., and purified according to the procedure reported by Kagama *et al.* (12). Centriprep-30 and Centricon-30 were bought from Amicon. Other chemicals were of the highest purity commercially available.

Enzyme Preparations and Assays--Highly purified cytochrome *caa*$_3$ and F_1F_0-ATP synthase from alkaliphilic *Bacillus pseudofirmus* OF_4 were prepared and assayed essentially as reported previously (3,5).

Preparation of Maleimide Spin-Labeled (MSL) Cytochrome *caa*$_3$--Alkaliphile, *Bacillus pseudofirmus* OF_4 cytochrome *caa*$_3$, 20 mg/ml in 20 mM Tris-Cl, pH 8.0, containing 0.35 M NaCl, 1 mM EDTA, 0.1 mM PMSF, 0.05 % dodecyl maltoside, and 10 % glycerol was incubated with a 5 molar excess of 4-maleimide-2,2,6,6-tetramethyl-1-piperidinyl-N-oxyl (MSL) for 1 hour at room temperature. The stock solution of MSL (10 mM) was made in 10 mM Tris-Cl /sucrose buffer, pH 8.0, containing 20% methanol. After incubation, the unreacted MSL was removed by passage through a D-Salt™ Excellulose Desalting Column from Pierce, equilibrated with 10 mM Tris-Cl buffer, containg 0.05 % dodecyl maltoside. Fractions containing MSL-cytochrome *caa*$_3$ were pooled and concentrated by Centriprep-30 and Centricon-30 to a protein concentration of approximately 20 mg/ml. MSL-cytochrome *caa*$_3$ obtained by this method contains no free spin-label. The absence of free spin-label in the preparation was confirmed by the conventional EPR spectra.

Preparation of Cytochrome *caa*$_3$ and F_1F_0 Complex-Phospholipid Vesicles--The protein-phospholipid vesicles were prepared by the cholate-dialysis method reported by Racker (13). Cytochrome *caa*$_3$ complex, with or without MSL labeling, alone or in combination with F_1F_0, at a protein concentration of approximately 30 mg/ml, was mixed with an asolectin micellar solution (20 mg/ml in 50 mM phosphate buffer, pH 7.4) and a sodium cholate solution [20% (w/v) in water]. The final solution contained 7 mg/ml protein, 10 mg/ml sodium cholate, and 10.5 mg/ml asolectin. After incubation at 4^{o}C for 30 min, the solution was dialyzed overnight against 500 volumes of 50 mM phosphate buffer, pH 7.4, with four changes of buffer to form vesicles. The protein-phospholipid vesicles formed were collected as precipitated by centrifugation at 80000g for 1 h and were respended in 50 mM phosphate buffer, pH 7.4, to a protein concentration of suitable number. The suspensions were used for the DSC and STEPR experiments.

Differential Scanning Calorimetry--All calorimetric measurements were performed with a CSC 6100 NanoII DSC from Calorimetry Science Corp. The reference and sample solutions were carefully degassed under vacuum for 15 min prior to use. A 0.50-ml sample in 50 mM K^+/Na^+ phosphate buffer, pH 7.4, was placed in the sample capillary cell, and the same amount of buffer was placed in the reference capillary cell. All DSC scans reported in this study were run at a rate of 1^{0}C/min. After the first scan, the samples were cooled to the original temperature and rescanned. Since after the first scan the protein was completely and irreversibly denatured, no thermotransition peaks were observed in the second scan. Thus the second scan could be used as a baseline. All thermodynamic analyses were carried out according to the program known as CpCal from the Nano DSC program group.

EPR Measurements--All EPR measurements were made with a Bruker EMX EPR spectrometer, using an aqueous quartz flat cell. The temperature of the microwave cavity was controlled by circulation of cooled nitrogen gas from a modified variable temperature housing assembly equipped with an electric temperature sensor. Conventional EPR spectra were recorded with instrument settings as follows: field modulation frequency, 100 kHz; modulation amplitute, 8 G; microwave frequency, 9.757 GHz; microwave power, 10.78 mW; time constant, 1310.72 ms. Saturation transfer EPR spectra were recorded using the same instrument settings as those described by Thomas *et al.* (14) and Poore *et al.* (15). A field modulation of 8 G and microwave frequency of 9.757 GHz were employed with phase-sensitive detection at 100 Hz (second harmonic) 90^0 out of phase. Incident microwave power was 107.80 mW. The phase was adjusted to minimize the second harmonic signal. Approximate rotational correlation time (τ_2) was obtained from the ratio of the two field lines (L"/L). The calibration curve of Thomas *et al.* (14) derived from isotropic tumbling of MSL-labeled hemoglobin was used in the calculation.

Other Analytical Methods--Protein concentration was determined by the biuret method (16), using bovine serum albumin as the standard (assuming 1 mg/ml has an A_{279} of 0.667). Absorption spectra were measured in a Shimadzu UV-2401 PC spectrophotometer.

Results and Discussion

Thermotropic Properties of Cytochrome *caa*$_3$ and F_1F_0-synthase Embedded in Phospholipid Vesicles--To unambiguously study the interaction between cytochrome *caa*$_3$ and F_1F_0-synthase from alkaliphilic *Bacillus pseudofirmus* OF_4, DSC studies were carried out with both complexes embedded in phospholipid (asolectin) vesicles, because these enzymes in protein-phospholipid vesicles should have an environment similar to that in membrane. The isolated complexes, singly or in combination, were embedded in phospholipids vesicles by the cholate dialysis method (13). A constant phospholipid to protein ratio of 1.5 was used. The ratio between cytochrome *caa*$_3$ and F_1F_0-synthase varies from 0.25 to 1.5. If the two lipoprotein complexes have no specific interaction, then no difference in DSC characteristics should be observed between phospholipids vesicles embedded with a mixture of two complexes and a mixture of phospholipids vesicles embedded with one or the other complex. In other words, differences in the thermodenaturation temperatures (Tm) and enthalpy changes (ΔH) would suggest formation of a physical complex between these two lipoproteins.

Figure 26 shows the differential scanning calorimetric thermograms of alkaliphilic *Bacillus pseudofirmus* OF_4 F_1F_0-synthase and cytochrome *caa*$_3$ embedded in phospholipids singly or in combination. When F_1F_0-synthase was incorporated into phospholipid vesicles and subjected to DSC analysis, an exothermic peak at 57.2 ^{0}C with the enthalpy change of -4.22 kcal/mol of protein was observed (see Fig. 26A). Purified cytochrome *caa*$_3$ also shows a single transition with ΔH = -8.19 kcal/mol of protein and Tm = 68.5 ^{0}C when embedded into phospholipids vesicles as shown in Fig.26B. As expected, when the mixture of protein-phospholipid vesicles formed individually from

F_1F_0-synthase and cytochrome *caa*$_3$ was subjected to DSC analysis under the identical condition, two exothermic transient peaks at 56.8 and 68.9 ^{0}C with the ΔH of -12.3 kcal/mol of protein were obtained (see Fig. 26D). These data are summaries of the thermotropic properties of F_1F_0-synthase-phospholipid vesicles and cytochrome *caa*$_3$-phospholipid vesicles. However, the protein-phospholipid vesicles formed from a mixture of F_1F_0-synthase and cytochrome *caa*$_3$ have Tm_1 = 45.5 ^{0}C and Tm_2 = 74.6 ^{0}C with ΔH = -9.45 kcal/mol of protein (see Fig. 26C). These data are significantly different from those observed with a mixture of phospholipids vesicles embedded individually with F_1F_0-synthase or cytochrome *caa*$_3$, suggesting that there is some interaction between these two complexes.

Figure 27 compares the thermodenaturation enthalpy changes of phospholipid vesicles formed with mixtures of cytochrome *caa*$_3$ and F_1F_0-synthase at various molar ratios and of mixtures of phospholipid vesicles of individual complexes. The value of the difference in ΔH increases as F_1F_0-synthase is increased. The maximum difference is obtained when approximately one mol of F_1F_0-synthase per mol cytochrome *caa*$_3$ is used. This suggests that the interaction between cytochrome *caa*$_3$ and F_1F_0-synthase is specific. The accuracy of assessment of the stoichiometry between the two complexes may have been compromised by uncertainty concerning the intactness of each complex.

As discussed earlier (11,17-19), the energy for the exothermic transition of an electron transfer complex embedded in phospholipids vesicles is derived from the collapse, upon thermodenaturation, of a strained interaction between unsaturated fatty acyl groups of phospholipids and a protein surface on the electron transfer or other lipoprotein complex which was exposed, by removal of an interacting protein from a

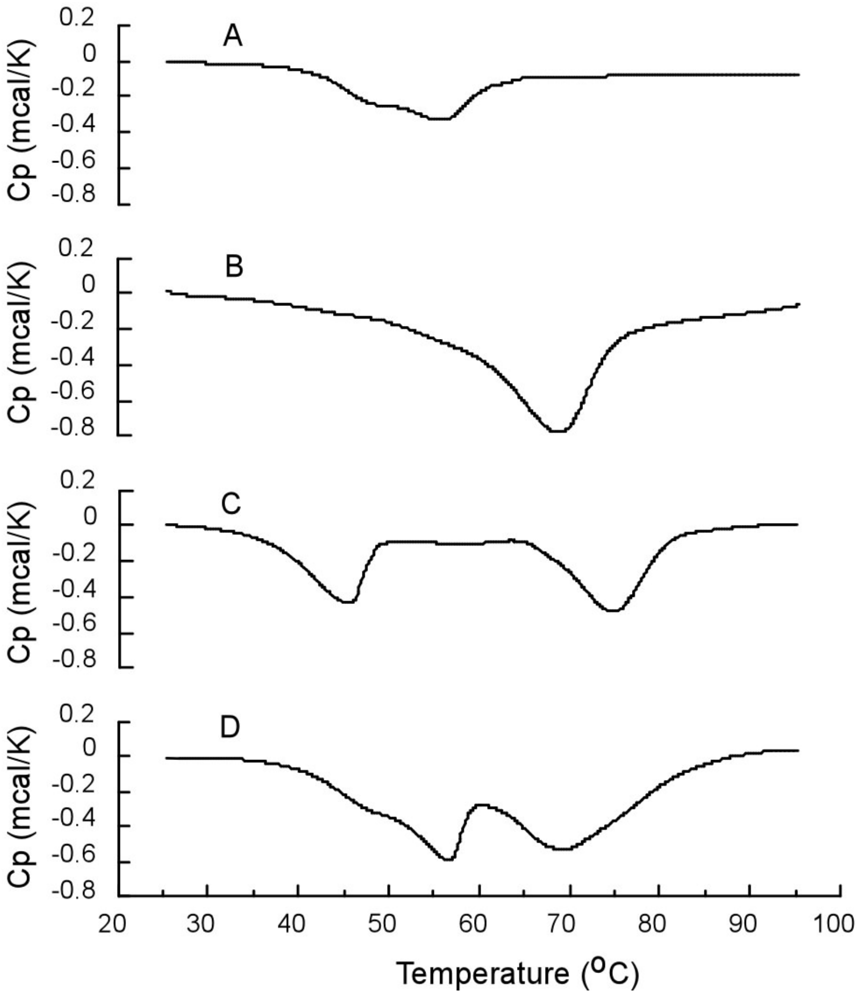

Figure 26. DSC curves of alkaliphile *B. pseudofirmus* OF4 F_1F_0 and cytochrome *caa*$_3$ embedded in phospholipids singly or in combination. The molar ratio of F_1F_0 and *caa*$_3$ is 1 and the weight ratio of phospholipids to protein is 1.5 in all cases. These vesicles are prepared by the cholate dialysis method. Spectrum A shows the exothermic thermodenaturation of 0.5 mg F_1F_0 embedded in phospholipid vesicles. Spectrum B is the DSC thermogram of 0.105 mg *caa*$_3$ embedded in phospholipid vesicles. Spectrum C is the DSC profile of phospholipid vesicle embedded with a mixture of 0.5 mg F_1F_0 and 0.105 mg *caa*$_3$. Spectrum D is a mixture of phospholipid vesicles, which include 0.5 mg F_1F_0 embedded in phospholipid vesicles and 0.105 mg *caa*$_3$ embedded in phospholipid vesicles.

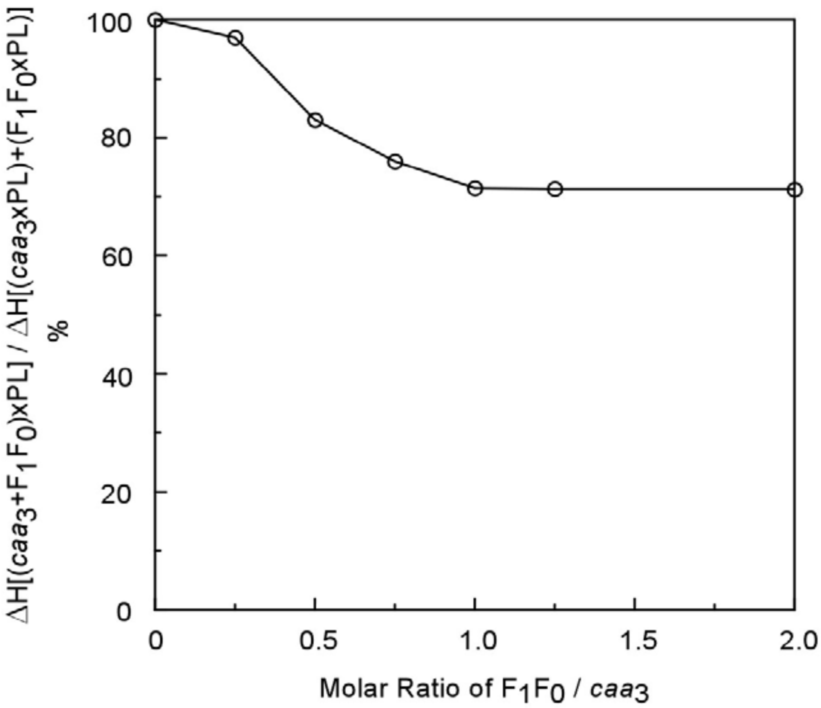

Figure 27. Comparison of thermodenaturation enthalpy changes of phospholipids vesicles formed with mixtures of cytochrome *caa*$_3$ and F$_1$F$_0$-synthase from alkaliphile *B. pseudofirmus* OF4 at various molar ratios and of mixtures of phospholipids vesicles of individual complexes. The molecular masses used in calculation of molar ratios were 517,000 and 105, 500 daltons for F$_1$F$_0$-synthase and cytochrome *caa*$_3$, respectively. The ratio of phospholipids to protein was 1.5 by weight in all cases.

complex or a complex from a supermacromolecular complex, during the isolation. Such an interaction occurs only when a vesicle is formed. Little exothermic transition was observed in mitochondrial or submitochondrial preparations because there is no such exposed area in the native complex or supercomplex to interact with phospholipids under strained conditions. When two interacting complexes are mixed together before being embedded in phospholipids vesicles, the exposed area on the protein surface is greatly diminishes through the protein-protein interaction. Therefore, less strained interaction occurs upon vesicle formation, and less enthalpy change of exothermic denaturation is observed. It has been reported that thermodenaturation of the mitochondrial membrane under aerobic condition is accompanied by a heat release,which was attributed to the autooxidation of iron-sulfur protein (20). This explanation is not applicable to the present study because there are no iron-sulfur proteins in either cytochrome *caa*$_3$ or F_1F_0-synthase.

ST-EPR Studies of Spin-labeled Cytochrome *caa*$_3$ Embedded in Phospholipid Vesicles in the Absence and Presence of F_1F_0-synthase--To confirm the existence of a specific interaction between cytochrome *caa*$_3$ and F_1F_0-synthase, cytochrome *caa*$_3$ was labeled with 4-maleimide-2,2,6,6-tetramethyl-1-piperidinyl-N-oxyl (MSL) as described under "Experimental Procedures". This MSL-cytochrome *caa*$_3$, which is enzymatically active, was embedded in phospholipids vesicles alone or together with F_1F_0-synthase. The electron paramagnetic resonance (EPR) measurements of these electron transfer complex-phospholipid vesicles show typical spin-immobilized spectra. The spectra are identical regardless of whether the protein-phospholipid vesicles contained only cytochrome *caa*$_3$ or cytochrome *caa*$_3$ and F_1F_0-synthase complexes (see spectra A and B of Figure 28). This suggests that the difference in mobility of the spin-label on cytochrome *caa*$_3$, in the absence and presence of F_1F_0-synthase, is too small to be measured by conventional EPR. Therefore, the protein rotational diffusion of the spin-labeled complex was measured by saturation transfer electron paramagnetic resonance (ST-EPR). From the change of the ratio of two low-field signals (L''/L) (see spectra C and D of Figure 28), rotational correlation times (τ_2) can be calculated according to methods reported (14,15). Table 11 shows the effect of additions on the rotational correlation time of spin-labeled cytochrome *caa*$_3$. When mixed with F_1F_0-synthase from alkaliphilic *Bacillus pseudofirmus* OF_4 before being embedded in phospholipids vesicles, a significance increase in τ_2 was observed compared to that of spin-labeled cytochrome *caa*$_3$ embedded in phospholipids vesicles alone. However, the τ_2 of spin-labeled cytochrome *caa*$_3$ was not affected by the addition of cytochrome *bc*$_1$ complex or ATP-synthase from bovine heart prior to the formation of vesicles; and the mixture of spin-labeled cytochrome *caa*$_3$ complex and F_1F_0-synthase phospholipids vesicles showed the same τ_2 as that of cytochrome *caa*$_3$ phospholipid vesicles alone (see Table 11).

A similar effect of succinate-Q reductase on τ_2 of spin-labeled ubiquinol-cytochrome *c* reductase (18), and of F_1F_0-synthase on τ_2 of spin-labeled cytochrome *c* oxidase from bovine mitochondria (11), has been reported from this group. It is conceivable that at least part of the observed effect resulted from a change in the fluidity of the membrane by inclusion of protein complexes other than the spin-labeled complex. Also, it should be mentioned that the rotational correlation time obtained from ST-EPR is only an approximate value; it is based on the calibration curve derived from the isotropic motion of spin-label. The values obtained, however, agree with those obtained by other methods, such as flash photolysis (21). Although in this study our main concern is with the relative

τ_2 of spin-labeled cytochrome *caa*$_3$ in the absence and presence of the F_1F_0-synthase from alkaliphilic *Bacillus pseudofirmus* OF_4, the τ_2 values obtained are in agreement with the DSC data.

From the results of DSC and ST-EPR experiments, we conclude that cytochrome *caa*$_3$ and F_1F_0-synthase from alkaliphilic *Bacillus pseudofirmus* OF_4 may exist as a supermacromolecular complex in the membrane. This conclusion differs significantly from the free diffusible model of electron transfer complexes derived from results of membrane fusing (22) and fluorescence recovery, after photobleaching, measurements (23). However, it has been clearly established that some mitochondrial electron-transfer complexes specifically interact to form supermolecular structures called supercomplexes from the work on the yeast *Saccharomyces cerevisiae* (24,25), beef (11,18,25,26), and plants (27-30). Similar supermolecular structures were also described for the respiratory chains of bacteria (31-35). The roles that have been attributed to respiratory supercomplexes are substrate-channeling, catalytic enhancement, sequestration of reactive intermediates (25), stabilization of protein complexes (36), increasing the capacity of the inner mitochondrial membrane for protein insertion (24), and generating mitochondrial cristae morphology (37). Furthermore, the dynamic formation of such supercomplexes is speculated to serve some regulatory function in the energy generation in mitochondria from plants (27) and beef (11). Similarly, the formation of a supermacromolecular complex between cytochrome *caa*$_3$ and F_1F_0-synthase from alkaliphilic *Bacillus pseudofirmus* OF_4 may help control energy generation in this alkaliphilic bacterium. The formation of supermacromolecular complexes from some electron transfer and F_1F_0-

synthase complexes indicates that some of these complexes do not follow the random diffusion model, even though they are capable of doing so.

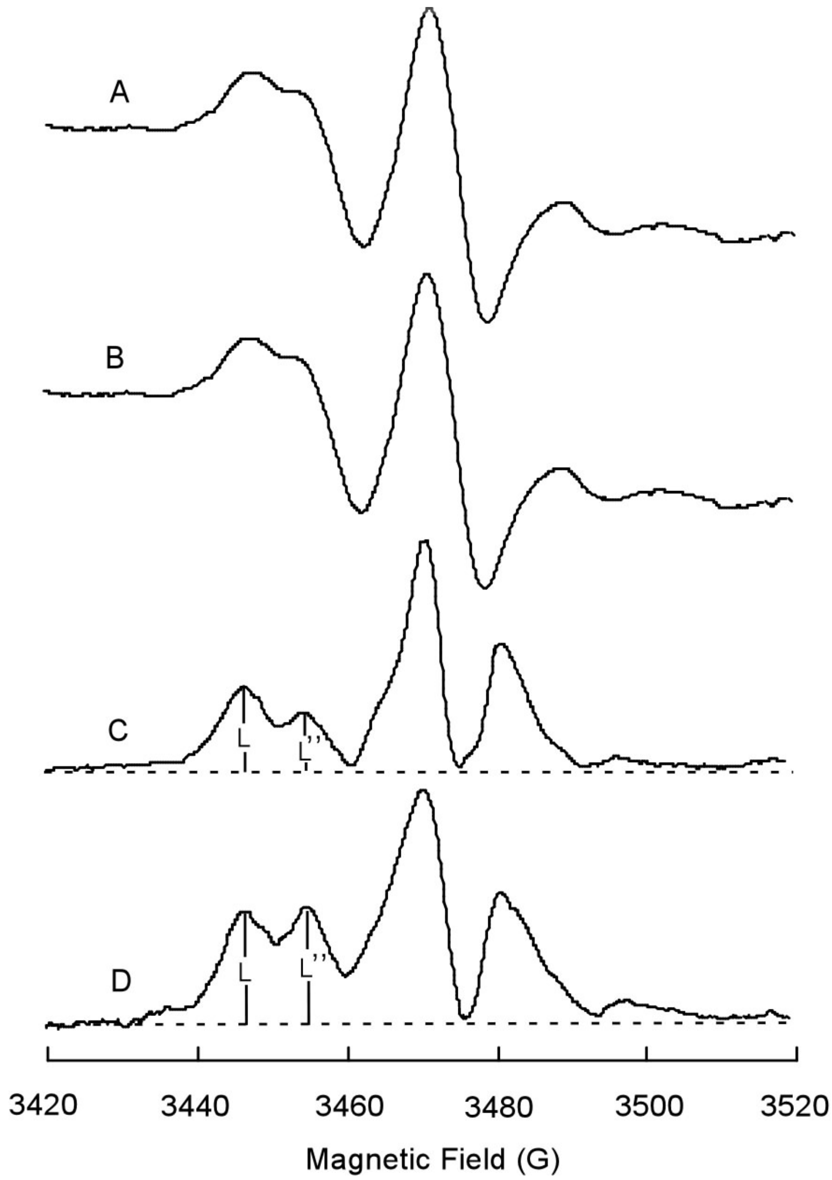

Figure 27. EPR spectra of spin-labeled alkaliphile *B. pseudofirmus* OF4 cytochrome *caa*$_3$ in the absence and presence of OF4 F_1F_0-synthase complex. Spectra A and B are conventional EPR spectra of spin-labeled OF4 cytochrome *caa*$_3$ embedded in phospholipid vesicles in the absence or presence of OF4 F_1F_0-synthase complex. Spectra C and D are the saturation transfer EPR spectra of the same samples. The protein concentrations were 6 and 36 mg/ml for cytochrome *caa*$_3$ and (cytochrome *caa*$_3$+F_1F_0-synthase) vesicles, repectively.

Table 11. Effect of additions on the rotational correlation time (τ_2) of spin-labeled cytochrome *caa*$_3$[1]

Preparations	L''/L	τ_2 (μs)
(MSL-*caa*$_3$ × PL)	0.70	65
[(MSL-*caa*$_3$ + bF_1F_0[2]) × PL]	1.06	270
[(MSL-*caa*$_3$ × PL) + (bF_1F_0 × PL]	0.71	70
[(MSL-*caa*$_3$ + mF_1F_0[3]) × PL]	0.71	70
[(MSL-*caa*$_3$ + m*bc*$_1$[4]) × PL]	0.70	65

[1]The molar ratio of cytochrome *caa*$_3$ to other proteins used was 1:1.

[2]The bF_1F_0 was F_1F_0-synthase from bacterial alkaliphile B. firmus OF4.

[3]The mF_1F_0 was F_1F_0-synthase from bovine mitochondria.

[4]The m*bc*$_1$ was cytochrome *bc*$_1$ complex from bovine mitochondria.

References

1. Krulwich, T. A., Ito, M., Gilmour, R., Hicks, D. B., and Guffanti, A. A. (1998) *Adv. Microb. Physiol.* **40**, 401-438
2. Gilmour, R., and Krulwich, T. A. (1997) *J. Bacteriol.* **179**, 863-870
3. Quirk, P. G., Hicks, D. B., and Krulwich, T. A. (1993) *J. Biol. Chem.* **268**, 678-685
4. Quirk, P. G., Guffanti, A. A., Plass, R. J., Clejan, S., and Krulwich, T. A. (1991) *Biochim. Biophys. Acta* **1058**, 131-140
5. Hicks, D. B., and Krulwich, T. A. (1990) *J. Biol. Chem.* **265**, 20547-20554
6. Mitchell, P. (1961) *Nature* **191**, 144-148
7. Krulwich, T. A. (1995) *Mol. Microbiol.* **15**, 403-410
8. Krulwich, T. A., Ito, M., Gilmour, R., Sturr, M. G., Guffanti, A. A., and Hicks, D. B. (1996) *Biochim. Biophys. Acta* **1275**, 21-26
9. Cherepanov, D. A., Feniouk, B. A., Junge, W., and Mulkidjanian, A. Y. (2003) *Biophys. J.* **85**, 1307-1316
10. Wang, Z., Hicks, D. B., Guffanti, A. A., Baldwin, K., and Krulwich, T. A. (2004) *J. Biol. Chem.* **279**, 26546-26554
11. Qiu, Z. H., Yu, L., and Yu, C. A. (1992) *Biochemistry* **31**, 3297-3302
12. Kagawa, Y. (1971) *Tanpakushitsu Kakusan Koso* **16**, 775-786
13. Racker, E. (1972) *J. Membr. Biol.* **10**, 221-235
14. Thomas, D. D., Dalton, L. R., and Hyde, J. S. (1976) *J. Chem. Phys.* **65**, 3006-3024
15. Poore, V. M., Fitzsimmon, J. T. R., and Ragan, C. I. (1981) *Biochim. Biophys. Acta* **693**, 113-124
16. Gornall, A. G., Barwawill, C. J., and David, M. M. (1949) *J. Boil. Chem.* **177**, 751-766
17. Gwak, S. H., Yu, L., and Yu, C. A. (1985) *Biochim. Biophys. Acta* **809**, 187-198
18. Gwak, S. H., Yu, L., and Yu, C. A. (1986) *Biochemistry* **25**, 7675-7682
19. Yu, C. A., Gwak, S. H., and Yu, L. (1985) *Biochim. Biophys. Acta* **812**, 656-664
20. Tsong, T. Y., and Knox, B. E. (1984) *Biophys. J.* **45**, 296a
21. Cherry, R. J. (1979) *Biochim. Biophys. Acta* **559**, 289-327
22. Schneider, H., Lemasters, J. J., Hochli, M., and Hackenbrock, C. R. (1980) *J. Biol. Chem.* **255**, 3748-3756

23. Gupte, S., Wu, E. S., Hoechli, L., Hoechli, M., Jacobson, K., Sowers, A. E., and Hackenbrock, C. R. (1984) *Proc. Natl. Acad. Sci. U S A* **81**, 2606-2610

24. Arnold, I., Pfeiffer, K., Neupert, W., Stuart, R. A., and Schagger, H. (1998) *EMBO J.* **17**, 7170-7178

25. Schagger, H., and Pfeiffer, K. (2000) *EMBO J.* **19**, 1777-1783

26. Schagger, H., and Pfeiffer, K. (2001) *J. Biol. Chem.* **276**, 37861-37867

27. Eubel, H., Jansch, L., and Braun, H. P. (2003) *Plant Physiol.* **133**, 274-286

28. Eubel, H., Heinemeyer, J., and Braun, H. P. (2004) *Plant Physiol.* **134**, 1450-1459

29. Krause, F., Reifschneider, N. H., Vocke, D., Seelert, H., Rexroth, S., and Dencher, N. A. (2004) *J. Biol. Chem.* **279**, 48369-48375

30. Dudkina, N. V., Eubel, H., Keegstra, W., Boekema, E. J., and Braun, H. P. (2005) *Proc. Natl. Acad. Sci. U S A* **102**, 3225-3229

31. Berry, E. A., and Trumpower, B. L. (1985) *J. Biol. Chem.* **260**, 2458-2467

32. Sone, N., Sekimachi, M., and Kutoh, E. (1987) *J. Biol. Chem.* **262**, 15386-15391

33. Iwasaki, T., Matsuura, K., and Oshima, T. (1995) *J. Biol. Chem.* **270**, 30881-30892

34. Niebisch, A., and Bott, M. (2003) *J. Biol. Chem.* **278**, 4339-4346

35. Stroh, A., Anderka, O., Pfeiffer, K., Yagi, T., Finel, M., Ludwig, B., and Schagger, H. (2004) *J. Biol. Chem.* **279**, 5000-5007

36. Acin-Perez, R., Bayona-Bafaluy, M. P., Fernandez-Silva, P., Moreno-Loshuertos, R., Perez-Martos, A., Bruno, C., Moraes, C. T., and Enriquez, J. A. (2004) *Mol. Cell* **13**, 805-815

37. Paumard, P., Vaillier, J., Coulary, B., Schaeffer, J., Soubannier, V., Mueller, D. M., Brethes, D., di Rago, J. P., and Velours, J. (2002) *EMBO J.* **21**, 221-230

Vita

Xing Gong

Candidate for the Degree of

Doctor of Philosophy

Thesis: STRUCTURAL AND FUNCTIONAL STUDIES OF ELECTRON TRANSFER COMPLEXES

Major Field: Biochemistry and Molecular Biology

Biographical:

Education: Graduated from the first High School of Xinshao, Hunan, China in July 1992; received Bachelor of Science degree and Master of Science degree in Chemistry from Lanzhou University, Gansu, China in July 1996 and July 1999, respectively. Completed the requirements for the Doctor of Philosophy degree with a major in Biochemistry and Molecular Biology at Oklahoma State University in December, 2005.

Experience: Employed as a research assistant by College of Chemistry and Chemical Engineering, Lanzhou University from September 1996 to July 1999; employed as a teaching and research assistant by College of Chemistry and Chemical Engineering, Lanzhou University from July 1999 to December 1999; employed by Oklahoma State University, Department of Biochemistry and Molecular Biology as a graduate research assistant from January 2000 to present.

Professional Membership: American Biophysical Society.

Publications: 1. Gong, X., Xie, T., Yu, L., Hesterberg, M., Scheide, D., Friedrich, T., and Yu, C. A. (2003) The ubiquinone-binding site in NADH:ubiquinone redoreductase from *Escherichia coli*, *J. Biol. Chem.* **278**, 25731-25737; 2. Gong, X., Yu, L., Xia, D., and Yu, C. A. (2005) Evidence for electron equilibrium between the two hemes b_L in the dimeric cytochrome bc_1 complex, *J. Biol. Chem.* **280**, 9251-9257.

Name: Xing Gong Date of Degree: December, 2005

Institution: Oklahoma State University Location: Stillwater, Oklahoma

Title of Study: STRUCTURAL AND FUNCTIONAL STUDIES OF ELECTRON TRANSFER COMPLEXES

Pages in Study: 144 Candidate for the Degree of Doctor of Philosophy

Major Field: Biochemistry and Molecular Biology

Scope and Method of Study: As an effort to understand the structure-function relationship of the electron transfer complexes, we chose *Escherichia coli* and *Rhodobacter sphaeroides* to study NADH:ubiquinone oxidoreductase (Complex I) and cytochrome bc_1 complex (Complex III), respectively. The mechanism of electron transfer and its coupling to proton translocation in Complex I is poorly understood. Knowledge of ubiquinone (Q) binding is essential for mechanistic studies for this enzyme. We identified a Q-binding peptide of NuoM in *E. coli* complex I by photoaffinity labeling with a photoactivatable azido-Q derivative. One of most unexpected findings in the structural analysis of mitochondrial bc_1 complexes is the inter-monomer b_L-b_L electron transfer during the catalysis. We obtained the evidence for electron equilibrium between the two hemes b_L through the molecular genetic manipulation of *R. sphaeroides* bc_1 complex together with biochemical and biophysical measurements. Although bacterial bc_1 complexes have simpler subunit composition than their mitochondrial counter parts, the sizes of core subunits are generally larger. We probed the role of one of extra fragments of cytochrome *b* (residues 309-326) through site-directed mutagenesis at various positions of this fragment in *R. sphaeroides* bc_1 complex. The interaction between cytochrome caa_3 and F_1F_0-ATP synthase from alkaliphilic *Bacillus pseudofirmus* OF4 was studied by differential scanning calorimetry (DSC) and saturation transfer electron paramagnetic resonance (ST-EPR).

Findings and Conclusions: The photoaffinity labeling results suggest that the Q-binding peptide corresponds to amino acid residues 184-206 of subunit NuoM in *E. coli* complex I. This Q-binding site is located in the transmembrane helix 5 toward the cytoplasmic side of the membrane or in helix 4 toward the periplasmic side of the membrane depending on the secondary structures of NuoM predicted by different programs. Molecular genetic studies of *R. sphaeroides* bc_1 complex demonstrate the aromatic group at position 195 of cytochrome *b* is involved in electron transfer reaction of the bc_1 complex. The rate of superoxide anion generation is 3 times higher in the F195A complex than in the wild-type, suggesting the idea that the interruption of electron transfer between the two b_L hemes enhances electron leakage to oxygen and thus decreases the bc_1 activity. The extra fragment of *R. sphaeroides* cytochrome *b* (residues 309-326) is found to be involved in the structural stability of the Qo site in the bc_1 complex. The results of DSC and ST-EPR indicate that at least a part of cytochrome caa_3 and a part of F_1F_0-ATP synthase form a supermacromolecular complex in the membrane of alkaliphilic *Bacillus pseudofirmus* OF4.

ADVISER'S APPROVAL: Chang-An Yu